Master's thesis

NTNU
Norwegian University of Science and Technology
Faculty of Engineering
Department of Marine Technology

Sindre Grøftrem

Probabilistic investigation into time domain analysis of feed barge mooring systems

Master's thesis in Marine Technology
Supervisor: Pål Lader
Co-supervisor: Martin Søreide
June 2022

NTNU
Norwegian University of
Science and Technology

Sindre Grøftrem

Probabilistic investigation into time domain analysis of feed barge mooring systems

Master's thesis in Marine Technology
Supervisor: Pål Lader
Co-supervisor: Martin Søreide
June 2022

Norwegian University of Science and Technology
Faculty of Engineering
Department of Marine Technology

NTNU
Norwegian University of
Science and Technology

Abstract

Norwegian rainbow trout and salmon farming volumes has not increased noteworthy for the past several years (SSB, 2021). This is because of strict requirements from the government to the industry, in regards to factors like lice density, fish welfare and environmental impact. It would seem that the Norwegian fjords are filled with aquaculture facilities. As long as the fish farmers are unable to show the government that they are able to uphold requirements, the government will not provide more licenses. A possible solution for both the fish farmers and the government, is to move the aquaculture to offshore sites. Naturally, this revolutionary change comes with some challenges. One of which is the topic of this thesis, feed barge mooring in exposed locations.

This thesis was motivated by concern from the aquaculture industry, that the new revised standard, NS9415, might not contain adequate requirements for exposed feed barge mooring. More specifically, at locations with significant wave heights up to 6m, compared to traditional locations with significant wave heights up to 3m. This thesis presents various commonly used mooring concepts, both for the aquaculture industry as well as the oil and gas industry. The components most important for aquaculture mooring is also presented. Different theories for modelling and analysing mooring lines are derived and explained. The newest aquaculture regulations regarding feed barge mooring is reviewed and presented. A qualitative risk assessment is performed by comparing feed barge mooring to offshore vessel mooring.

Two commonly used methods for mooring analysis were identified to be *coupled* and *uncoupled* analysis. Which one of these methods to use in various cases are not specified in the revised standard NS9415. It was therefore decided that an investigation into these methods would fulfill the main goal of this thesis. A comparison between these two methods of analysis were then conducted. To facilitate such a comparison, state of the art analysis software SIMA, developed by SINTEF, was utilized. Two identical models were created, with the only difference being that one was uncoupled and the other coupled. The specifications for these models were given from ScaleAQ, which had conducted model-tests of an identical setup. Several analyses were then performed for varying environmental conditions, matching that of ScaleAQ's model tests, to aid verification/comparison of the SIMA models. From the numerical analyses performed in SIMA, vessel response and line tension from leeward and windward lines were stored and post-processed. The results for coupled and uncoupled models were then compared.

It was found that the coupled model was able to predict the vessel response and tension rather accurate, although this was not confirmed by the small-scale model test results supplied by ScaleAQ. On the other hand, the uncoupled model vastly over-predicted both vessel response and line tensions. Based on the filtered response spectrums, it was concluded that this was caused by eigenmode excitation (especially yaw-motion), due to lack of damping from mooring lines. Even though the uncoupled analysis was roughly 20 times faster than the coupled, the results were too inaccurate to be useful. It was proposed that manually adding damping to the uncoupled model, to substitute for lack of mooring line damping and thus improve accuracy, might be

subject for further work. Also subject for further work, is investigating whether or not there was numerical errors in the uncoupled model, as this could not be ruled out.

A study of a specific requirement in NS9415, regarding the use of regular instead of irregular waves, were also conducted. It was found that this requirement under-predicted the max vessel response and over-predicted the mean response value. Meaning that the requirement is not conservative for ULS design, and should therefore be avoided. It should be noted that the standard does mention that irregular waves should be considered in cases where slowly varying drift forces are important, which is the case for moored structures.

Sammendrag

Norsk regnbueørret -og lakse oppdretts volumer har ikke økt nevneverdig de siste årene (SSB, 2021). Dette er på grunn av strenge krav fra staten til industrien, krav til faktorer som tetthet av lus, fiskevelferd og påvirkning på miljøet. Det kan virke som norske fjorder har nådd maksimal kapasitet av oppdrettsanlegg. Så lenge oppdretterne ikke klarer å opprettholde kravene, så deler ikke staten ut flere lisenser. En mulig løsning på denne problemstillingen for både oppdretterne og staten, er å flytte oppdretten til mer eksponerte lokasjoner, utenfor fjordene. Slike revolusjonerende endringer kommer naturligvis med utfordringer. En av disse utfordringene er tema for denne avhandlingen, nemlig fortøyning av forflåter i eksponerte forhold.

Denne avhandlingen ble motivert av bekymring fra oppdrettsnæringen og forskningsmiljøet rundt at den nye reviderte standarden, NS9415, muligens ikke inneholder tilstrekkelige krav for eksponerte forflåter. Mer spesifikt, på lokasjoner med signifikant bølgehøyde opp mot 6m, sammenlignet med tradisjonelle lokasjoner med signifikant bølgehøyde opp mot 3m. Denne avhandlingen presenterer forskjellige vanlige fortøyningsmetoder og konsepter, både brukt i oppdrett og olje -og gass næringen. Fortøyningskomponenter som er viktig for oppdrett blir også presentert. Forskjellige teorier for modellering og anlyse av fortøyningsliner blir utledet og forklart. En kvalitativ risikovurdering hvor førtyning av forflåte blir sammenlignet med offshore fortøyning blir utført. De nyeste reguleringene til oppdrett blir presentert.

To ofte brukte metoder for fortøyningsanalyse ble funnet å være *koblet* og *ukoblet* analyse. Hvilken av disse som skal brukes i forskjellige scenarioer blir ikke presisert i NS9415. En sammenligning av disse to analysemetodene ble utført. For å legge til rette for en slik sammenligning ble det topp moderne analyseprogrammet SIMA, utviklet av SINTEF, brukt. To identiske modeller, hvor eneste forskjell var at den ene var koblet og den andre ukoblet, ble lagd. Spesifikasjonene til disse modellene ble gitt av ScaleAQ, som hadde utført modelltester på et identisk oppsett. Flere analyser med forskjellige miljølaster ble utført, laster som samsvarte med modelltestene til ScaleAQ, for å legge til rette for verifisering av SIMA-modellene. Fra de numeriske analysene i SIMA ble fartøysrespons og linestrekk fra den mest og minst utsatte lina hentet ut og post-prosessert. Resultatene fra den koblede og ukoblede analysen ble deretter sammenlignet.

Det ble funnet at den koblede modellen greide å forutsi fartøysrespons og linestrekk bra. På den andre siden så over-estimerte den ukoblede modellen både fartøysrespons og linestrekk i stor grad. Basert på de filtrerte respons spektrumene ble det konkludert med at de store utslagene ble forårsaket av eksiterte egenmoder (spesielt i yaw), grunnet mangel på demping fra fortøyningslinene. Selv om de ukoblede analysene gikk 20 ganger raskere enn de koblede, så er resultatene for unøyaktig til å være brukbare. Det ble foreslått å legge til manuell demping i den ukoblede modellen for å forbedre resultatene, og at dette kunne være gjenstand for fremtidig arbeid. I tillegg kunne ikke numeriske feil i den ukoblede modellen avvises, og fremtidig arbeid kan derfor være å utforske dette.

En studie av et spesifikt krav i NS9415, som omhandler bruk av regulære bølger istedenfor irregulære, ble også utført. Det ble oppdaget av dette kravet førte til un-

dervurdering av maks respons, og overvurdering av gjennomsnittlig respons. Dette betyr at kravet ikke er konservativt i henhold til ULS design, og burde derfor ikke brukes for slike konstruksjoner. Det må nevnes at en merknad i standarden sier, at der hvor saktevarierende andreordens krefter dominerer, så burde irregulære bølger tas hensyn til.

Acknowledgements

I would like to thank my supervisor, Professor Pål Lader, for his valuable guidance and discussions throughout this project. His knowledge of the aquaculture industry and its challenges aided in the final shape of this thesis. The enthusiasm he has displayed in my work has contributed a lot to my own motivation and enthusiasm.

I would also like to express gratitude to ScaleAQ, especially co-supervisor Martin Søreide, CTO in ScaleAQ. Martin introduced me to this topic, and explained how this research would be helpful for the aquaculture industry. Kasper Wåsjø, ScaleAQ mooring department manager, also deserves thanks for assisting with technical mooring insight.

For the introduction into risk assessment, i want to thank Professor Stein Haugen.
For the digital introductory course in SIMA modelling, i would like to thank Marit I. Kvittem, scientist at SINTEF Ocean.
For invaluable guidance and aid in SIMA, senior researcher in SINTEF, Gro S. Baarholm and PhD candidate Irene R. Arreba deserves gratitude.
For aid in finding relevant theory and for professional discussions, Adjunct Professor Kjell Larsen deserves acknowledgement.
For access to SINTEF Exposed project hydrodynamic data, i would like to thank senior consultant in SINTEF, Ørjan Selvik.

Table of Contents

List of Figures

List of Tables

Acronyms

ALS Accidental limit state. 43, 45, 46

CDF Cumulative distribution function. xi, 25, 26, 28

COG Center of gravity. 36, 55

DAF Dynamic amplification factor. 45

DOF Degree of freedom. 39

FEM Finite element method. 63, 64, 67

FFT Fast Fourier transform. 63

FLS Fatigue limit state. 43, 45, 46, 82, 100, 102

FPSO Floating, production, storage and offloading vessel. xi, 7–9

FSO Floating storage and offloading vessel. 51

Hs Significant wave height. 22

HSE Health, safety and environment. 42

JONSWAP Joint north sea wave project. xi, 22, 23

MBL Minimum breaking load. 43

MODU Mobile offshore drilling unit. 9, 10

MOU Mobile offshore unit. 50

MTO Man, technology and organizational. 49

PAL Pioneer adjustable lever. 49

PDF Probability density function. xi, 25, 26, 44

PM Pierson–Moskowitz. xi, 22, 23

PSA Petroleum safety authority. 50, 52–54

RAO Response amplitude operator. 56, 63, 65

SLS Serviceability limit state. 43, 46

TLP Tension leg platform. 6, 7, 32

ULS Ultimate limit state. ii, 42, 43, 46, 82, 100–102

1 Introduction

The introduction will present the motivation behind this thesis and why this research was needed. Previous work by the author will be presented, as well as the thesis' main objectives.

1.1 Motivation

This thesis was formed on the background of concern from both academics and stakeholders in the aquaculture industry, regarding feed barge mooring systems. The aquaculture industry is known for severe accidents, and is the 2nd most risk exposed industry in Norway (Holmen and Thorvaldsen, 2018).

The aquaculture industry in Norway is experiencing a transition from fish farming deep inside calm fjords, to more exposed farming in rougher conditions. This transition is driven by requirements from the government regarding factors such as lice density, fish welfare and pollution. The fjords appear to be filled with conventional fish farming facilities. Therefore, to achieve further growth in the industry, one possible solution is to move the aquaculture outside the fjords. Such a massive transition naturally comes with many challenges, one of which is the topic of this thesis. This being feed barge mooring in exposed conditions. Mooring failure of these structures could result in fish escapes and risk to human life.

More specifically, there exists uncertainty for what risk level the current feed barge mooring design standards allows for, especially considering more exposed aquaculture sites. Analysis of irregular sea is rather new to the industry, and quite important for mooring systems. Therefore, an investigation into different methods of analysis and how varying weather conditions affect the results, is needed to better understand these complex systems.

1.2 Objectives

The main objective of this Master thesis is to investigate the various load components acting on a feed barge mooring system in irregular waves for different state of the art analysis methods. To test various exposed sea states against another to see if important load components change accordingly.

This will be reviewed in light of the newly revised Norwegian aquaculture standard NS9415 (Standard Norway, 2021), to find potential improvements to the standard with risk in mind. Focusing especially on irregular waves.

1.3 Relation to the specialization project

During the fall of 2021, the author of this thesis wrote a project intended as a foundation for this master thesis. The project, titled "*Preliminary investigation*

into theory, risk assessment and analysis of aquaculture feed barge mooring systems" (Grøftrem, 2021), provided insight into various mooring systems, theory regarding both mooring and risk assessment and software applicable to mooring analysis.

This master thesis can be seen as a continuation of this work, therefore some of the material from the project work will be reused. Although most of the material has been revised to some degree, the sections containing reused materials is listed below and will not be referenced further.

- The various existing state of the art mooring systems and concepts in Section 2.
- The literature review from Section 3 to Section 3.8.2.
- Previously performed risk assessments in Section 4.
- The breakdown of analysis software SIMA in Section 5.1.4.

2 Mooring systems

This section will present various mooring systems, and their components. Their characteristics will be discussed in connection with the needs of a feed barge.

2.1 Mooring concepts

There exists many ways of mooring a structure, depending on the specific needs of the structure and the environment it operates. Mooring is usually performed by either connecting the mooring lines directly to the structure, or through a grid mooring system. For feed barges, the direct mooring strategy is used because it is a stand-alone structure.
This section will present various mooring concepts without much technical derivation.

2.1.1 Spread mooring

Often for larger weight and volume structures, spread mooring systems are used. This is because these structures often stand alone without other structures connected, in addition to them being heavy and large and therefore requiring its own mooring system. Examples of such structures are feed barges, offshore aquaculture installations and closed fish pens. The spread mooring system is often made such that you have mooring lines in each *corner* of the vessel, giving adequate stiffness in all horizontal directions, as illustrated in Figure 1. The term *spread mooring* or *catenary mooring*, is regularly used for all mooring systems that relies on geometric stiffness in the mooring lines. The principle difference between these two concepts can be seen in Figure 2, where taut mooring relies on elastic stiffness instead of geometric stiffness. This implies that taut mooring need a different kind of anchor, e.g. a suction anchor, to handle vertical forces. For most spread mooring systems, a combination of geometric and elastic line segments are used to obtain the desired stiffness characteristics. This relation is explained in detail in Section 3.1.4.

As a rule of thumb, a ratio of $\frac{1}{3}$ is used between water depth and mooring horizontal length. This is because there is a trade-off to how much capacity is needed and how stiff the system should be. There must be enough capacity to ensure no vertical forces on the anchor, as some anchors only can take horizontal forces. Simultaneously, the vessel must be kept in place according to the specific requirements of the system.

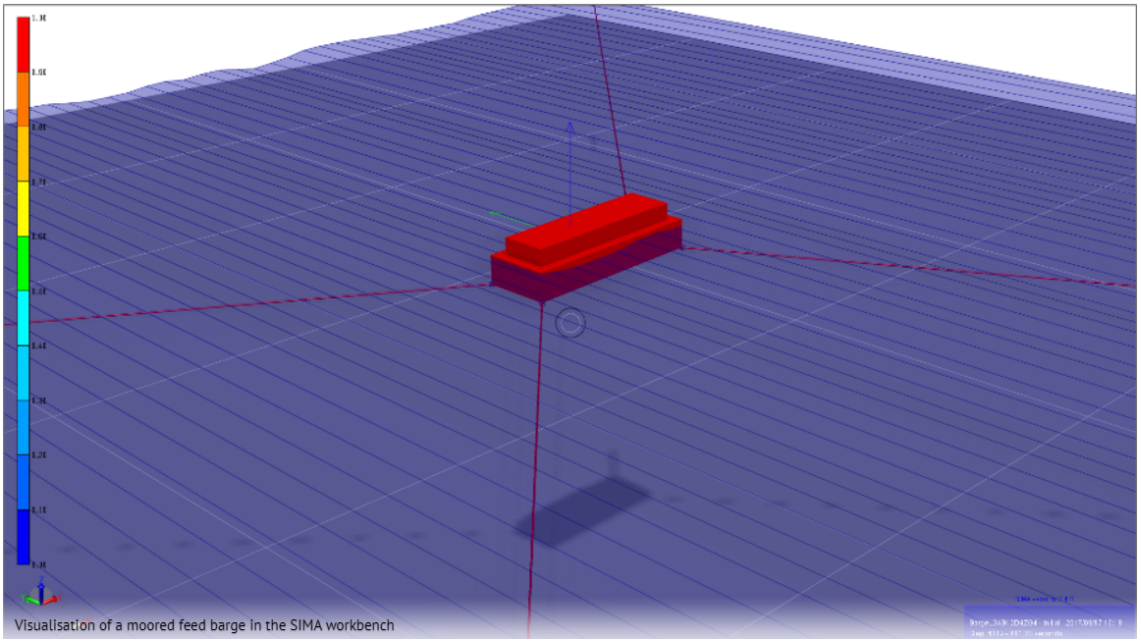

Figure 1: Visualisation of moored feed barge in SIMA workbench (Fon, 2021).

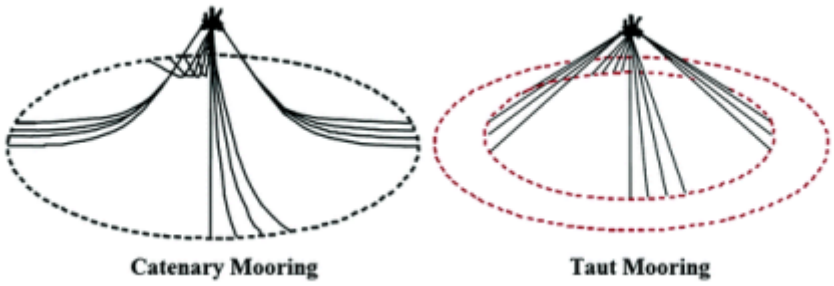

Figure 2: Comparison between catenary and taut mooring concepts (Ikhennicheu et al., 2020).

2.1.2 Hinged steel cages

Typically for square net pens close to shore, hinged steel structures are used. Where the catenary mooring lines are connected directly to the hinged steel elements, as can be seen illustrated in Figure 3. This is a very rigid and *safe* system, in the sense that it is capable of large loads. However, since the elements are rigid, the hinges are particularly vulnerable for high stresses and fatigue. To mitigate this, floating elements, as seen in Figure 3, are attached to the mooring lines to transfer vertical loads from the mooring to horizontal loads on the bridge elements.

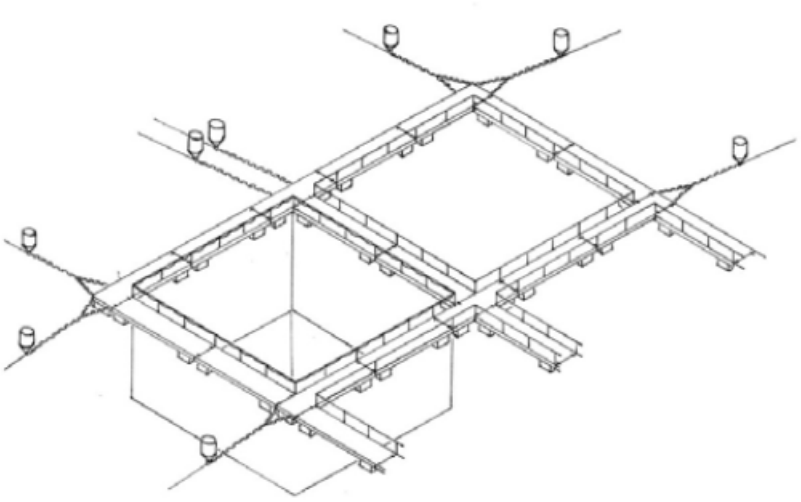

Figure 3: Hinged steel mooring concept (Lader, 2021).

2.1.3 System mooring

For classical floating collar circular net pens, a frame system mooring is commonly used. This consists of a submerged frame system connected to spread catenary mooring lines, allowing service boats to access the net pens. While also allowing simple replacement of nets. This configuration is illustrated in Figure 4. As can be seen in Figure 5, these systems require large seabed areas. Since feed barges are located close to these fish cages, it is important that both the spread system mooring and the feed barge spread mooring does not come into contact, since that could cause mechanical damage to the mooring lines.

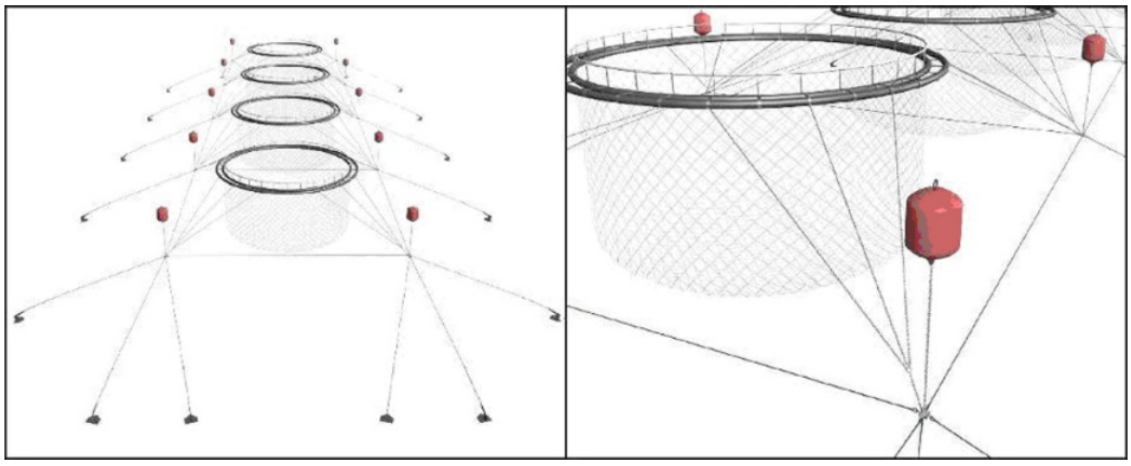

Figure 4: Illustration of system mooring (Lader, 2021).

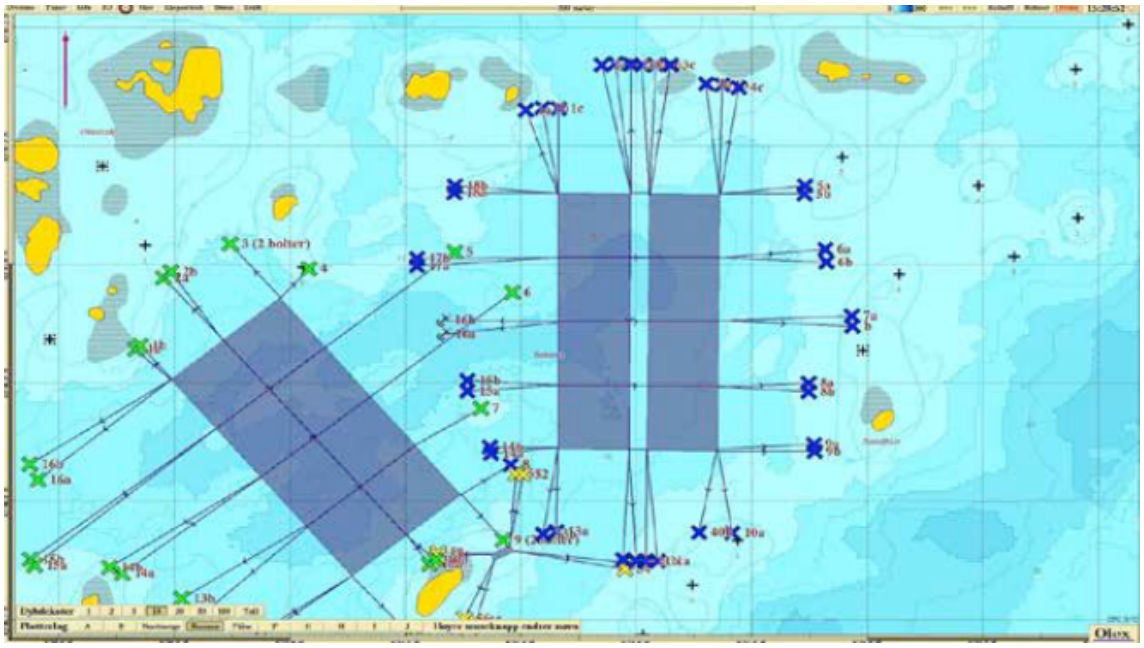

Figure 5: System mooring size illustrated on a map (Lader, 2021).

2.1.4 Tension leg mooring

Sometimes used to moor oil/gas production platforms, is the tension leg mooring system. Quite unlike the spread catenary mooring system where the anchor must experience no vertical forces, the tension leg relies on vertical forces. This of course implies that different anchors must be used, e.g. suction anchors. The tension leg platform is constructed such that the mooring *legs* is under constant tension due to excess buoyancy of the platform. A Tension leg platform (TLP) with components is illustrated in Figure 6. This solution reduces the environmental impact compared to other mooring systems, but has difficult installation and maintenance procedures. This mooring system are never used for feed barges for these reasons, and will therefore not be discussed in further detail in this thesis.

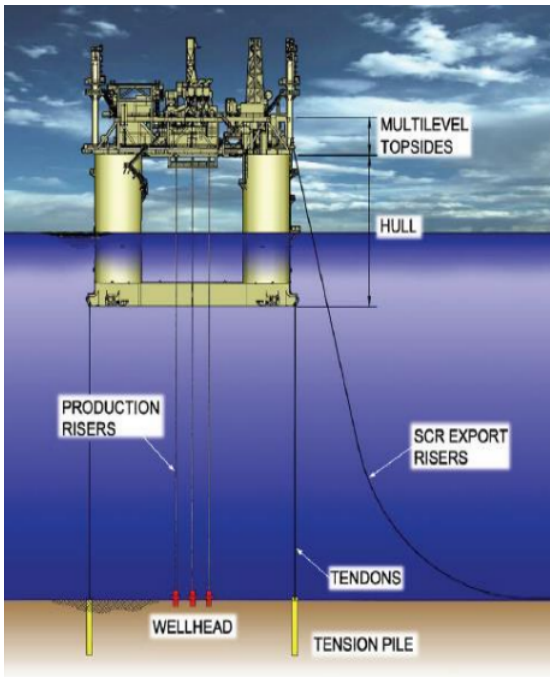

Figure 6: Illustration of tension leg platform components (Energo Engineering, 2018).

2.1.5 Turret mooring

Turret mooring system is made of a turret assembly which is integrated in a vessel and permanently fixed in place by a taut mooring system. The unique part of this mooring concept is the turret system which allows the vessel to rotate around a fixed geostatic point. Specifically useful for floating oil/gas production vessels, that needs to rotate in order to face the sea head on. This concept is quite area demanding in comparison with e.g. the TLP solution, but allows for rotation of the moored vessel which reduces the environmental loads. A turret mooring for a Floating, production, storage and offloading vessel (FPSO) installation is illustrated in Figure 7.

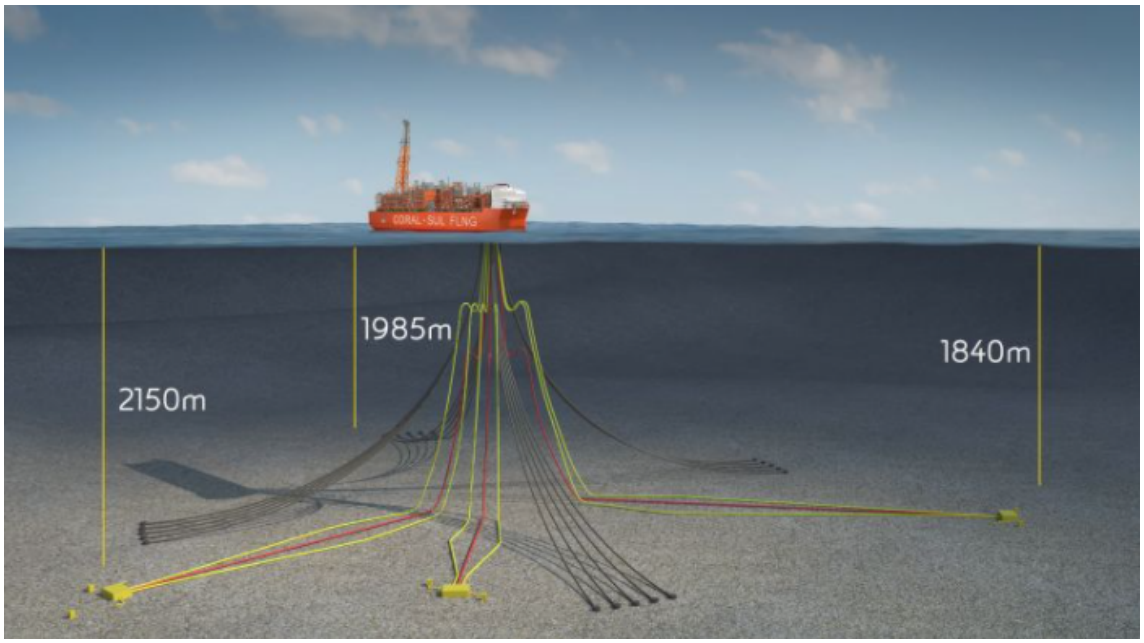

Figure 7: Illustration of turret mooring for a planned FPSO installation (Hydro, 2021).

2.1.6 Single point mooring

Single point mooring is as the name implies, mooring with one line at a single point. Commonly used in smaller leisure vessels and sometimes commercial vessels out at sea. The advantage of this system is that they are simple and has low site impact. There are several reasons why this is not adopted in other applications, mostly because its very area demanding, with no redundancy. Additionally, it is not acceptable to drift around a mooring point for many installations.

2.2 Mooring components

The main components of a mooring system consists of (Chakrabarti, 2005):

- Chain, rope or wire
- Anchors or piles
- Rigging consisting of stoppers, block and/or shackles
- Fairleads, bending shoes or padeyes
- Power supplies

This section will elaborate on some of these components.

2.2.1 Chain

Wire and chain generally make up the line of the mooring system, providing the geometric stiffness.

There are mainly two kinds of chain constructions. The stud link chain (see Figure 8a) is usually used for mooring of Mobile offshore drilling unit (MODU) and FPSOs in shallow water. The studs make the links stable and helps to facilitate laying down the chain while handling. For more permanent mooring, studless chains (see Figure 8b) are used. This is because it reduces weight per unit strength and increases fatigue life (Chakrabarti, 2005).

Chains are made in a variety of sizes and qualities, and the chain properties is important to account for in mooring design. To get a sense of the dimensions used in aquaculture, a table of the chains supplied by ScaleAQ can bee seen in Table 1.

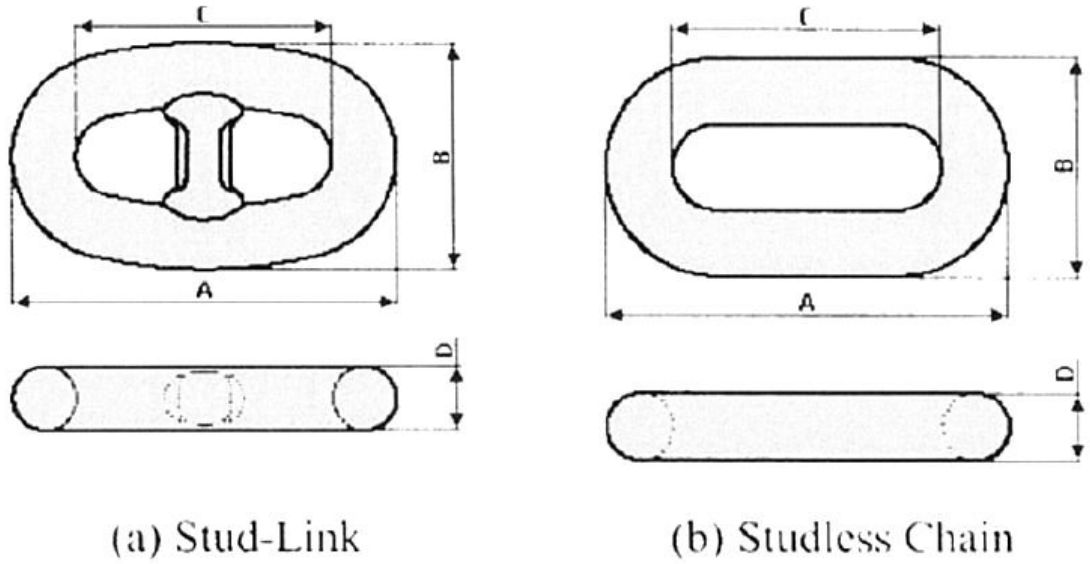

Figure 8: (a) Stud-link and (b) Studless chain (Chakrabarti, 2005).

Table 1: Chains supplied by ScaleAQ (ScaleAQ, 2021a).

Item no.	Description	Dimension (mm)	Fracture strength (t)	Weight per lock (kg)
300344	Anchor chain studless	30	47,6	505
300346	Anchor chain studless	36	68,5	760
301737	Anchor chain studless	40	85,5	935
302123	Anchor chain studless	48	121,9	1351

2.2.2 Wire rope

Wire rope is made from individual wires that are wound in helical patterns, forming *strands*. The pitch of the helix is what determines the axial stiffness and flexibility of the wire.

Wire ropes can either be single stranded or multi stranded. Six-strand wire rope are most commonly used in MODUs and temporary mooring systems for their ease of handling, like the stud-chain. The multi stranded ropes can contain either a fibre or metallic core, which is important for the support of the outer wires and sometimes to absorb shock loading. However, the fiber core option is not much used for heavy marine installations. The common wire strands can be seen in Figure 9.

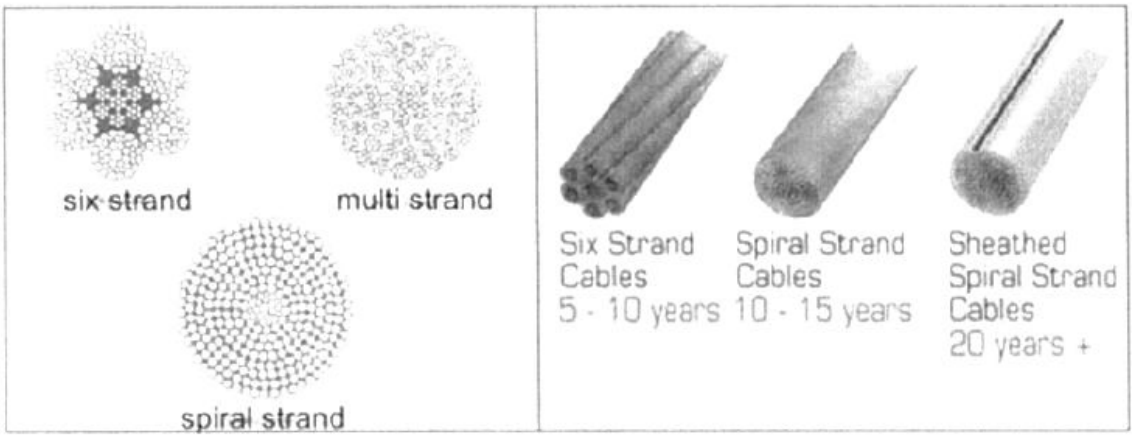

Figure 9: Wire rope constructions (Chakrabarti, 2005).

Single strand ropes are used more commonly in large permanent installations, like stud-less chain. The wire is wound in such a way that creates *torque balancing*, which prevents twisting of the rope under load. Such spiral strands are more resistant to fatigue than multi stranded rope. To ensure long lifetime, corrosion resistance is essential. The chains are either coated in polyurethane, galvanised or protected using zinc anode wires (Chakrabarti, 2005).

2.2.3 Synthetic fiber rope

Synthetic fiber ropes provides stiffness in an alternative way. These ropes are highly elastic with low weight and are therefore often used in taut mooring systems that relies on elastic stiffness. They are sometimes used together with chain or wire to provide beneficial damping effects. Synthetic lines are easy to handle and install, but is more prone to abrasion than chain (Bjørkøy, 2017).

2.2.4 Connectors

Connectors are used to connect the different mooring components. Essential for these connectors is safe and reliable connections that abide by the technical requirements given in the regulations. The connectors has to be designed to withstand the full breaking load of the chain or wire its connecting (Chakrabarti, 2005).

Shackles
Shackles are used to connect chain or rope segments to each other and also to connect the anchor chain to the anchor. A shackle is made up of a bow that is closed with a

pin. NS9415 requires that shackles are secured with two pins and that they are made of corrosion resistant material (Bjørkøy, 2017; Standard Norway, 2021). An example of such a doubly secured corrosion resistant shackle can be seen in Figure 10a.

Mooring plate
The mooring plate is the connector between many of the system mooring components like the mooring frame, lines, bridles and buoys. Therefore this part is essential for ensuring safe position keeping of the entire net pen installation. Like other connectors, NS9415 demands that it should be designed such that the lines connected to it experience yielding first (Standard Norway, 2021). This is because one anchor line failure is far less critical than a mooring plate failure. An example of a mooring plate can bee seen in Figure 10b.

(a) Shackle

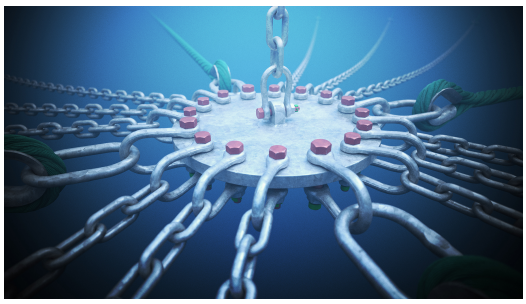

(b) Mooring plate

Figure 10: Common connectors in aquaculture mooring systems (ScaleAQ, 2021e,f).

2.2.5 Seabed attachment

Seabed attachment equipment has a sole function of transferring loads from the mooring system to the seabed. What kind of bottom attachment is used typically depend on what kind of seabed the relevant location has. For rock bottoms, rock pins are used and for sand/mud bottoms, anchors are used.

Rock pins
Rock pins are, simply put, steel cylinders that can penetrate rock. Typically, two types are used for anchoring: the T-pin and eye-pin. T-pins are have a T shape at the top, which allows shackles to be connected to the bolt stem. While eye-pins have a hole in the top where shackles then can be connected through. It is piled into the rocks by a piling hammer or a vibrator, it is then fastened by use of grout or by expanding the bottom part of the pin. An example of such a T-pin can be seen in Figure 11b.

Anchors
The holding power of an anchor must be sufficient to sustain the design load. What kind of anchor to be used and its size, will be affected by the geological conditions of the site and the weight of the installation.

For fish farm applications, fluke anchors are often used. They have a high holding

capacity to weight ratio, since they dig deep and displace large soil volumes. An example of such an anchor can be seen in Figure 11a.

(a) Fluke anchor

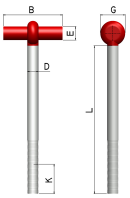

(b) T-type rock pin

Figure 11: Common anchoring concept (ScaleAQ, 2021b,c)

2.2.6 Fairleads

Fairlead is a piece of equipment which guides chain or rope around an object or to stop it from moving laterally. It can be both hooks, or simply a reinforced hole in the hull of a ship, as can be seen in Figure 12

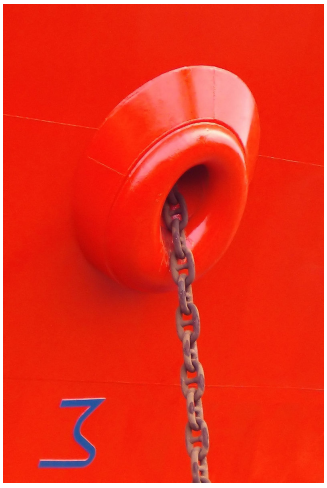

(a) Hole-type fairlead (Wikipedia, 2021).

(b) Hook-type fairlead (Pike, 2021).

Figure 12: Common fairlead types.

Padeye

There is another type of fairlead that can be used to either guide a line or function as an attachment point. This is called a padeye, and can resemble a shackle. The main difference between them is that the padeye is bolted to a fixed location, and not used to attach line segments. A typical padeye can be seen in Figure 13.

Figure 13: A typical illustration of a padeye (eSubsea, 2021).

3 Literature review

Essential to solving any problem, is thoroughly understanding the physics behind it. Including theories that explains the physics. In this chapter, theory regarding hydrodynamic load, responses and catenary lines are presented. This will give a basis for fundamentally understanding the behaviour of a mooring system.

3.1 Catenary lines

Mooring lines are generally expressed through the Catenary equations. These are equations describing a line that hangs in between two fixed points.

From Figure 14, the static equilibrium equations for a Catenary line in water can be established (Faltinsen, 1990).

$$dT' = \left[w \cdot sin\varphi - F\left(1 + \frac{T'}{EA}\right)\right] ds \tag{1}$$

$$T' = \left[w \cdot cos\varphi + D\left(1 + \frac{T'}{EA}\right)\right] ds \tag{2}$$

Where $T' = T - \rho g A z$, corrected for buoyancy because w is the weight per unit length of cable in water.

Both Equation 1 and Equation 2 are non-linear and generally hard to solve for an explicit solution. However, for most normal mooring line components, the line tension is lower than the line's axial stiffness. Therefore, one can assume $\frac{T}{EA} << 1$, and therefore neglect this term in equation (1) and (2). Which allows an analytical solution (K. Larsen, 2018). In other words, this solution gives only the geometric stiffness of the mooring line, while neglecting the elastic stiffness.

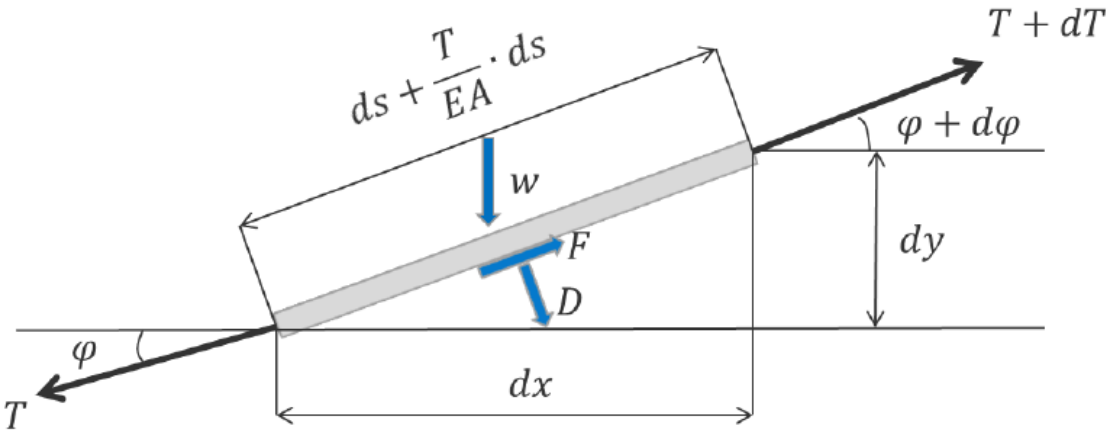

Figure 14: Sketch of forces acting on a two-dimensional mooring line from K. Larsen, 2018

Where

- T = Line tension [N]
- w = Weight per unit length of cable in water [N/m]
- φ = Angle of line relative to the seabed (or x-axis) [rad]
- F = External force on the line in tangential direction
- D = External force on the line in horizontal direction
- E = Young's modulus of the specific line
- A = Cross section area of line
- s = Length of line

3.1.1 Stiff catenary lines

By using the equations presented in the previous section, equations to describe the stiff mooring system can be established. Following the procedure given in K. Larsen, 2018, neglecting stiffness gives:

$$dT' = [w \cdot sin\varphi - F]\, ds \tag{3}$$

$$T' = [w \cdot cos\varphi + D]\, ds \tag{4}$$

Then define:

$$P = w \cdot sin\varphi - F$$

$$Q = w \cdot cos\varphi + D$$

And divide Equation 3 by Equation 4, we get:

$$\frac{dT'}{T'} = \frac{P(\varphi)}{Q(\varphi)} d\varphi \tag{5}$$

By integration gives

$$T'(\varphi) = T_0 \cdot exp\left[\int_{\varphi_o}^{\varphi} \frac{P(\beta)}{Q(\beta)} d\beta\right] \tag{6}$$

The line length (s), horisontal and vertical position (x,y), is then found by integrating these relations:

$$ds = \frac{T'(\varphi)}{Q(\varphi)} d\varphi$$

$$dx = cos\varphi \cdot ds$$

$$dy = sin\varphi \cdot ds$$

These integrals are simplified if the current loads are neglected (F=D=0). After some calculation the follow expressions for the inelastic cable in still water remain:

$$s = \frac{T'_x}{w} \cdot sinh\left(\frac{w \cdot x}{T'_x}\right) \tag{7}$$

$$y = \frac{T'_x}{w} \cdot \left[cosh\frac{w \cdot x}{T'_x} - 1\right] \tag{8}$$

$$tan\varphi = \frac{s \cdot w}{T'_x} \tag{9}$$

$$x = \frac{T'_x}{w} \cdot ln\left[1 + \frac{y \cdot w}{T'_x} + \sqrt{\left(1 + \frac{y \cdot w}{T'_x}\right)^2 - 1}\right] \tag{10}$$

The notations given in these equations are illustrated in Figure 15.

By combining the above equations, the equation for the line characteristics can be derived (Equation 11). This equation gives a relation between the vessel offset and the horizontal force for a catenary line with given weight and water depth:

$$X_l = l + \frac{T'_x}{w} \cdot cosh^{-1}\left(1 + \frac{w \cdot y}{T'_x}\right) - \sqrt{y \cdot \left(y + \frac{2T'_x}{w}\right)} \tag{11}$$

3.1.2 Elastic catenary lines

There are situations where the elasticity of the mooring lines has to be accounted for. High tension levels in the mooring lines, long lines and/or synthetic line segments are all factors that make elasticity increasingly important. Including the elastic stiffness in the catenary equation makes an analytical solution generally impossible, it is therefore suggested to use a numeric approach. As suggested in K. Larsen, 2018, we know that the horizontal line tension is given by

$$T_y = w \cdot s \tag{12}$$

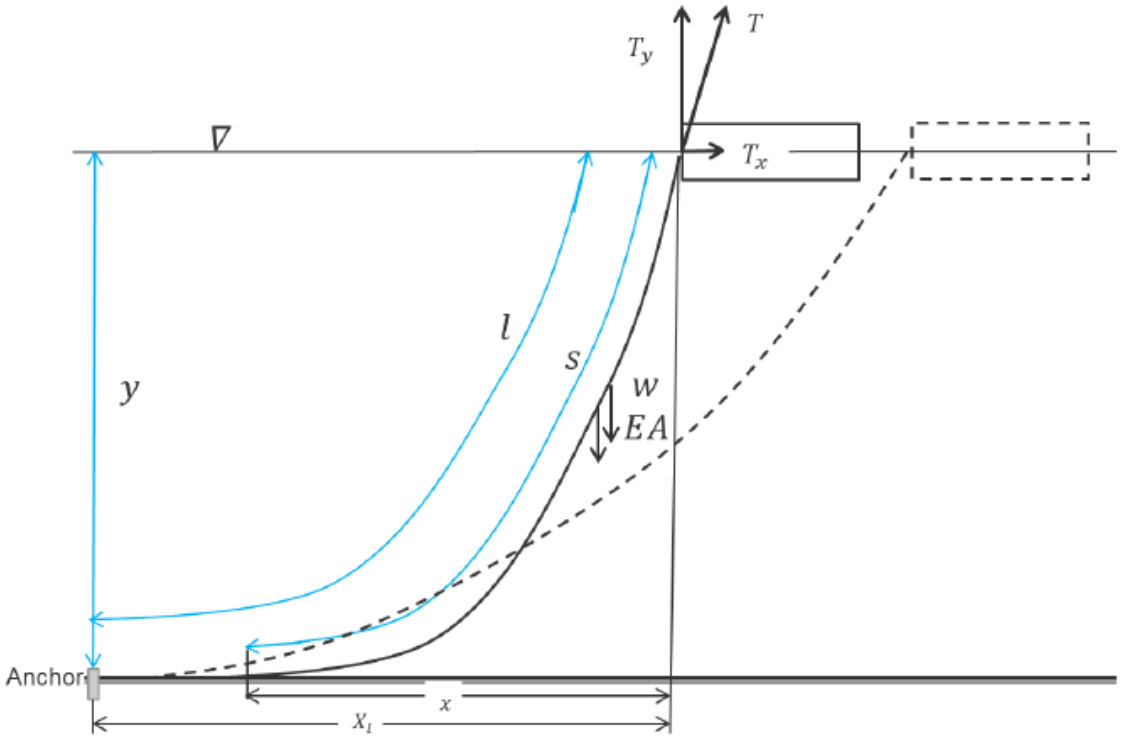

Figure 15: Illustration of the notations defining the line characteristics, as presented in K. Larsen, 2018.

And we can show that

$$T_x = \frac{T_y^2 - \left(w \cdot y - \frac{T_y^2}{2 \cdot EA}\right)^2}{2 \cdot \left(w \cdot y - \frac{T_y^2}{2 \cdot EA}\right)} \tag{13}$$

And then

$$x = \frac{T_x}{w} \cdot sinh^{-1}\left(\frac{T_y}{T_x}\right) + \frac{T_x \cdot T_y}{w \cdot EA} \tag{14}$$

With equation 12, 13 and 14, the following procedure is proposed by K. Larsen, 2018:

1. The following must be known, water depth y, weight w, elastic stiffness EA and the initial length l_0
2. Then a value for the vertical tension $T_y > w \cdot y$ has to be assumed
3. Equation 13 and Equation 14 can then be used to calculate T_x and x
4. The line characteristics can then be calculated for this step by $X_l = (l_0 - \frac{T_y}{w}) \cdot (1 + \frac{T_H}{EA} + x)$, which then gives a coordinate for the line characteristics (X_l, T_x).

5. To get the next step in the iteration, T_y should be increased, and the procedure should be repeated from step 3.

3.1.3 Polymer/fiber catenary lines

Another method of iteration can be used if one assume no weight ($w \approx 0$). This can be useful for initial design of taut mooring systems with synthetic lines.

The procedure goes as follows:

1. The following must be known, water depth y, elastic stiffness EA, and a stretched length l_0 that corresponds to a known pretension force T_0. With this the initial top angle φ_0 and horizontal distance to anchor can be calculated using simple trigonometry.
2. The horizontal distance from the top point of the mooring to the anchor should be increased an increment $dx = dx + \Delta x$
3. New top angle $\varphi = tan^{-1}\frac{y}{x_0+dx}$
4. Increment of line length $dl = cos\varphi \cdot dx$
5. Line tension $T = T_0 + \frac{EA}{l_0} \cdot dl$
6. Horizontal component of line tension $T_H = T \cdot cos\varphi$. This gives a coordinate to the line characteristics (x_0+dx, T_H). To get the next coordinate, the procedure should be repeated from step 2.

3.1.4 Comparison between catenary types

In order to get a sense of how these different ways of modelling a catenary line would work, a simple Matlab script was made. This script can be found with all values included in appendix D. The geometric lines with and without stiffness included was calculated for a total line length of 2000m, with a water depth of 200m. While the taut mooring line was approximately 2000m with 200m depth, where the other values where made to give roughly the same stiffness as the geometric lines.

From Figure 16, we can see that there is small differences in line tension and offset from geometric lines with and without elasticity included (elasticity of steel was used). In the first section with low tension, the stiffness of the geometric mooring line may appear slightly linear, before curving drastically for higher tensions. The picture is quite different for the elastic line with no geometric stiffness, which has a linear behaviour for the entire curve.

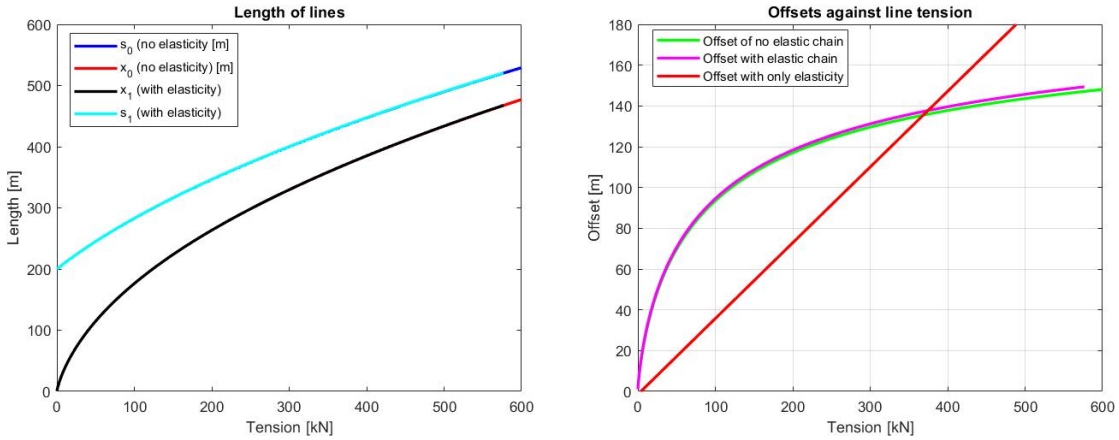

(a) Comparison between geometric lines with and without elasticity. Where s and x is the actual length of active line and horizontal length of active line, respectively.

(b) Comparison between geometric lines with and without elasticity, and a line with only elastic stiffness (taut). Offset and tension are both horizontal components.

Figure 16: Plots from Matlab code comparing catenary lines, code given in appendix D.

3.2 Wave theory

In order to analyse the forces that acts on a feed barge, good understanding of the underlying theory and its assumptions is important. This chapter will present this theory briefly while focusing on the assumptions made.

3.2.1 Potential flow theory

Potential flow theory is the foundation on which the hydrodynamic load analysis is largely built. Good sources exist on this topic, and I will therefore only point out the assumptions that are made, and how this translates to wave modelling. Faltinsen, 1990 provides a good walk through of potential flow theory.

Potential flow theory describes how water particles moves in water. Ultimately giving a potential function which describes the velocity field as a gradient of scalar functions. The following is assumed to make this possible:

1. Irrotational flow and incompressible fluid gives the Laplace equation ($\nabla^2\varphi = 0$)
2. Kinematic bottom boundary condition states that there can be no flow through the seabed. ($\frac{\partial\varphi}{\partial z}|_{z=-d} = 0$)
3. The flow cannot permeate through the surface of a body.
4. Two free surface boundary conditions.
    - The kinematic free surface boundary condition says that a water particle located at the free surface will remain there. ($\frac{\partial\varphi}{\partial z}|_{z=0} = \frac{\partial\zeta}{\partial t}$)

- The dynamic free surface boundary condition says that the pressure at the free surface is constant and equal to the atmospheric pressure. ($\zeta = -\frac{1}{g}\frac{\partial \varphi}{\partial t}|_{z=0}$)

Where,

- φ is the potential function which describes the velocity field as a gradient of scalar functions.
- z is the water depth, where 0 is at the free surface and -h is a the seabed.
- t is the time.
- ∇^2 is the Laplace operator.

3.2.2 Linear wave theory

Based on linear potential flow theory, linear wave theory can be established to describe the propagation of waves. This is done by linearization of the boundary conditions presented in Section 3.2.1. This procedure is given in e.g. Newman, 1977. The regular wave profiles derived have sinusoidal shape, which is not entirely accurate. Real waves have higher crests than troughs. However, for some assumptions the regular waves are quite accurate. These are:

- Wave amplitude has to be small compared to the wave length.
- The object has to stay still.
- The body moves in the same order as the wave amplitude.

For deep water ($d > \frac{\lambda}{2}$) we have the following equation for the wave profile:

$$\zeta = \zeta_0 sin(\omega t - kx) \tag{15}$$

Where,

- ζ is the wave elevation of the free surface from the middle value.
- ζ_0 is the wave amplitude.
- ω is the wave frequency.
- k is the wave number, given by $k = \frac{2\pi}{\lambda}$ where λ is the wave length.

3.3 Irregular waves

While regular waves, as represented in Equation 15, is fine for studying effects of singular propagating waves, it does not accurately represent real sea behaviour. Real sea conditions is chaotic and unpredictable and is often modelled in a stochastic manner.

3.3.1 Modelling of irregular waves

To model a wave surface as a stochastic field, some assumptions has to be made. The wave field is assumed *stationary* in time and homogeneous in space, giving a constant standard deviation and mean value across time. Although, it is known that weather conditions change with time, and for that reason it is normal to only apply this stationary assumption for time intervals between 20 minutes to 3 hours. Which is often referred to as short-term description of wave fields (C. Larsen et al., 2019).

The wave field has to be assumed *ergodic*. This means that the entire wave process is assumed to be accurately represented by a single time series sample of said process. In practical mathematical terms is means that the expected value and variance for the wave process can be calculated from a single time series (C. Larsen et al., 2019).

The last assumption is that the wave elevation is Gaussian distributed. This implied zero mean value and constant variance. Then, the wave elevation can be represented as a Gaussian random variable.

By applying all of the assumptions above, the wave elevation of a long-crested irregular wave can be modelled by summing an adequate number of regular wave components (Faltinsen, 1990), as such:

$$X(t) = \sum_{i=1}^{N} A_i cos(\omega_i t - k_i x + \varepsilon_i) \tag{16}$$

Where,

- A_i is the wave amplitude
- ω_i is the wave frequency
- k_i is the wave number
- ε_i is a random phase angle

Another, perhaps more practical way of representing irregular sea states, is to use the ocean surface energy per area. This is called a wave energy spectrum, S(ω) (Faltinsen, 1990):

$$\frac{1}{2} A_i^2 = S(w_i)\Delta\omega_i \tag{17}$$

Then, by using Equation 17 into Equation 16, an equation for representing irregular sea elevation dependant on the wave spectrum is acquired:

$$X(t) = \sum_{i=1}^{N} \sqrt{2S(\omega_i)\Delta\omega_i} cos(\omega_i t + \varepsilon_i) \tag{18}$$

3.3.2 Pierson-Moskowitz Spectrum

There are several types of wave spectrum. Which one is best suited depends on the studies frequency range, the integrability of the spectrum and how many parameters the spectrum has (C. Larsen et al., 2019).

The most basic of wave spectrum, is the Pierson–Moskowitz (PM) spectrum, and is given on the following form:

$$S(\omega) = \frac{A}{\omega^5} exp\left(-\frac{B}{\omega^4}\right) \tag{19}$$

Where A and B are constants that vary depending on application (Haver, 2019). This spectrum is only valid for fully developed sea states and unlimited fetch. They have a steep slope for low frequencies and only one peak. The most used variations of this spectrum is (C. Larsen et al., 2019) :

- The standard PM spectrum is dependant only on the wind speed V. The constants in the formulas for A and B are calculated from North Atlantic data.
- The modified PM spectrum which is based on including the Significant wave height (Hs) parameter in addition to the wind speed V.
- The ISSC spectrum uses the Hs parameter in addition to the mean individual wave frequency $\bar{\omega}$

3.3.3 JONSWAP Spectrum

Another commonly used spectrum is the Joint north sea wave project (JONSWAP) spectrum. This spectrum is based on the PM spectrum, but also accounts for developing sea states. The way this is done, is multiplying the PM spectrum with a *peakedness* factor γ^{α}. The spectrum then becomes:

$$S(\omega) = \frac{\bar{\alpha} g^2}{\omega^5} exp\left(-1.25\frac{\omega_p^4}{\omega^4}\right) \gamma^{\alpha(\omega)} \tag{20}$$

Where,

$$\alpha = exp\left(-\frac{(\omega - \omega_p)^2}{2\sigma^2\omega_p^2}\right) \tag{21}$$

$$\sigma = \begin{cases} \sigma_A = 0.07, & \text{if } \omega \leq \omega_p. \\ \sigma_B = 0.09, & \text{otherwise.} \end{cases} \tag{22}$$

$$\omega_p = 0.87\frac{g}{V} \tag{23}$$

$\bar{\alpha}$ is a parameter that shapes the high frequency area of the spectrum. This can be expressed differently depending on application. For North sea applications, the following expression is used (C. Larsen et al., 2019):

$$\bar{\alpha} = 5.058\frac{H_s^2}{T_p^4}(1 - 0.287 \cdot ln(\gamma)) \tag{24}$$

The *peakedness* factor is dependant on how developed the seastate is, and for $\gamma = 1$ the spectrum reduces to the modified PM spectrum. For a typical north sea storm, a γ value of around 3 is used (C. Larsen et al., 2019).

Generally, the JONSWAP spectrum gives a higher wave spectrum density when compared to the PM spectrum, as shown in Figure 17

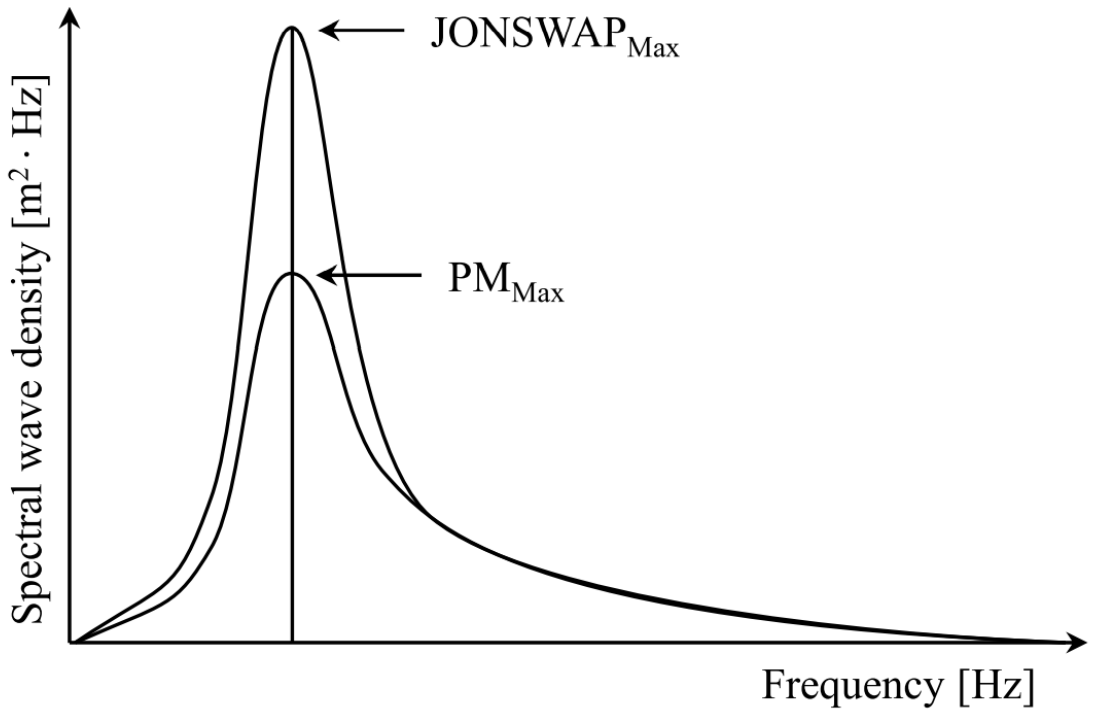

Figure 17: Representative comparison between JONSWAP and PM spectrum (Bruset, 2019)

When performing analysis in the time domain it is important to consider the effect of irregular waves, because it changes erratic over time and has no repeating cycles.

This means that you can have sudden unexpected large wave amplitudes, and unexpected wave frequencies. For this, wave spectra is a good way of representing sea states. A summary of the spectra presented in this section can be seen in Table 2, here the wind speed V is transformed into peak frequency using Equation 23 for better comparison between formulas.

Table 2: Summary of common wave spectrum, their parameters and equations.

Spectrum	**Parameters**	**Equation**
Standard PM	ω_p	$S(\omega) = \frac{\alpha g^2}{\omega^5} exp\left(-1.25\frac{\omega_p^4}{\omega^4}\right)$
Modified PM	H_s, ω_p	$S(\omega) = 0.3125 H_s \frac{\omega_p^5}{\omega^5} exp\left(-1.25\frac{\omega_p^4}{\omega^4}\right)$
ISSC	$H_s, \bar{\omega}$	$S(\omega) = 0.1107 H_s \frac{\bar{\omega}^4}{\omega^5} exp\left(-0.4427\frac{\bar{\omega}^4}{\omega^4}\right)$
JONSWAP	$H_s, \gamma, \omega_p, \omega$	$S(\omega) = \frac{\bar{\alpha} g^2}{\omega^5} exp\left(-1.25\frac{\omega_p^4}{\omega^4}\right) \gamma^{\alpha(\omega)}$

3.4 Stochastic environment

In order to analyse any structure, the load has to be defined. For the case of floating structures, the weather loads are best described as stochastic of nature, and should therefore be modelled as such. This chapter will contain some stochastic concepts useful for later analyses.

3.4.1 Response spectrum

Similarly to wave spectrums presented in Section 3.3.1, the energy density of a structures response can be presented dependant on the load frequency. This is called a response spectrum. For each load frequency, the structure will have a linear response dependant on the load amplitude, with equal frequency as the load. A response spectrum S_x can be modelled as a product of the response transfer function H_x and the wave spectrum S_ζ (C. Larsen et al., 2019):

$$S_x(\omega) = H_x^2(\omega) \cdot S_\zeta(\omega) \tag{25}$$

Where the response transfer function H_x is given as:

$$H_x(\omega) = H_M(\omega) \cdot H_H(\omega) \tag{26}$$

Where,

- H_M Is a mechanical transfer function that defines the linear relation between load and response amplitude.

- H_H Is a hydrodynamic transfer function that defines the linear relation between wave amplitude and load amplitude.
- S_ζ Is a wave spectrum, derived in Section 3.3.

The response spectrum is useful to locate peak frequency ω_P and the structure eigenfrequency ω_0, as illustrated in Figure 18.

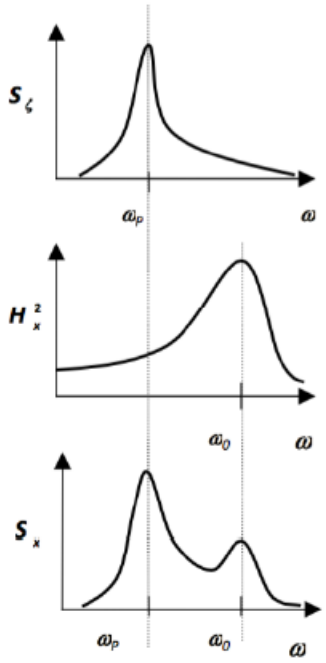

Figure 18: Illustration of response spectrum calculation (C. Larsen et al., 2019).

3.4.2 Short term statistics

A statistical description of either waves or response can be achieved by observing response over a relatively short period of time. However, for design purposes, a description for longer periods of time is useful. These short period descriptions can then be generalized for larger time periods, as will be shown in this section and the next.

The short term distribution is given by a Cumulative distribution function (CDF), which describes the probability of a response value x, being less than a given response X, and is generally expressed as follows:

$$P(X \leq x) = F_X(x) = \int_{-\infty}^{x} f_X(y)dy \tag{27}$$

Where $f_X(x)$ is the Probability density function (PDF) and $F_X(x)$ is the CDF. The PDF is used to describe the probability of a random variable being greater than x. The following relationship is then implied (C. Larsen et al., 2019):

$$f_X(x) = \frac{dF_X(x)}{dx} \tag{28}$$

This relationship is illustrated in Figure 19.

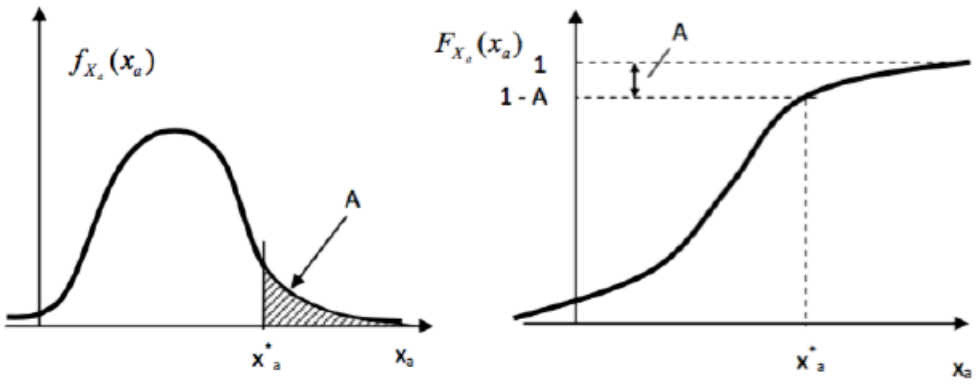

Figure 19: Illustration of a PDF to the left, and a CDF to the right (C. Larsen et al., 2019).

A common distribution used to describe a stochastic process that is Gaussian distributed and has statistically independent individual maximas, is the Rayleigh probability distribution (a special case of the Weibull distribution) (Bjørkøy, 2017):

$$F_X(x) = P(X \leq x) = 1 - exp\left(-\frac{x^2}{2\sigma_x^2}\right) \tag{29}$$

Which, by using Equation 28, corresponds to the following CDF:

$$f_X(x) = P(X > x) = \frac{dF_X(x)}{dx} = \frac{x}{\sigma_x^2} exp\left(-\frac{x^2}{2\sigma_x^2}\right) \tag{30}$$

Where X represents a random maximum response taken from a stationary stochastic process X(t), with variance σ^2.

The Rayleigh distribution has some limitations in addition to the assumptions made. It is only valid for narrow-banded signals, which means that the frequency spectrum needs to be narrow, have no negative maximas and only one maximum between each zero up-crossing. The difference between a narrow banded, and broad banded signal can be seen in Figure 20. For broad banded signals, E.g. the Rice distribution can be used (C. Larsen et al., 2019).

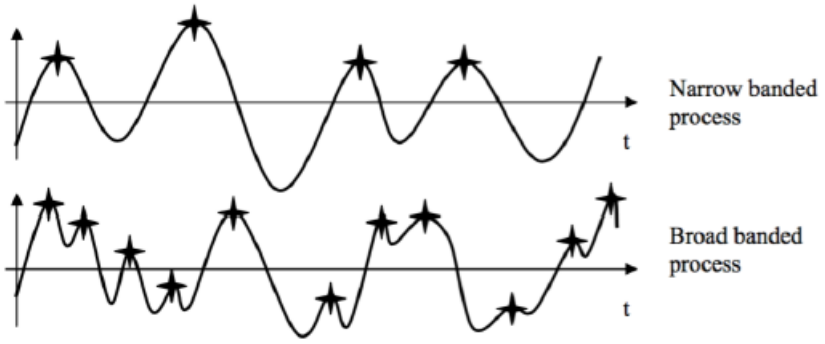

Figure 20: Illustration of narrow and broad-banded signals (C. Larsen et al., 2019).

3.4.3 The extreme value distribution

When designing a marine installation, the extreme value distribution describes the response in storm condition. This distribution can be of interest, since it is based on parameters that describe short term conditions. These parameters are the significant wave height H_s and spectral peak period T_p, as well as the storm duration (C. Larsen et al., 2019).

The extreme value can be described as a stochastic variable since the largest maximum of each individual short term series will vary independently. This extreme value theory is based on having several independent, equally Rayleigh distributed storm samples. Where the extreme value of each sample is found as $X_{max} = max[X_1, X_2, ..., X_N]$. Then, the distribution is given as follows:

$$F_{X_{max}}(x_{max}) = P(X_{max} < x_{max}) = [F_X(x_{max})]^N \tag{31}$$

Where X_{max} is given as the largest response from all the N storm samples. This process from four different storm samples are illustrated in Figure 21.

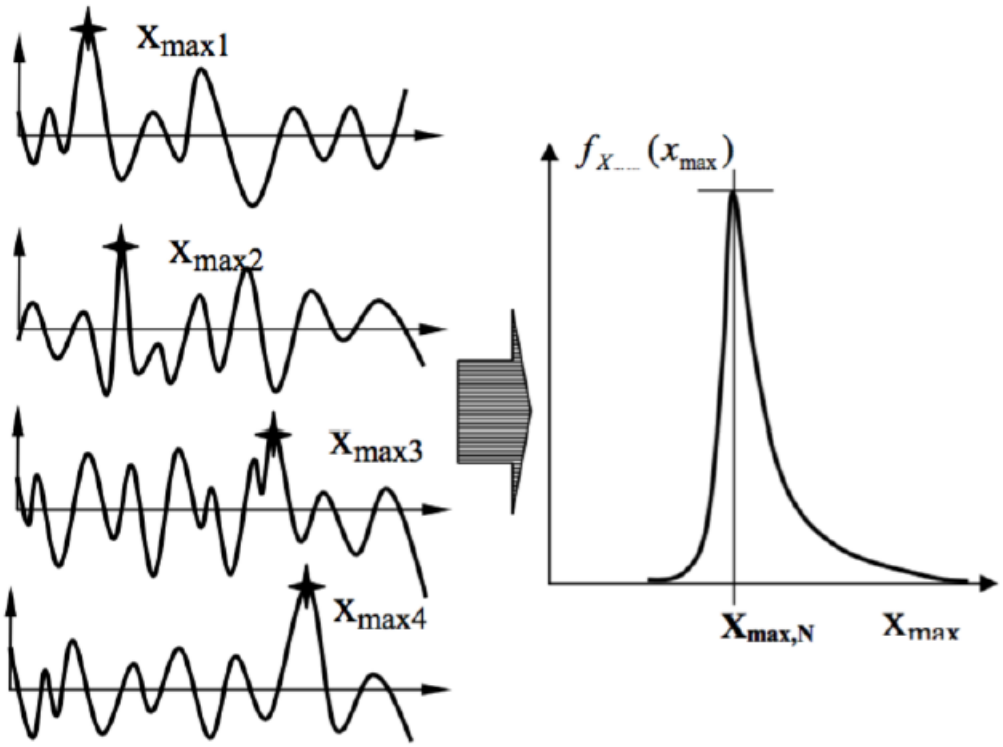

Figure 21: Illustration of storm samples creating an extreme value distribution (C. Larsen et al., 2019).

This extreme value distribution function for 3 hour response is often approximated by the Gumbel distribution, while the type 1 extreme value distribution is used for maximum (Haver, 2019). The Gumbel distribution is given as follows:

$$f_{X_{max}}(x_{max}) = \frac{1}{\beta} exp\left(-\left(\frac{x_{max}-\alpha}{\beta} + exp\left[-\left(\frac{x_{max}-\alpha}{\beta}\right)\right]\right)\right) \tag{32}$$

With the corresponding CDF:

$$F_{X_{max}}(x_{max}) = exp\left(-exp\left[-\left(\frac{x_{max}-\alpha}{\beta}\right)\right]\right) \tag{33}$$

Where α is the *location* parameter, and β is the *scale* parameter of the distribution. The practical meaning of these are represented in Figure 22.

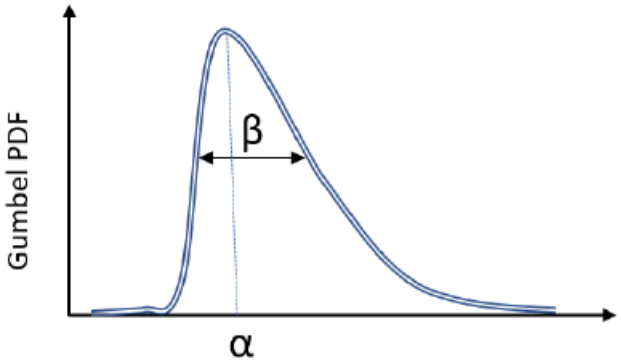

Figure 22: Gumbel distribution parameters illustration (Bjørkøy, 2017).

If one use the same assumptions as for the Rayleigh distribution, the Gumbel parameters can be obtained by the *method of moments*, since the following relations between α, β, mean value μ and standard deviation σ are valid (Haver, 2019):

$$\mu = \alpha + 0.5772\beta \tag{34}$$

$$\sigma_x = \frac{\pi}{\sqrt{6}}\beta \tag{35}$$

Which is then called a fitted Gumbel distribution by the moment method.

For practical application of this distribution in design applications, a quantile of the fitted distribution is often used. The fraction is described by $100(1-\mu)\%$ where μ typically has a value around 0.1. The quantile function of the Gumbel distribution then becomes (Haver, 2019):

$$Q(p) = \alpha - \beta ln(-ln(p)) \tag{36}$$

Where p is the probability given by the parameter μ. E.g. when $\mu = 0.05$, the function is given as:

$$Q(0.95) = \alpha - \beta ln(-ln(0.95)) \tag{37}$$

A comparison between distributions can be seen in Figure 23. **A** represents a normal Gaussian distribution, **B** shows a Rayleigh distribution and **C** represents the extreme value distribution for various number of storm samples N.

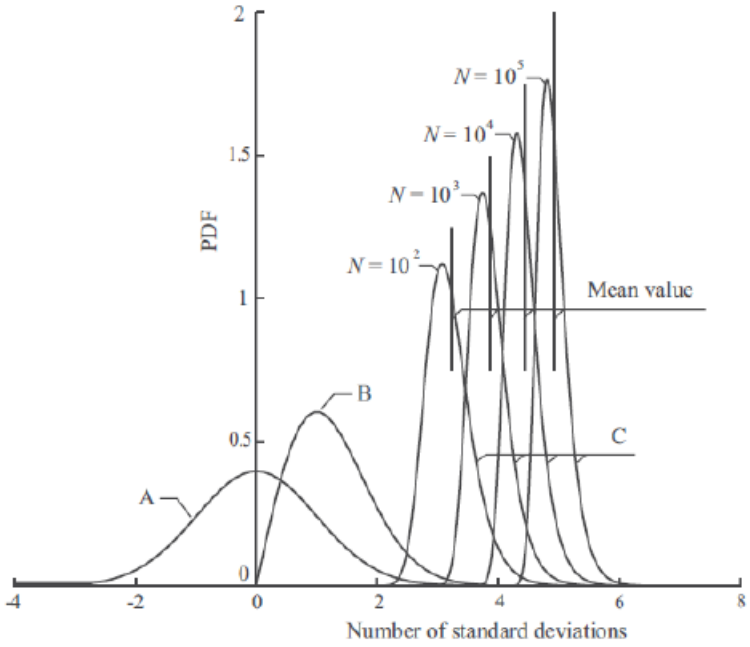

Figure 23: Comparison between statistical distributions (Bjørkøy, 2017).

3.5 Loads on feed barges

The loads acting on a feed barge is dynamic, and has to be understood thoroughly in order to design a safe and reliable mooring system. Feed barges are subjected to wind, waves and current loads, all contributing to different dynamic responses.

It is useful to classify structures in waves as either large- or small-volume structures, in order to predict which wave loads will dominate. For small volume structures, the incident wave will not be affected much by the structure itself. Therefore, the loads can be modelled as if the body is not there. By using this *long wave approximation*, small volume structures can be classifies as either drag or inertia dominated. For large volume structures however, the body will affect the incident wave and therefore experience diffraction loads. Thus, the long wave approximation is not valid (Faltinsen, 1990).

The classification of such structures is not straight forward and is often presented in the case of a cylinder. For a cylinder with diameter D in waves with wave length λ, the following apply. If $\frac{\lambda}{D} > 5$, the structure is classified as small volume. While $\frac{\lambda}{D} < 5$ is considered large volume. These limits serves as guidelines however, as the environmental conditions and the specific case in question could change which loads will be dominating (Pettersen, 2007).

The classification of wave loads can be seen illustrated in Figure 24. As the focus of this thesis is to study feed barges, long wave theory might not be applicable. This is due to feed barges being rather large, with a normal width of $\approx 10 - 20$m, and normally twice the length (ScaleAQ, 2021d).

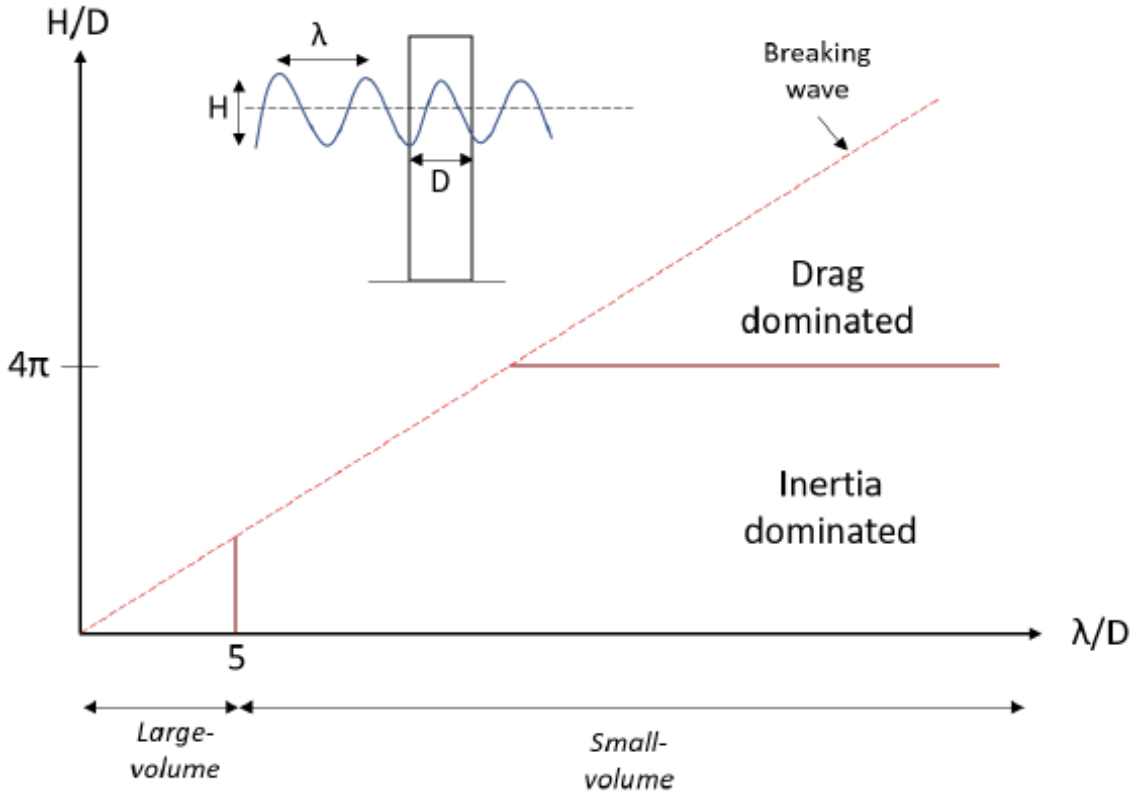

Figure 24: Classification of wave loads for small/large volume structures.

3.5.1 Diffraction forces

For this thesis, the diffraction forces will be highly relevant as barges are generally considered large volume structures (Berstad et al., 2014). Diffraction theory is based on considering the forces that acts on a body in waves when the body is restrained from oscillating. These forces consists of two contributions, the Froude-Krylov and diffraction loads. These are found by integrating the incident wave dynamic pressure and the diffraction dynamic pressure along the mean wetted surface, respectively (Faltinsen, 1990).

The resulting excitation force, F_i, for a given degree of freedom, i, is given in Equation 38.

$$F_i = \underbrace{-\int\int_S pn_i \, ds}_{Froude-Krylov} + \underbrace{A_{i1a1} + A_{i2a2} + A_{i3a3}}_{Diffraction} \tag{38}$$

Where,

- p is the hydrodynamic pressure on the wetted surface
- n_i is the surface normal vector
- A_{ij} is the added mass coefficient

- a_j is the acceleration

3.5.2 Second-order effects

Irregular waves introduces second-order effects that are especially important for moored structures. The forces acting on structures in irregular waves are usually categorized based on their frequency. We have (1) wave-frequency, which consists of oscillating first order forces with wave frequencies. Then there is (2) low-frequency forces, which are second-order forces that are not oscillatory, with low frequency compared to the wave frequency. Lastly there is (3) high-frequency forces, which are second-order of nature. For example can second order sum-frequency loads be important for design of TLPs, since such high frequency loads can cause excitation of *ringing* eigenmodes. However, for the design of moored barges these forces are not that relevant (OrcaFlex, 2021).

It is important to understand how these loads effect the feed barge design. For the (1) wave-frequency loads, the stability and structural integrity of the barge itself is the main concern. The (2) low frequency forces are often small when compared to wave frequency loads, and does not impact stability in the same way. These forces does however cause the barge to drift away from its original position, and the mooring system has to be designed to avoid this. It is important to remember that the spread mooring system is only supposed to keep the vessel stationary and counter the static forces, not the dynamic forces (Lader, 2021).

This means that is it (2) low frequency forces that will be of most importance to this thesis. This is often referred to as *wave drift forces*. When considering regular sea states, as explained in Section 3.2, one can model wave drift forces by use of *Maruo's drift force* or direct pressure integration (Faltinsen, 1990).

Methods for expressing wave drift forces in regular sea
Maruo's drift forces for a 3D body assumes no current and no energy dissipation. Then the following expressions for the wave drift force, F_i, applies.

$$\bar{F}_1 = \frac{\rho g}{4} \int_0^{2\pi} A^2(\theta) \left(cos(\beta) - cos(\theta)\right) d\theta \tag{39}$$

$$\bar{F}_2 = \frac{\rho g}{4} \int_0^{2\pi} A^2(\theta) \left(sin(\beta) - cos(\theta)\right) d\theta \tag{40}$$

Alternatively, one can use direct pressure integration. This method is derived from the Bernoulli equation and can yield all three forces and three moments. However, one has to take care when making assumptions regarding the velocity potential to avoid bad results. After some derivation and making the assumption of small wavelengths, the drift force and moments, F_i, is given by:

$$\bar{F}_i = \frac{\rho g \zeta_a^2}{2} \int_{L_1} sin^2(\theta + \beta) \eta_i dL \tag{41}$$

For further derivation of these methods, see Faltinsen, 1990.

Where,

- ρ is the water density
- g is the gravitational constant
- $A^2(\theta)$ is derived from the sum of radial and diffraction wave amplitudes generated by the body far away
- β is the wave propagation angle relative to the x-axis
- θ is defined as $x = rcos(\theta)$
- ζ_a^2 is the wave amplitude squared
- L_1 is the length of each element
- η_i is the normal vectors
- i represents the 6 degrees of freedom

Methods for expressing wave drift in irregular sea
As explained in Section 3.3, real sea conditions are not adequately modelled by regular sea. One must consider irregular sea to get real life conditions. This is done by superimposing the results from mean wave loads in regular sea (Faltinsen, 1990).

From the direct pressure integration method presented above, summation gives:

$$\bar{F}_i^s = \sum_{i=1}^{N} \left(\frac{\bar{F}_i(\omega_j, \beta)}{\zeta_a^2} \right) A_j^2 \tag{42}$$

Which can also be expressed independent of the individual wave amplitude A_j, by using the following relation between the individual wave height A, and wave spectrum, S:

$$\frac{A_j^2}{2} = S(\omega_j) \frac{\omega_{max} - \omega_{min}}{N} \tag{43}$$

which then gives:

$$\bar{F}_i^s = 2 \int_0^\infty S(\omega) \left(\frac{\bar{F}_i(\omega; \beta)}{\zeta_a^2} \right) d\omega \tag{44}$$

These expressions will give wave drift forces more accurate to real life conditions when compared to the regular sea expressions. It should be noted that it is important to remember which assumptions has been made through these examples, and if they

are applicable for relevant scenarios. For further derivation and explanation, see Faltinsen, 1990.

Where,

- ω_j is the individual wave frequency
- A_j is the individual wave height
- $S(\omega)$ is the wave spectrum defined by Equation 43
- N is a number of sub-intervals

3.6 Complete moored system damping

As explained in section 3.5.2, the relevant loads on a feed barge are first order wave frequency forces, and second order drift forces. Specifically motions in the horizontal plane caused by drift forces are important for the mooring system, since they can cause high line loads. The frequency of the drift forces might correspond to the vessels natural frequency. Therefore, it is essential to quantify the level of damping for the system, since this will determine the resonant response (Chakrabarti, 2005).

The moored vessel will introduce viscous flow damping, due to the relative motion between the hull and fluid where both viscous drag and eddy-making forces contribute. In addition, the vessel introduces wave drift damping, caused by an increase in drift force magnitude when a vessel is going through waves (Pettersen, 2007).

3.6.1 Barge damping

To express damping quantity in a system, the damping ratio ξ, is commonly used. This is the ratio between the damping and the critical damping of the system, as given in Equation 45 (Weiby, 2018).

$$\xi = \frac{B}{B_c} \tag{45}$$

Where the critical damping B_c is given by the restoring stiffness C, and mass M, of the system. This relationship in given in Equation 46 (Weiby, 2018).

$$B_c = 2\sqrt{M4C} \tag{46}$$

From here one can use Equation 47 and Equation 48 to find the natural frequency ω_0, and the damped natural frequency ω_d of the system.

$$\omega_0 = \sqrt{\frac{C}{M+A}} \tag{47}$$

$$\omega_d = \omega_0 \sqrt{1 - \xi^2} \tag{48}$$

Where A is the added mass of the system in water (Pettersen, 2007).

Estimating the damping in roll and pitch is especially important for feed barges, since the natural frequency often lays within the wave-frequency range. The damping contributions consists mainly of frictional and eddy making forces (Pettersen, 2007).

The frictional damping coefficient can be estimated by Equation 49 (Zang, 2017).

$$B_{f0} = \frac{4}{3\pi} \rho S R_e^3 R_0 \omega C_f \tag{49}$$

Where the frictional coefficient C_f is given by

$$C_f = 1.328 \left(\frac{2\pi\nu}{3.22 r_e^2 R_0^2 \omega} \right)^{0.5} \tag{50}$$

If the barge is designed with straight corners, the bilge keel radius r_e can be taken as 1 (Zang, 2017).

For the Eddy making damping, the damping coefficient can be found by Equation 51 (Zang, 2017).

$$B_{e0} = \frac{2}{\pi} \rho L D^4 \left(H_0^2 + 1 - \frac{OG}{D} \right) \left(H_0^2 + \left(1 - \frac{OG}{D} \right)^2 \right) R_0 \omega \tag{51}$$

Where H_0 is given by the following equation

$$H_0 = \frac{B}{2D} \tag{52}$$

The empirical damping can be found as a sum of these frictional and Eddy making damping forces, through interpolation. The formulas above are made for roll, but the procedure is identical for pitch, except that length is switched with breadth and the GM value for the longitudinal direction is used instead of the transverse (Zang, 2017). This method is further derived and explained in Negi and Dhavalikar, 2009, where it is also shown that the method gives good results compared to model tests.

Where,

- R_0 is the roll motion amplitude in radians.
- S is the wetted surface area.
- ν is the kinematic viscosity of sea water.
- B is the width of the barge.

- D is the draft of the barge.
- OG is the difference in draft and COG.
- GM is the metacentric height.

3.6.2 Mooring damping

The mooring system itself also contributes to the total system damping. According to Chakrabarti, 2005, these are the main effects:

1. Hydrodynamic line drag damping
   When the vessel moves horizontally, the mooring line will travel through the water column with higher velocity than the vessel itself, illustrated in Figure 25. The drag force experienced by the mooring line will then give energy dissipation for every cycle of tension. The velocity of the line, and thus the drag damping is dependant on the water depth, line pre-tension and the line weight. According to DNV, 2013, if the drag force is given in a classic Morrison manner, like in Equation 53, then the drag coefficients C_D is given in Table 3.

$$f_d = \frac{1}{2}\rho C_D D v|v| \tag{53}$$

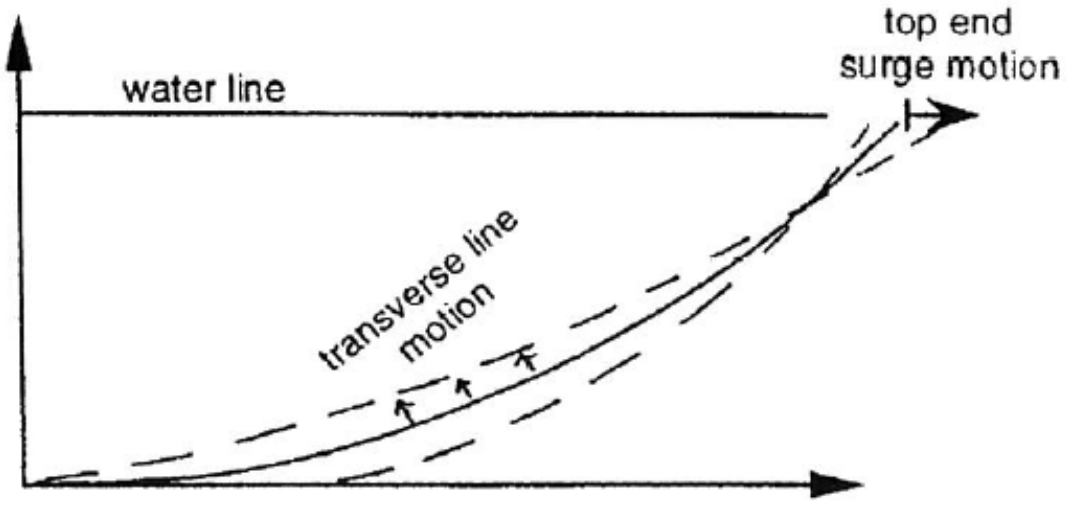

Figure 25: Illustration of line motion caused by vessel translation (Chakrabarti, 2005).

Table 3: Drag coefficients from DNV, 2013.

Mooring component	**Transverse**	**Longitudinal**
Stud chain	2.6	1.4
Stud less chain	1.4	1.15
Stranded rope	1.8	-
Spiral rope without plastic sheathing	1.6	-
Spiral rope with plastic sheathing	1.2	-
Fibre rope	1.6	-

2. Vortex induced vibrations
   Vortex shedding behind the mooring line cause oscillating forces transverse to the flow. The frequency of these forces can excite the line natural frequency, and thus cause large transverse motions. This will cause a significant increase to the drag forces, and thus also damping. This effect occurs on cylinder shaped bodies, and is therefore considered important for wires and negligible for chains.

3. Line internal damping
   Material damping between wires and chain links cause damping. This contribution is often small and therefore negligible. In addition, not much work has been done on this.

4. Seabed interaction
   Friction between the mooring line and the seabed leads to reduced tension fluctuations in the inactive part of the line, thus increasing line stiffness. It has been shown that in-plane effects from seabed interaction can cause significant increase in peak tension values.

According to Matsumoto, 1991, the levels of mooring line damping can be large when compared to vessel damping in some situations. Figure 26 shows a comparison between wave drift, viscous and mooring line damping for a spread catenary mooring of a model tanker in 200m water depth. From this figure the importance of mooring line damping becomes clear.

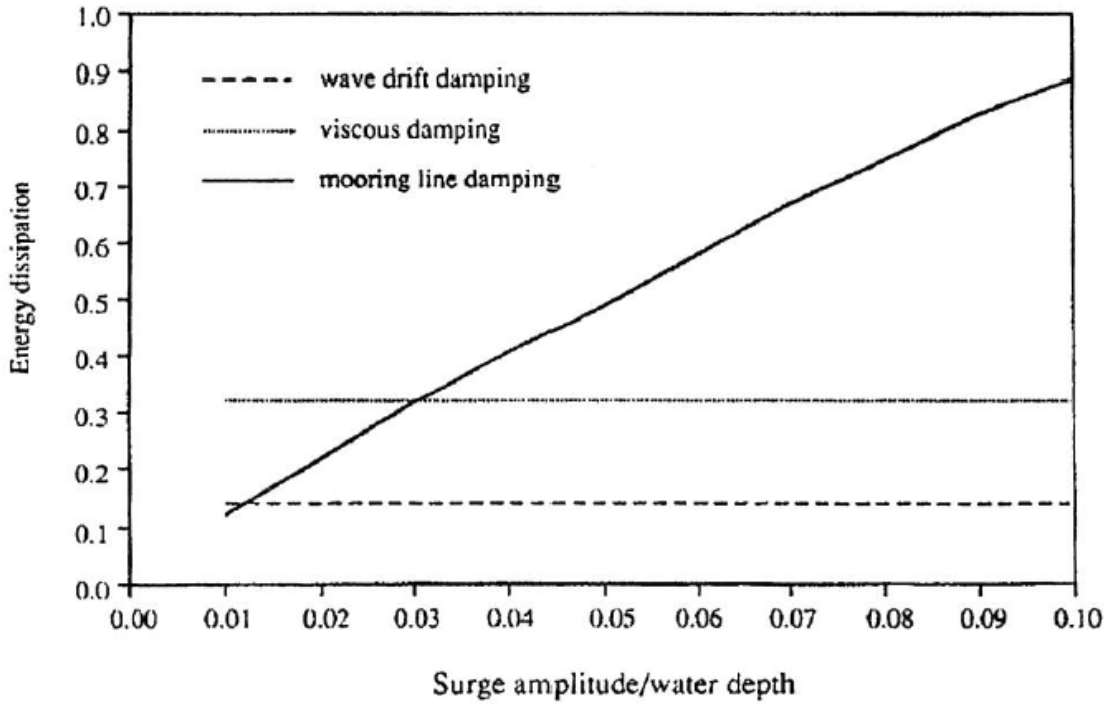

Figure 26: Relative energy dissipation from wave drift, viscous and mooring line damping caused by various surge amplitudes. (Chakrabarti, 2005).

3.7 Mooring system design principles

There are several methods for catenary mooring system design. This section will contain a general description of the most common methods and when they are beneficial to use. The methods should be read in conjunction to certification standards that are applicable, such as NS9415. (Chakrabarti, 2005; Standard Norway, 2021).

3.7.1 Static design

When first considering a mooring concept design, the static design approach can be used. This method uses catenary line theory, presented in Section 3.1. This design principle is based on finding static equilibrium for the system. Looking at the forces acting in horizontal direction, one can calculate the mean wave drift force for the roughest design sea state, as shown in Section 3.5.2. Then, equilibrium considerations can be applied to find the horizontal force that each catenary mooring line has to endure. From here, it is a matter of using the catenary equations, presented in Section 3.1, to find the line characteristics. The result from such analyses are often presented in a diagram like Figure 27. Where the static load components are applied to the vertical axis, and vessel displacement on the horizontal axis. The dynamic offset can then be approximated by empirical formulas.

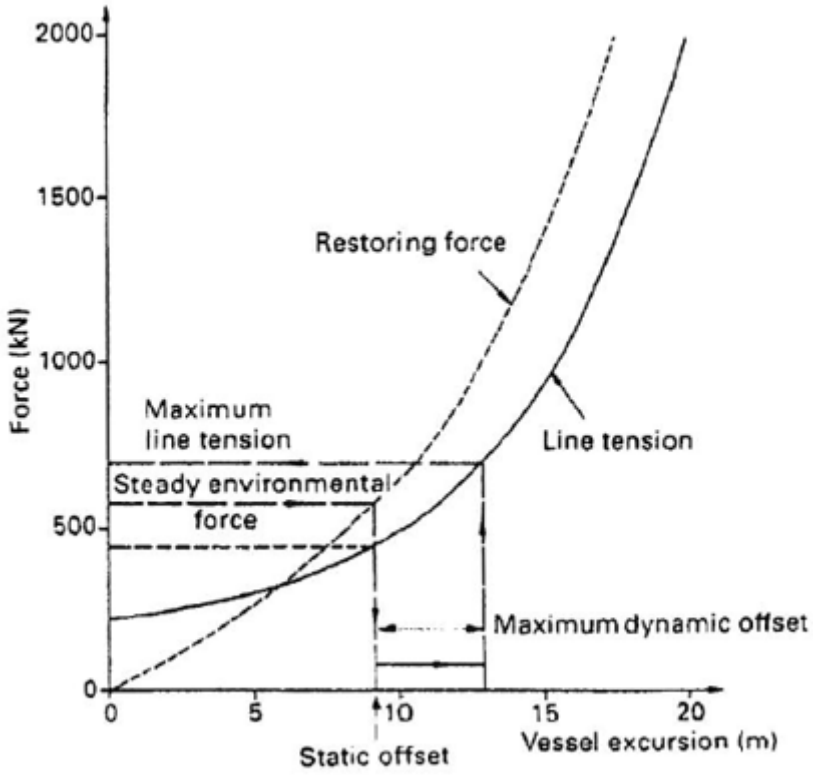

Figure 27: Restoring force and most loaded line tension against vessel excursion for a caternary mooring system (static analysis). Figure from Chakrabarti, 2005.

Once a system satisfies all requirements (line length, no upward force at anchor and max line tension), the analysis is performed again for a case in which the most loaded line breaks. This is to ensure proper redundancy in the system, reducing risk of complete mooring system failure.

This method has the disadvantage that conservative estimations are made. Unidirectional environment is assumed, which is almost never the case for aquaculture sites in the fjords of Norway. Also, the important dynamic features are absent for this method, meaning that large safety factors has to be used (Chakrabarti, 2005).

3.7.2 Quasi-static design

This approach is, as the name implies, static to some degree. It can be thought of as the next level of complexity for a mooring design. These analyses are usually performed in either the time or frequency domain. For the time domain simulations, vessel forces and response is calculated for the relevant wave drift frequencies while wind and current forces are considered steady. The mooring stiffness curve is used (as in Figure 27) without the dynamic part. The frequency domain simulation assumes a linear stiffness curve, and calculates dynamic response for the relevant frequencies from both wave drift and wind. To simplify the calculations, these contributions are calculated as for a single Degree of freedom (DOF) system (Chakrabarti, 2005).

The main differences between this *quasi-static* approach and the static approach are the following.

- Quasi-static analysis usually include the catenary stiffness at each time-step of horizontal offset within the equation of motion. This allows for non-linear stiffness behaviour, which is the case for geometric stiffness systems as can be seen in Section 3.1.4. Simultaneously, stiff catenary or taut elastic mooring systems does have practically linear stiffness characteristics, in which this feature is wasted.
- Some contributions of added mass and damping are included. However, these are mostly connected to the vessel and not the mooring systems itself. Therefore they tend to be inaccurate.
- Even though frequency domain solutions are possible, as stated above, they are subject to gross assumptions due to the linearisation of stiffness and damping.

This approach solves the equation of motion: $(m+A)\ddot{x}+B\dot{x}+B_v\dot{x}|\dot{x}|+Cx = F_x(t)$, where m, A, B and B_v refers to vessel mass, added mass, linear and viscous damping respectively. The simulations should cover at least 18 hours of full scale analysis to provide sufficient response data for the low frequency range (Chakrabarti, 2005). Such long time-domain simulations are very time-consuming when compared to static analyses.

3.7.3 Dynamic design

Full scale dynamic analysis methods are frequently used in design, even though there is no universal agreement of mooring line damping values. Mooring line damping can influence vessel response and line loads to a large extent. Especially in deep water. Generally, the methodology goes as follows (Chakrabarti, 2005):

- A static configuration must first be established, with a non-linear time domain solution. Lines are often decomposed into straight bar elements with linear shape functions, except for the mass which is lumped at the end nodes (Moen, 2003). Normally, the vessel motions are calculated independently from the line dynamics. However, as mentioned earlier, for deep water scenarios, mutual interaction between the vessel and mooring system is of significance. In this case coupling between mooring and vessel must be included.
- Dynamic methods should not only include the mooring restoring force, but also the hydrodynamic damping effects introduced by relative motion between line and fluid, as explained in Section 3.6.

Simulations use lumped mass finite element or finite difference schemes to model line sections, because its shape is affected by the water resistance (Moen, 2003).

Dynamic analysis is performed in the time-domain, which is computationally expensive. Compared to static and quasi-static, this is the most time-consuming analyses. Some of the difficulties are:

- Sufficiently small time steps to ensure that high frequency mooring line oscillations are included (see Section 3.6).
- Simulations must be long enough the account for low-frequency forces, like wave-drift. In deep water these periods may be around 5 minutes.
- Normally, real life weather is multi-directional. Resulting in a number of test cases that must be considered. However, for Norwegian fjords, the weather is typically coming from the open sea. Which means that one already know which directions the weather will hit hardest, reducing the number of direction on has to consider.

Top-end line oscillation must be included in simulations, because of vessel motions at combined wave and drift frequencies. If this is not included, dynamic tension components might be underestimated or line damping contributions can be neglected. Line dynamics can in some cases lead to a doubling in top tension when compared to static line tension (Chakrabarti, 2005).

3.8 Technical regulations

The aquaculture act of 2006 states that *The purpose of this Act is to promote the profitability and competitiveness of the aquaculture industry within the framework of a sustainable development and contribute to the creation of value on the coast.* This act regulates the licensing system and the bureaucracy around it.

The main objective for technical regulations and standards in Norwegian aquaculture, is to prevent fish escapes. The operational, design and technical integrity of an installation must be reviewed to prevent escape (NYTEK, 2011). The high focus on fish escapes are due to several factors, most importantly:

- Fish escapes threatens the wild fish stocks because of interbreeding, which may lead to new species that are not suited for wild life. Farmed fish may also introduce diseases and claim space and food from the wild stocks.
- Economic loss for the farmer due to fish escape. The farmer has to take the loss of the fish itself and also the cost related to handling the escape incident.

NYTEK sets the technical regulations for Norwegian aquaculture and refers to the technical standards for details, e.g. NS9415.

3.8.1 NYTEK

NYTEK is the Norwegian national regulation of technical standards for floating aquaculture installations, which is issued by the Norwegian ministry of trade, fisheries and industry. This includes regulations for certification and inspection of aquaculture facilities. The inspections has to be passed and equipment must be certified for the fish farmer to get a license. More specifically, mooring analysis and site surveys has to be documented. In addition, all main components must be controlled and verified by independent certified inspection-companies.

NYTEK does not only apply to fish farmers however, both manufacturers and suppliers are subject to this regulation. While farmers has to verify their farming cite, manufacturers and suppliers has to certify their products. NYTEK is not a technical standard, and it refers to NS9415 for technical specifications.

NYTEK's main purpose is to reduce the risk of technical failure and to ensure high quality of components (NYTEK, 2011). Specifically relevant for feed barge mooring is perhaps NYTEK §17,18,19 which describes requirements for site survey, mooring analysis and mooring installation.

3.8.2 NS 9415

NS9415 is the Norwegian standard regarding technical requirements for design, dimensioning, installation and operation of Norwegian aquaculture. It is relevant for all main components of a fish farm, such as mooring systems, floating net pens and barges. These requirements are derived mainly to prevent fish escapes, but also focus on Health, safety and environment (HSE) for people. The technical requirements consists of strength analyses, lifetime analyses, safety limits and specifications for load calculation (Standard Norway, 2021). The standard was first drafted in 2003, then revised in 2009 before it was again revised in 2021. The newest edition will take effect in 2022, and it is this version that has been reviewed in this report. The elaboration of this standard presented in this section will focus on the mooring system and load analysis, but also contain information that could be relevant to identify potential risk areas for feed barges in general.

3.8.3 Partial coefficient method

NS9415 (Standard Norway, 2021) uses a common method for establishing design criteria, called the partial coefficient method. This is used in *limit state design*, and consists of applying safety factors to both the design load and material properties, depending on which *limit state* is considered.

The different limit states are:

- Ultimate limit state (ULS):
  This design criteria is based on designing for extreme environmental load cases.

- Accidental limit state (ALS):
  This design criteria is based on designing for accidental load cases, such as explosions, mooring line failures, fires and ship collisions.
- Serviceability limit state (SLS):
  The serviceability limit state design criteria considers normal operation of the structure in question, and how safe this operation can be performed.
- Fatigue limit state (FLS):
  This limit state considers fatigue during a structures design lifetime. Fatigue occurs when a structure is under cyclic loading, which is the case for most floating structures due to waves, tides etc.

The partial coefficient method is given mathematically as follows (Standard Norway, 2021):

$$S_c \cdot \gamma_f \leq \frac{R}{\gamma_M} \tag{54}$$

Where,

- S_c is the characteristic load (calculated load)
- γ_f is the load factor
- R is the characteristic capacity
- γ_M is a material factor

The standard gives values for which load factor γ_f and material factor γ_M that should be used for the different limit states. The factors can also depend on which analysis method is applied (Standard Norway, 2021).

The characteristic capacity of a component is given from the manufacturer, and is commonly set to the Minimum breaking load (MBL) of the component. This value comes from the 90% quantile of the components capacity distribution (Bjørkøy, 2017).

The characteristic load S_c, is a bit more tedious to calculate. This value comes from extreme value analysis of the selected limit state. The standard gives 3 combinations of current, wind, wave and ice load return periods that has to be considered to find the characteristic load for ULS design, this can be seen in Table 4. The combination that gives highest load is then used.

Table 4: Return period (years) for load combinations to be controlled in ULS design (Standard Norway, 2021).

Combinations	Current	Wind	Wave	Ice
1	50	10	10	-
2	10	50	50	-
3	10	10	10	50

The theoretical principle behind this method is rather straight forward. One assumes that both the load and strength of a component follows a probability distribution, and the purpose of the method is to reduce the probability of failure, or the area in which both the Probability density function (PDF) share. This is illustrated in Figure 28.

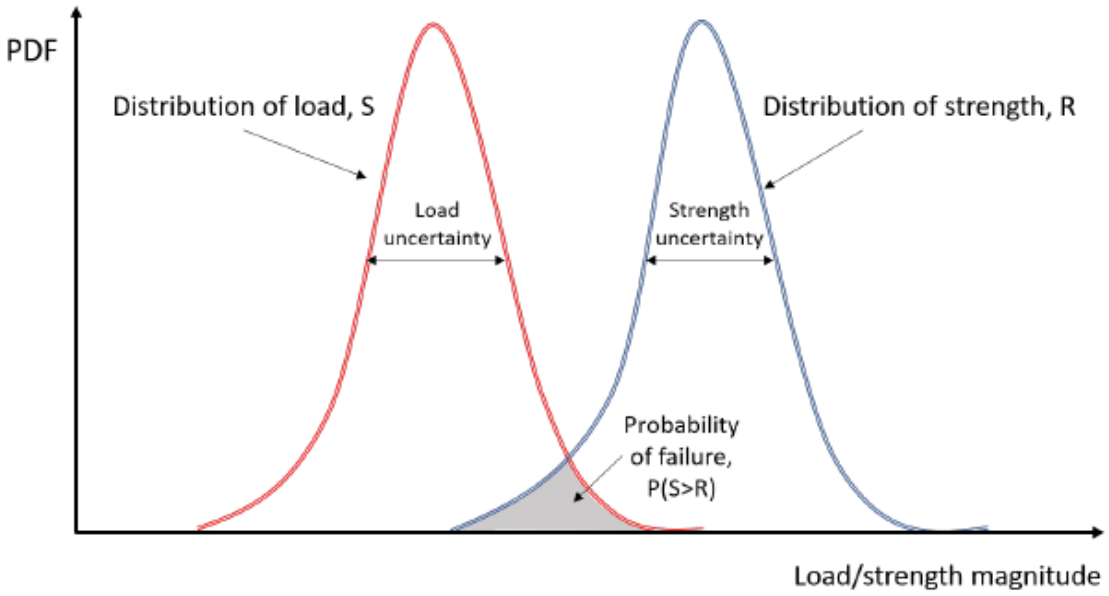

Figure 28: Illustration of the partial coefficient method (Bjørkøy, 2017).

3.8.4 Requirements for site survey and establishing environment data

NS9415 (Standard Norway, 2021) gives numerous requirements for measuring wind, current and wave conditions at a site. It is required to perform a site survey that shall be documented and used in the design of the aquaculture facility (Standard Norway, 2021). Section 8 of the standard is used for this purpose, and the most important aspects are as follows:

- Values for current, wind and waves must be given for minimum 8 evenly distributed sectors over 360°.
- Local tide values, as well as extreme low and high tide with return period of 50 years must be established.
- Design current speed with return period of both 10 and 50 years must be established. For this, measurements on 5 and 15 meter water depth over a minimum period of 3 months must be made. It shall also be stated which current component is most important for the extreme current.
- Design wind speed must be established for extreme values with 10 and 50 year return period. It must be established both wind load and wind generated waves.

- Waves with extreme value return period of 10 and 50 years must be established through numerical analysis. The standard sets requirements to what this analysis should contain. It is stated that the numerical analysis can be supported by wave measurements, but does not go into further detail on this.

3.8.5 Requirements for load interpretation and analysis

Section 9 of NS9415 (Standard Norway, 2021) specifies how loads on aquaculture facilities should be interpreted, analysed and handled. The standard states: *A floating aquaculture facility shall be designed to withstand all loads that can appear during the designed lifetime of said facility.* Since this thesis is focused on feed barge mooring, information specific to other structures will not be presented in this subsection.

The standard states that the mooring system should be designed to withstand line failure. Most importantly, the most loaded line should be able to fail, without progressive line failure or unacceptable loss of position for the moored structure. It also requires that failure of each single mooring line should be considered and documented. Mooring analysis of ALS conditions shall use material factors given in Table 5, divided by 1,5.

As explained in Section 3.8.3, load factors differ for which limit state is being analysed, as can be seen in Table 6. The standard states that the safety factor for FLS design should be at least 1, without further detail. It is also specified that Table 6 should be multiplied with a Dynamic amplification factor (DAF) for quasi-static (see Section 3.7.2) analysis, with value of at least 1,1. The choice of this DAF must be explained and documented.

The standard allows the use of regular waves in limit state design under the following equation:

$$H = H_{max} = 1,9H_s \tag{55}$$

Where,

- H Is the regular wave height [m].
- H_{max} is the largest wave height for a sea state [m].
- H_s is the dimensioning significant wave height for a sea state with duration of 3 hours and return period of 50 years [m].

As explained in Section 3.5.2, regular waves are no good for mooring design, because it is the second order slowly varying forces that dominate. Luckily, the standard does have a remark for this exact reason stating: *Irregular sea state is of particular importance for systems that have slowly varying motions of importance.*

Table 5: Material factors for various mooring components given in NS9415 (Standard Norway, 2021).

Type	**Material factor**
Synthetic rope	2,5
Synthetic rope with knot	5,0
Chain and chain components	2,0
Used chain	5,0
Connection plates and other connectors of steel	2,0
Steel wire	3,0
Shackles	2,0
Rock pins and fluke anchors	3,0

Table 6: Load factors for mooring systems and some other components, given in NS9415 (Standard Norway, 2021).

Limit state	**Load factor**
ULS	1,15
ALS	1,0
SLS	1,0
FLS	≥ 1

3.8.6 Floating feed barge requirements

Section 12 of NS9415 (Standard Norway, 2021) specifies requirements for feed barges, and covers the following points:

- **General functional requirements, of which the standard states the following sub-requirements:**
  The barge must have sufficient buoyancy with payload included. Optionally, the standard also allows the barge to be connected to other components that can ensure buoyancy. The barge must have adequate robustness concerning accident situations. This particular formulation is quite vague and seem open to interpretation. Regarding inspections, relevant areas should be accessible such that its condition can be controlled.

- **Requirements for steel barge dimensioning:**
  Section 6.3 of the standard, concerning steel structures, shall be used for dimensioning. This section refers largely to the standard NS-EN 1993. It is required to prepare profile, plane and cut drawings that contains the dimensions of the structure. It also specifies how certain welds should be performed, and states that welded joints should be controlled by use of non-destructive tests.

- **The following requirements apply for concrete barges:**
  Section 6.5 of the standard, concerning concrete structures, is to be used for

dimensioning. This section refers to NS-EN 1992 for dimensioning and to NS-EN 13670 for casting execution. It also refers to DNGL-ST-C502 which is developed for concrete marine structures, which could be relevant. For feed barges, an exposure class of XS3 (according to NS-EN 1992) is required for all outside concrete surfaces, while other exposure classes can be used for inside surfaces. The exposure class gives requirements for how deep steel reinforcements need to be in the concrete, to avoid corrosion.

- **Requirements for stability and watertight integrity for fully detached barges:**
  The barge should have adequate stability for both intact condition and damaged condition. The standard does not specify what is meant by damaged condition, but this is probably linked to incidents identified as potential accidents, like ship collision. For most vessels, incline tests are mandatory to confirm point of gravity and light ship weight precisely, and aquaculture feed barges are no exception. The standard does, however, state that in some special cases this test can be avoided. There are also requirements for minimum freeboard depending on the barge length and what sea state it is designed for. Watertight sections shall be marked on drawings and these sections should be designed to withstand the pressures they may face. The standard demands a minimum of 3 such watertight sections on a feed barge, with additional sections if necessary. The governing rule is that one section should be able to flood and the barge should still have intact stability and buoyancy for all design conditions.

- **Requirements for mooring and documentation:**
  Section 12 gives some generic description of towing and required documentation that shall follow the feed barge. The required information is references to NS9415, design payload, maximum axle load of vehicles on the barge, date of finished build, tow points and its maximum load and the manufacturer. General mooring requirements for all aquaculture structures are given in section 13.

4 Risk assessment of modern feed barges

For this section i will attempt to perform a risk analysis of exposed moored feed barges, with a focus on the mooring systems. This analysis will be more qualitative than quantitative since there is no easily available data of feed barge incidents. I will use a mooring failure incident from the oil and gas industry as a benchmark for this analysis, more specifically the Ocean Vanguard incident in 2004 (Solheim et al., 2004; Vinnem and Røed, 2020).

The motivation behind this exercise consists of two parts. Firstly, the author believes that being aware of the risk picture will give a better understanding of a system and its critical components. Which will then contribute to a better shaped thesis, attacking the topic in question from the best suited angle. Secondly, is it required in section 5.2 of the governing standard NS9415 to perform a risk assessment when designing components for an aquaculture site (Standard Norway, 2021). For both of these reasons, it was concluded that this exercise would be useful.

4.1 Ocean Vanguard - Mooring failure incident

The semi submersible drilling platform Ocean Vanguard, experienced a serious accident on the 14. December 2004. During a storm, two anchor line winches failed, resulting in uncontrolled release of those anchor lines. Although this semi submersible is quite different in nature when compared to a feed barge, they are both floating moored structures in relatively exposed locations, which makes a comparison between the mooring systems reasonable.

4.1.1 Description of accident timeline

Ocean vanguard had stopped drilling, and at 20:00 prepared to disconnect the riser system due to bad weather. No specific operations were carried out before the incident. At the time of the incident, wind speeds were around 30ms and waves were around 15m.

At 22:40, anchor winch 1 and 2 failed, resulting in the uncontrolled release of the two mooring lines. Directly after this, the assisting sub sea engineer initiated decoupling of the lower marine riser package.

Soon after, the platform went into a steep heel, approximately 8-10deg according to witnesses. While this occurs, the riser system is under tremendous load and eventually fails. The riser pipe is torn off and falls into the sea. Roughly 3-5 minutes after the lines were released, the platform had drifted 160m off its initial position. At this point the crew was aware of what had happened and initiated the DP thruster system to regain control of the platform.

4.1.2 MTO analysis of Ocean Vanguard

In order to identify some risk aspects and potentially relevant barriers for a moored feed barge, a Man, technology and organizational (MTO) analysis of the Ocean Vanguard incident was carried out. This work was to some degree performed in the course TMR4555. This analysis can be seen in Appendix A

The analysis is made in accordance with Eltervåg et al., 2004. Where the event- and cause part of the diagram divides the accident into single sequential events and their causes. This part is made from the timeline of the incident.

The next part of the diagram is the change analysis. According to Vinnem and Røed, 2020, the background for the change analysis is *to assess how events in the accident progress have deviated from normal situation, or common practice.* Which can be thought of as factors indirectly initiating the direct causes.

The final part of the MTO diagram is the barrier analysis. Usually, when an accident event occurs, barriers that were in place to prevent such situations has been breached. This part of the MTO analysis is aimed at identifying these barriers. The barriers identified here can be used to further improve barrier strategies to ensure that similar events does not happen again. Simultaneously, it is important to find the barriers that held and preventing further escalation.

4.1.3 Aspects of Ocean Vanguard accident that applies to feed barges

Through the MTO analysis in Appendix A, described in Section 4.1.2, some aspects can be brought into the consideration of aquaculture feed barges. These are:

- **Failure to follow regulations for inspection, maintenance and documentation.**
  For most systems, inspection and maintenance is important to ensure proper function, mooring systems are no different. In the case of the Ocean Vanguard incident, the lack of proper maintenance was identified as one of the main contributing factors for the mooring anchor winch failure. For feed barges, the story is a bit different. Feed barges does not utilize such anchor line winches in their mooring system. Nonetheless, it is important to follow the regulation provided by the government and the manufacturers to ensure proper function and strength capacity of the mooring lines.

- **Failure to have proper redundancy in the mooring system.**
  According to NS9415, aquaculture mooring systems should be designed with potential accident and hazards in mind. Meaning that the mooring system should have adequate redundancy in case of mooring line failure. For Ocean Vanguard, there were redundancy systems in form of a Pioneer adjustable lever (PAL) fail-safe. The crew, however, did not know how to operate these and therefore they were not active.

  For feed barges, this redundancy has to be accounted for in the design phase of the systems. Seeing as there is no winch system in use for feed barges that the

crew has to operate. This is positive in the sense that there is less components that can fail or be operated wrong (Standard Norway, 2021; Vinnem and Røed, 2020).

- **Conflicting emergency protocols.**
  One of the factors that were identified contributing to late emergency protocol initiation for Ocean Vanguard, was conflicting emergency protocols. The platform manager had two sets of regulations that governed how he was supposed to respond in the emergency situation. This led to confusion and most likely slowed response. For time critical emergency situations where lives might be at stake, this is unacceptable.

  It is therefore important that governing regulations are clearly defined for feed barge operation and emergencies. Things like evacuations cannot be hindered by conflicting protocols. With that being said, the offshore oil production is prone to varying regulations from country to country, with Norway often having more rigorous standards. This is not so much the case for aquaculture, because it is not as international in its production and supply. Meaning that aquaculture manufacturers only has to consider Norwegian regulations.

4.2 Analysis of other mooring failures

Since documentation of feed barge mooring failure was unobtainable for this report, i have decided to look at statistics for moored oil and gas installations on the Norwegian continental shelf. A report from the Petroleum safety authority (PSA) has analysed mooring failures from 2010-2013 (Kvitrud, 2014). It should be noted that these failures might not be completely transferable to feed barges, because of the different environmental conditions between oil- and gas production and aquaculture sites. However, since the main concern behind this report is more exposed aquaculture sites, it can be argued that this exercise is valuable.

A similar report was provided by the PSA in 2006, where they analysed mooring failures in the period from 1996-2005. This report concluded with the number of incidents related to mooring systems on MOUs were too high. To remedy this, the report suggests better transference of experience, more mooring competence for the crew, more attention to maintenance and documentation of this. It also highlighted the importance for inspections, especially for older lines (typically older than 20 years). The most common line failures was fatigue in chain links and shackles. Since there is a lower amount of shackles in a line compared to chainlinks, the failure frequency of these were significantly largest. In addition, many fatigue fractures were caused by bending, most likely due to the fairleads. The reports therefore advise reconsideration for fairlead design. Fibre ropes had proven to be very vulnerable to mechanical exposure, and special care should therefore be taken when performing operations where this is a risk (Kvitrud, 2014).

For the 2010-13 incidents, 15 failures was considered. It was discovered that failure probability was largely dependant on what structure type was in question, as can be seen in Table 7. Although, this is most likely due to the low sample of accidents.

On the other hand, this could be used in comparison to feed barges to attempt to estimate mooring failure more accurately than taking a broad average from all vessels. When comparing a feed barge to the vessels in Table 7, it is probably the production semi-sub in which the feed barge has most in common. This is the only installation on the list that normally has a spread mooring system and is also permanently situated on a site. Using the failure probability from said semi-sub then gives one mooring line failure per 8 years for a feed barge. This simple comparison gives an estimate that could be used for risk evaluation. The lifetime of a feed barge is 20-30 years, which means that a feed barge will experience several mooring line failures. This is important to have in mind when designing for redundancy.

The overall failure probability per line-year for the period 1996-2005 was $100 \cdot 10^{-4}$, while it was $88 \cdot 10^{-4}$ for 2010-2013. Indicating that the failure probability has not improved much. From Table 8, the 15 failures has been categorized into component failure. As expected, chains are prone to fatigue and overload failure, while fibre ropes are prone to mechanical damage. Its also worth to note that steel wires both had overload and mechanical damage failures (Kvitrud, 2014).

Table 7: Annual risk of mooring failure for different oil and gas related vessels, according to Kvitrud, 2014.

	Annual risk of mooring line failure
FPSO	1/7
FSO	1/17
Drill ships	1/1.5
Drilling semi-sub	1/4
Production semi-sub	1/8

Table 8: Causes of the 15 failures on mooring line elements in 2010-13. Errors in winches or brakes are not included (Kvitrud, 2014).

	Fatigue	Overload	Mechanical damage
Chains	4	3	
Fibre ropes			3
Steel wires		2	1
Kenter link	1		
Socket connection		1	
Sum	5	6	4

Intuitively, older components should be the most accident prone. According to Figure 29, this might not be the case. It is observed that most components fail between 0-5 years of operating time, which suggest that current procedures and protocols for design and installation are not adequate (Kvitrud, 2014). The report goes on to list improvements to regulation and standards, as well as questioning the status quo where operators are responsible for inspecting themselves. A big part of the proposed improvements regards the need for high trace-ability for mooring components, and the need for documented inspection and maintenance.

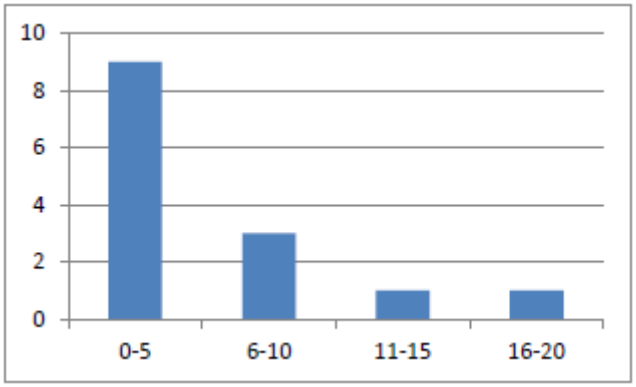

Figure 29: Number of failures as a function of the age of the failed elements. Double line failures are counted as one case (Kvitrud, 2014).

4.3 Barrier strategy for ultimate limit state (ULS) of aquaculture feed barges

From Section 4.1 and 4.2 we have gained some insight to which barriers that would be important to implement in a barrier strategy for an exposed feed barge. The PSA defines a barrier strategy as *"A plan for how barrier functions, on the basis of the risk picture, are implemented in order to reduce risk"* (Eltervåg et al., 2004). This assumes that one is able to get a reasonably good risk picture, which is not always the case.

4.3.1 Risk management process

If we follow the often used standard for risk management in the offshore industry, ISO 31000, Figure 30 shows the general procedure for establishing a risk management scheme. Under this description, the *Risk treatment* can be seen as the barrier strategy.

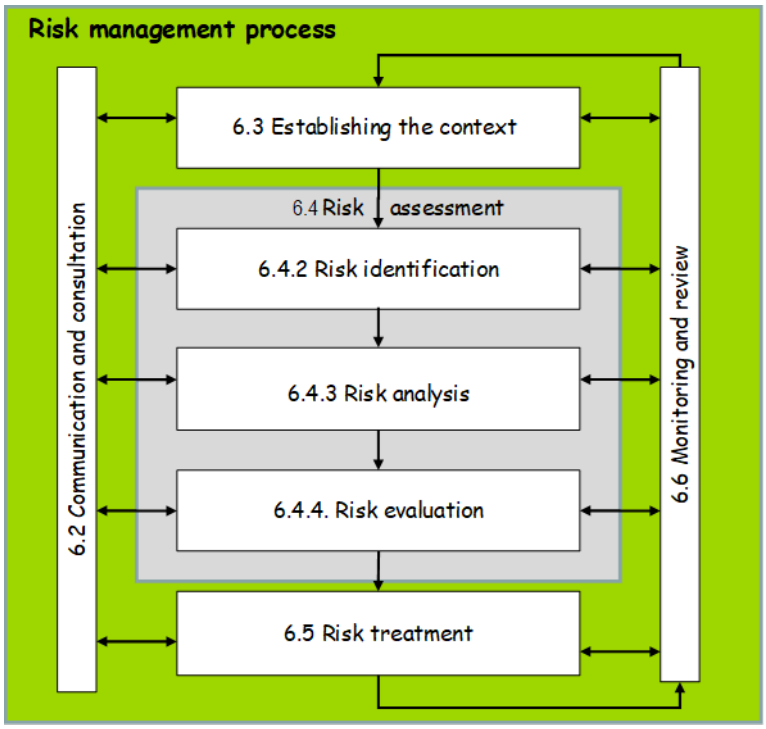

Figure 30: Overview of establishing a risk management scheme (ISO 31000, 2018).

As mentioned earlier, establishing a good risk picture without a decent quantitative risk analysis might be difficult. However, for cases with little accessible data, a qualitative analysis has a big value and should be used actively when designing structures like feed barges. This is because one is forced to consider and evaluate the risk picture in important design decisions (Vinnem and Røed, 2020).

4.3.2 Establishing a barrier strategy

The PSA proposes the strategy shown in Figure 31 to establish barrier strategies.

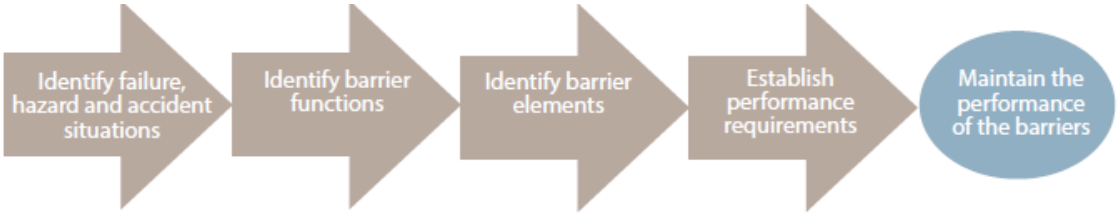

Figure 31: Key steps in barrier management (Eltervåg et al., 2004).

The main accident that this barrier strategy will focus on is naturally mooring failure for feed barges, with some inspiration from the oil and gas industry which was discussed earlier. A proposed barrier strategy can be seen in Appendix B. The main accident situation was identified to be mooring failure, as can be seen as the main function in the barrier strategy. Based on the common failures discussed in Section 4.1 and 4.2, sub-functions and barrier elements were established. Since i

have tried to transfer it to feed barges, winches among other things were excluded. To recap, the following factors were identified as key to reduce mooring failures:

- **Proper inspection and maintenance according to regulations.**
  At least for offshore oil and gas production facilities, the producers are responsible for controlling themselves. For many accidents, one have experienced little documentation of maintenance and inspection. Including generally bad traceability for mooring components. I would expect this to be less of a problem in aquaculture, due to more inspection from independent authorities. Still, it is an important aspect of risk reduction.

- **Revised design of fairleads to reduce bending moments in shackles and chain-links.**
  According to the PSA report (Kvitrud, 2014), fatigue fractures in chains and shackles were largely caused by bending which occurred while the components travelled through the fairleads (see Section 2.2.6 for more details of fairleads). This does also intuitively make sense, since the chains are designed for tensile stress only. Therefore it is reasonable to assume that a different fairlead design could improve this.

- **Proper mooring installation procedures to avoid installation damage.**
  The main cause for fiber rope failure is mechanical damage (see Table 8). Additionally, as we see in Figure 29, the short lifespan before failure suggests that installation might be an influencing risk factor. Better installation procedures to prevent such damage could help avoid these failures. It should be noted that proper training of crew is equally important to ensure that procedures are followed and executed correctly.

- **Redundancy included in mooring design.**
  Redundancy in such systems are essential, and is demanded in NS9415. The standard states that the most loaded line should be designed to fail without progressive failure (see Section 3.8.5). Which means that this design principle is quite important, since mooring lines fail rather frequently, once per 8 years according to my estimation in Section 4.2 (Kvitrud, 2014).

- **Clear procedures to follow in emergency situations.**
  One of the main lessons to be taken away from the Ocean Vanguard incident, is that emergency procedures must be clear and without other conflicting procedures. This is because response time is critical in such situations.

5 Method

The main goal of this thesis was to examine the effects of irregular *exposed condition* waves on a feed barge spread mooring system, up against the new governing design standard NS9415 (Standard Norway, 2021) for different analysis methods. In order to fulfill this goal, analyses of a generic feed barge mooring setup was performed for various environmental conditions using state of the art theory.

In order to create the simulation model for this thesis, several programs had to be utilized. This chapter will be dedicated to presenting these programs, the model set-up, explaining the decisions that were made and present which results were retrieved and examined.

5.1 Analysis software

This section will be dedicated to break down the various programs needed for the simulations in this thesis. The structure of the program, the theory it utilizes and some description of model setup will be presented.

5.1.1 GeniE

The software GeniE is the analysis tool for structural design in the total software package solution SESAM (DNV, 2022c). According to the user documentation, GeniE is especially good for modelling topsides, jackets, floating offshore structures and ships (DNV, 2020). This program in itself contains ton of functionality for structural analysis. However, for this thesis it will only be used for creating a panel model of the feed barge to be used in further analysis. For more documentation, see the user manual (DNV, 2020).

As mentioned, GeniE allows modelling of *panel models*. This basically means that the model is designed with the main outer dimensions with surfaces that we call panels. These panels are only defined by their geometric 3D property. Consequentially, the models Center of gravity (COG), mass and other properties has to be defined later.

The design process of the feed barge can be seen in Figure 32. The design concept of the model can be seen in Figure 32b, where the two guide planes can be seen in green. The orange blocks represents a *dummy force* that has been applied to the panels. This is to specify on which surface the water pressure in later analysis should act (DNV, 2020). Figure 32a shows the model mesh, which is just as simple as it looks. There is no point in having a finer mesh since no structural analysis will be performed on the barge. For further GeniE documentation, see the manual (DNV, 2020).

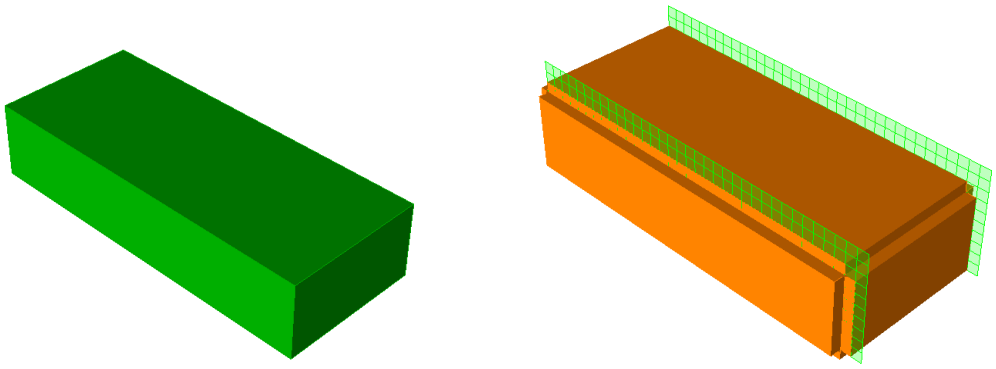

(a) GeniE model mesh.

(b) GeniE model with guide-planes and dummy hydrostatic force.

Figure 32: GeniE modelling process.

5.1.2 HydroD

The panel model that is made from GeniE then needs to be analysed in water to find how the structure will act. Another program from the SESAM package, HydroD, is suitable for this and also has high compatibility with the other programs used in this thesis (DNV, 2022b).

HydroD uses state of the art theory for hydrodynamic and stability analysis of arbitrary floating or fixed structures in waves. As with GeniE, HydroD is an extensive software with tons of features and applications. For this thesis however, a specific part of the functionality will be utilized. More specifically, the sub-program Wadam, which allows for linear frequency domain solution of the 3D radiation-diffraction problem for panel models (DNV, 2022a). When running this analysis, one can obtain RAO's for the selected wave frequencies and wave headings. These can then be used in further analysis to describe the vessel-wave interaction.

The design process follows Figure 33. As mentioned, the first step was performed in GeniE. The second step is to create an environment to be used in the analysis. For this specific case, it can be beneficial to use 8 equally spaced wave directions towards the vessel for the environment, as required by the standard for cite surveys (Standard Norway, 2021). For the frequency ranges, the specifications shown in Table 9 could be acceptable. Having a finer selection for high-frequency and wave-frequency waves, the RAOs will be accurately represented.

The next step is then to go through the modelling cycle, to define the mass and mass distribution of the model. After running the hydrostatic analysis, the response data is saved in a .SIF file, which can be used in further analysis. An example of such a transfer function for heave can be seen in Appendix C. For further HydroD documentation, see the manual (DNV, 2021).

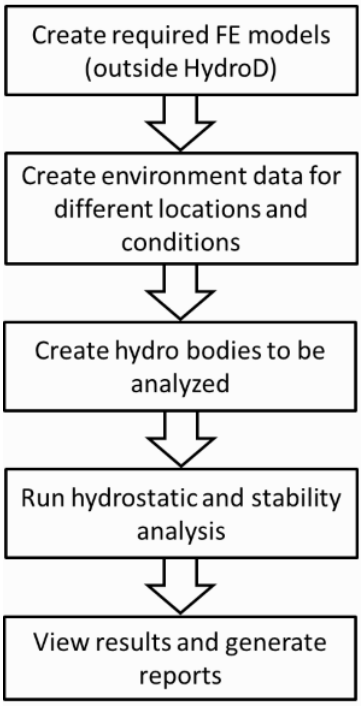

Figure 33: HydroD design process (DNV, 2021).

Table 9: Environment specifications used in HydroD software.

From [s]	**To** [s]	**Step** [s]
0,1	20	0,1
20	60	1

5.1.3 Alternative to HydroD

An alternative method of acquiring the hydrodynamic data for feed barges was identified since advanced software like HydroD, from experience, can be difficult to manage. If this proves to be the case, this alternative method will be used.

Through the *Centre for research based innovations* (Exposed, 2022), a summer project in 2017 were dedicated to establishing a SIMA database for hydrodynamic barge data (Zang, 2017). This is performed by using the theory presented in Section 3.6.1.

This database contains data for a large variation of feed barges. If it is to be utilized, it would simply be a matter of identifying the model in the database which is most similar to the barge which is to be analysed. This database is made with directions from 0° to 180° with a 10° spacing, and then assuming symmetry around the model for the last 180°. This means that the data is only valid for feed barges that are symmetric around the XZ-plane (when the X-axis goes along the length of the ship and Z-axis goes vertically), which is the case for most barges.

5.1.4 SIMA analysis software

SIMA workbench offers a complete solution for simulation and analysis of marine operations and floating systems. It supports the entire process from simulation definition to result interpretation and documentation (SINTEF, 2021). According to the SIMA user manual, the program has two main purposes.

- Be a tool for beginners to become proficient in modeling and analysis.
- Be a tool for experts that shorten the time it takes from project start to finish.

The following subsections will be used to explain the use of SIMA in this thesis, in addition to go deeper into the workings of relevant sub-programs. This is done because the thesis is largely based on simulation in this program.

5.1.5 Application of SIMA in this thesis

According to research performed in Section 3.7, accurate time domain dynamic analysis requires a coupled analysis between the vessel and mooring system. This can be done in SIMA by combining the two sub-programs SIMO and RIFLEX.

SIMO is a program for simulating motion and station-keeping of complex floating systems. Essential features include (Marintek, 2018):

- Flexible modelling of multi-body systems.
- Non-linear time domain simulations of both wave frequency- and low frequency response.
- Environmental forces from wind, waves and current.
- Passive and active control forces.
- Interactive and batch simulations.

Which means that SIMO is excellent for analysing moored vessels, since it takes into account the low frequency loads important to mooring, as discussed in Section 3.5.2. However, SIMO only allows a catenary type modelling of the mooring system, similar to what was done in Section 3.1.4. This means that SIMO alone cannot take the mooring dynamic effects, like hydrodynamic damping discussed in Section 3.6, into account. As expressed in Section 3.7.3, these dynamic effects are especially important for deep water conditions where line tension can double when compared to a static analysis.

To solve this problem, RIFLEX can be utilized. RIFLEX was developed to analyse flexible marine riser systems, but is also applicable for other types of slender structures. Such as mooring lines, conventional risers and umbilicals.

This program uses nonlinear finite element formulation. Key features include (Marintek, 2018):

- Flexible modelling of complex systems.
- Nonlinear time-domain analysis of motion and forces.
- Nonlinear cross section properties.
- For simplified analysis, generalized Morison load model can be used. Both in static, catenary linearized time domain and in frequency domain analysis.

This brings the option to have proper dynamic time domain simulation of the mooring lines, which can be coupled with the SIMA vessel analysis with help from the hydrodynamic response data gathered from HydroD. This will then give a solid dynamic analysis where both the dynamic effects from vessel and mooring systems are accounted for.

5.1.6 SIMO program structure

To use software for complicated calculations, some insight to how the program works is essential. This subsection will be used to explain the inner workings of SIMO.

The program is built according to Table 10, where the second column is the subprograms to SIMO, communicating through a common file system.

Table 10: SIMO program structure according to Marintek, 2018.

SIMO	INPMOD	File system for communication between modules	Input generation and presentation, interface to external sources of data
	STAMOD		Read input data, static analysis, define initial condition
	DYNMOD		Dynamic analyses, generation of time series
	OUTMOD		Post-processing of time series
	S2XMOD		Export of time series

A more detailed description of each module:

- **INPMOD - input data manipulation**
  This module provides interface to external input data sources, like hydrodynamic programs and then modifies the system description file.
- **STAMOD - initial condition and static equilibrium**
  The system description file made in INPMOD is read here. This module defines the initial conditions for the dynamic simulation described. Environmental conditions are also defined here, and saved to a file for use in DYNMOD. A static equilibrium analysis can be calculated here, with average environmental forces applied. From this, natural periods and eigenmodes can be calculated.

- **DYNMOD - dynamic response calculation**
  This module calculates response in the time-domain. Before calculation, through integration of the equation of motion, can start, the simulation parameters must be read from STAMOD and INPMOD.

- **OUTMOD - output module**
  The purpose of this program is to read the time series which are generated in DYNMOD and from this generate plots and statistical parameters.

- **S2XMOD - export of time series**
  This sub-programs main purpose is to export results from DYNMOD to other formats. For example, export time series to MATLAB-file, ASCII-file etc.

A flowchart of how these modules communicates through the file-system can be seen in Figure 34

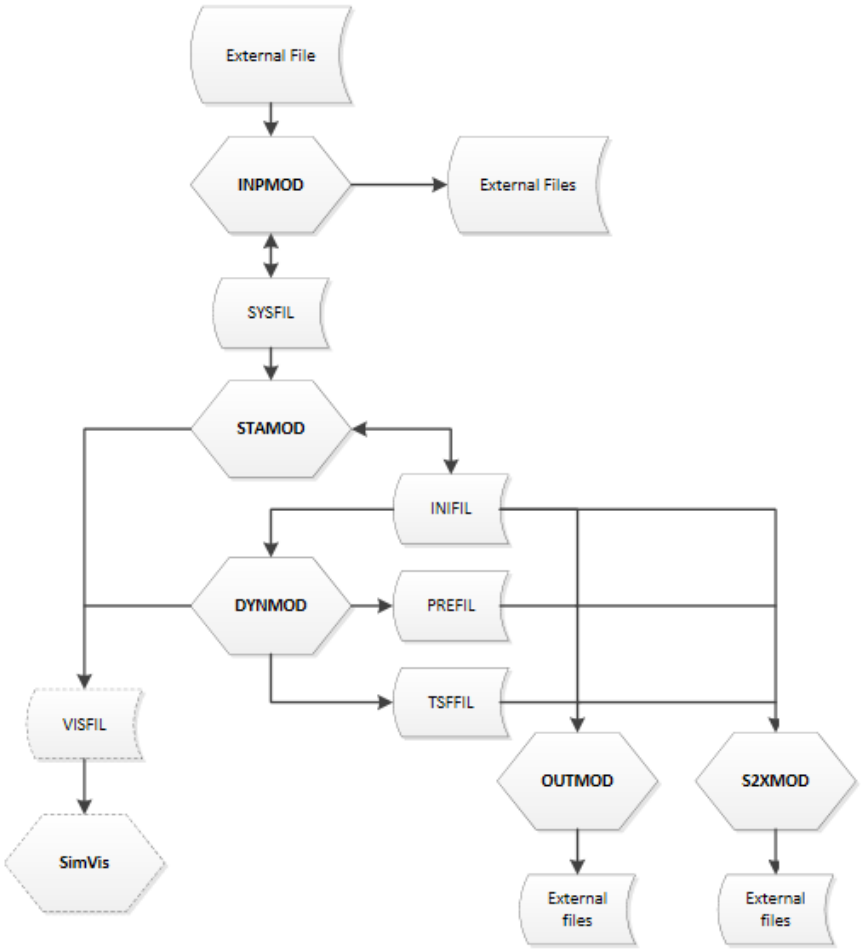

Figure 34: Flowchart of SIMO program structure from Marintek, 2018.

5.1.7 RIFLEX program structure

To use software for complicated calculations, some insight to how the program works is essential. This subsection will be used to explain the inner workings of RIFLEX.

This program is built quite similar to SIMO, and the structure can be seen in Table 11. The second column gives the sub-programs, which communicates through a common file-system.

Table 11: RIFLEX program structure according to Marintek, 2018.

RIFLEX	INPMOD	File system for communication between modules	Input data base organisation
	STAMOD		Static analyses
	DYNMOD		Time domain dynamic analyses
	FREMOD		Frequency domain dynamic analyses
	OUTMOD		Post-processing and output by print/plot

A more detailed description of each module:

- **INPMOD**
  This module reads the input data and organizes it for use in later analyses. Once this module has been run, several other analyses can be run without having to rerun this one. Unless the input data has been changed naturally.
- **STAMOD**
  The STAMOD module can run several types of static analyses. These results can be used in parameter studies, or to define initial conditions for succeeding dynamic analyses. Element mesh and key data for finite element analysis is also generated here, based on the input from INPMOD.
- **DYNMOD**
  This sub-program carries out dynamic time domain analyses on the basis of the final static configuration from STAMOD and environmental data as forces displacements. You can perform several runs in this module without running INPMOD or STAMOD again. The calculated dynamic response is stored for post processing in OUTMOD. It is also possible to calculate natural frequencies and modeshapes here.
- **OUTMOD**
  OUTMOD performs the post processing of results obtained in STAMOD and DYNMOD. It can also export time series data to various other file formats.

It should be noted that there were no additional information regarding the FREMOD module in the software manual, which is why it is not mentioned in the list above (Marintek, 2018).

A flowchart of how these modules communicate through the shared file-system can be seen in Figure 35.

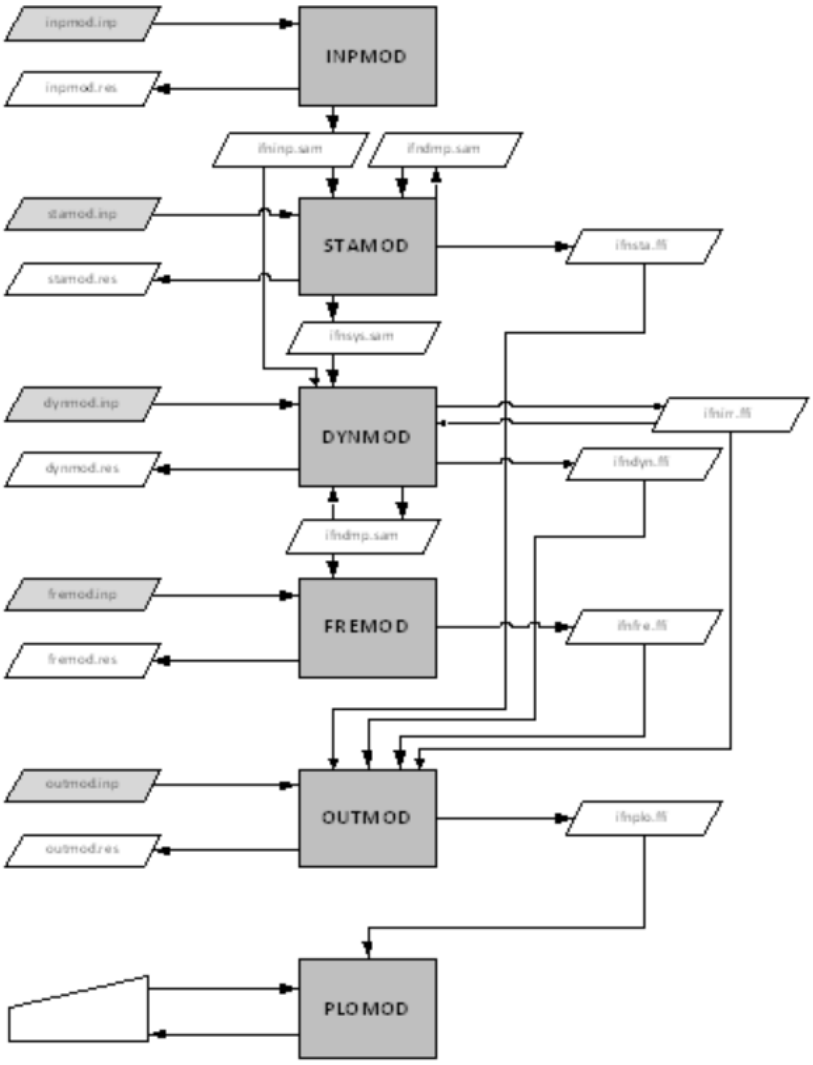

Figure 35: Flowchart of communication between RIFLEX modules, imported from Marintek, 2018.

5.1.8 Coupled and uncoupled analysis definition

The terms *coupled* and *uncoupled* analysis has been used several places in this thesis, and although a generic explanation was given in Section 3.7, a more precise definition of how this is performed in SIMA should be presented. The terms themselves refers to how the mooring system is incorporated into the process of solving the equations of motion (K. Larsen, 2022).

Uncoupled
The uncoupled procedure is best explained in steps:

1. Solve for a static condition of mooring and large volume vessel. As explained

in Section 3.7.1.

2. Go to next time-step in analysis.

3. Use stiffness from previous step to solve the vessels equations of motion with environmental condition of this step.

4. Use new position of vessel to statically solve for new mooring stiffness. Here it is important to note that the mooring is not affected by the dynamic environment such as current and waves. It is simply calculated from the static position of the vessel in this current step.

5. If the desired length of simulation is not reached, go back to step 2.

Since the stiffness from the mooring system is not calculated in the same time-step as the vessel motion, the line tension achieved is within the quasi-static category (see Section 3.7.2). This is the case whether or not the mooring is modelled as a catenary line or using a FEM method.

There are two methods for solving step 3 in SIMO, depending on what input is available:

- **Method A:** If RAOs for direct wave-frequency response is available, this method is selected.

  1. Wave frequency response is computed in frequency domain, and then inverse Fast Fourier transform (FFT) into time domain:

  $$\begin{aligned}&(m + A(\omega)) \cdot \ddot{x}_{WF} + (C(\omega) + D_l) \cdot \dot{x}_{WF} + K \cdot x_{WF} = q^1_{wa}(\omega)\\ &x_{WF}(\omega) = (-\omega^2(m + A(\omega)) + i\omega(C(\omega) + D_l) + K)^{-1} H^1(\omega) \cdot \zeta_a(\omega)\end{aligned} \tag{56}$$

  2. Low frequency response is calculated in the time domain, with the same realisation for the wave elevation as is used for the wave frequency response:

  $$\begin{aligned}&(m + A(\omega = 0)) \cdot \ddot{x}_{LF} + D_l \cdot \dot{x}_{LF} + D_q \cdot \dot{x}_{LF}|\dot{x}_{LF}| + K(x_{LF}) \cdot x_{LF}\\ &= q_{cu} + q_{wi}(t) + q^2_{wa}(t)\end{aligned} \tag{57}$$

  3. The total motion is then $X = x_{WF} + x_{LF}$.

- **Method B:** If wave-force transfer functions (retardation function) is known, the motion can be calculated directly using these. The equation of motion then becomes:

  $$\begin{aligned}&(m + A(\omega)) \cdot \ddot{x} + C(\omega)\dot{x} + D_l\dot{x} + D_q\dot{x}|\dot{x}| + K(x) \cdot x\\ &= q_{cu} + q_{wi}(t) + q^1_{wa}(t) + q^2_{wa}(t)\end{aligned} \tag{58}$$

  Where

  $$\begin{aligned}A(\omega) &= A_\infty + a(\omega)\\ C(\omega) &= C_\infty + c(\omega)\end{aligned} \tag{59}$$

Then, the total motion, x, is solved with numerical integration in the time domain using retardation functions $h(t)$. The retardation functions is used because of frequency dependant added mass, $A(\omega)$, and damping $C(\omega)$.

$$\begin{aligned}&(m + A_\infty) \cdot \ddot{x} + D_l \cdot \dot{x} + D_q \dot{x}|\dot{x}| + K(x) \cdot x + \int_0^t h(t-\tau) \cdot \dot{x} d\tau \\ &= q_{cu} + q_{wi}(t) + q_{wa}^1(t) + q_{wa}^2(t)\end{aligned} \tag{60}$$

Where

$$h(\tau) = \frac{2}{\pi} \int_0^\infty c(\omega) cos(\omega\tau) d\omega \tag{61}$$

Coupled
The coupled method calculates line forces in the same step as the vessel motions, to achieve equilibrium. The procedure goes as follows:

1. Solve for static condition of mooring and large volume vessel. As explained in Section 3.7.1
2. Go to next time-step in analysis.
3. Solve the equation of motion with both vessel and mooring forces being considered. Here, unlike the uncoupled method, the mooring lines are affected by the dynamic environment. Each element in the FEM formulation of the mooring lines takes wave and current forces into account.
4. If the desired length of simulation is not reached, go back to step 2.

This formulation allows for dynamic effects, as discussed in Section 3.7.3, from the mooring. The solution of step 3 uses *Method B* from the uncoupled description above.

5.2 Simulation model

It was decided in cooperation with co-supervisor Martin Søreide in ScaleAQ that it would be beneficial to look at a generic mooring setup instead of designing a site-specific case, due to the nature of the thesis and best use of the time available. Therefore, ScaleAQ provided some model specifications, for a generic feed barge mooring case, given in Table 12 and Table 13. These are the specifications on which the model was built.

Table 12: Barge specifications given by ScaleAQ. **Values given with reference coordinate system in middle of vessel.*

Variable	**Variable name (Unit)**	**Value**
Length between perpendiculares	(m)	33.0
Breadth	(m)	13.5
Draught, midship	(m)	3.888
Sinkage	(m)	0
Trim	(deg)	0
Displacement	(tonnes)	1698.0
Vertical center of buoyancy	KB (m)	-
Vertical center of gravity	VCG (m)	3.888*
Longitudinal center of buoyancy	LCB (m)	-
Longitudinal center of gravity	LCG (m)	16.5
Block coefficient	Cb	0.953
Water plane area coefficient	Cw	1
Prismatic coefficent	Cp	-
Mid section are coefficent	Cm	0.965
Longitudinal metacentric height	GM1	-
Transverse metacentric height	GMt	-
Roll radius of gyration	r44	5.063*
Pitch radius of gyration	r55	8.250*
Yaw radius of gyration	r66	8.250*
Roll-yaw radius of gyration	r46	0.000*

Table 13: Mooring specification given by ScaleAQ.

Mooring lines	**Symbol**	**Unit**	**Value**
Type: Octogonal	-	-	-
Total length of mooring lines	L	m	210
Length top line	L	m	27.5
Length of middle line	L	m	100
Length of bottom line	L	m	82.5
Stiffness of mooring	k	N/m	149 798
Number of mooring lines	-	-	8

5.2.1 Barge configuration

The barge was modelled as a box, illustrated in Section 5.1.1, not considering the geometry of the topside. Since wind loads are not considered in this thesis, a box geometry was found to be adequate.

Several attempts to use HydroD, as described in Section 5.1.2, to obtain hydrodynamic data were performed without success. Some of the RAOs did not compute correctly, which led to odd results in the later analyses. Therefore, the alternative method, presented in Section 5.1.3, was utilized. A similar barge was selected from

the large database, and the hydrodynamic data from this barge was adapted to fit into this analysis. A comparison between main specs of the two barges can be found in Table 14. The main parameters of the barge was found to be a good fit. Additionally, since this thesis focuses on the mooring, as long as the configuration is the same for all runs, making comparisons good, it is not paramount to have *perfect* barge response.

Table 14: Comparison between main specifications of the barge given by ScaleAQ and the barge found in the hydrodynamic database (Zang, 2017.)

Variable	**Simulation Barge**	**Database barge**
Length	33 (m)	34.05 (m)
Breadth	13.5 (m)	12 (m)
Vertical centre of gravity	3.888 (m)	4.076 (m)
Roll radii/breadth	0.375 (-)	0.35 (-)
Pitch radii/length	0.25 (-)	0.25 (-)

5.2.2 Mooring line configuration

The main mooring line specifications were given by ScaleAQ, as can be seen in Table 13. However, this data set is not a complete mooring description, information such as which dimension mooring lines to use, how much pre-tension to apply and which drag coefficients to use was decided by the author. These values can be seen in Table 15. The drag coefficients were taken from a DNV standard, as shown in Section 3.6 (DNV, 2013).

The dimensions of the mooring lines were chosen by approximating this 3D system, as a 2D catenary system. A MATLAB script applying 2D catenary theory, as presented in Section 3.1, were used to iteratively find adequate maximum stiffness of the system. Which ScaleAQ suggested to be around $150\frac{kN}{m}$, as seen in Table 13. The MATLAB script utilized was originally written by professor Pål Lader, and edited for use in this thesis. The script can be seen in Appendix E. After iterating with several line dimensions, the results shown in Figure 36 was found to be suitable, and thus corresponds with dimensions given in Table 15 and a pretension value of 38kN for all lines.

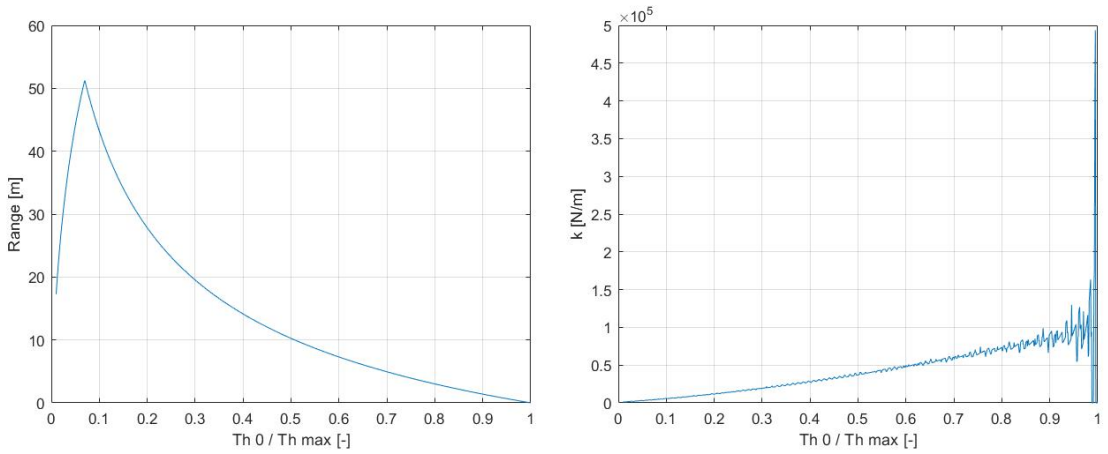

(a) 2D range approximation.

(b) 2D stiffness approximation.

Figure 36: Results from 2D approximation code given in Appendix E.

Table 15: Mooring line specifications selected by author.

Line type	**Dimension (mm)**	**Transverse drag coeff. (-)**	**Longitudinal drag coeff. (-)**	**E-mod (GPa)**	**Weight (kg/m)**
Top chain	30	1.4	1.15	210	18.36
Bottom chain	48	1.4	1.15	210	49
Middle fiber rope	72	1.6	-	20	3.6

The number of elements to be used in the FEM formulation of the mooring lines were selected based on trial and error. Too long elements caused numerical instability since element rotations became too large, especially in the point where the mooring line lifts from the seabed. Simultaneously, smaller elements allow for larger time-steps, since the rotation per element becomes smaller. The final values selected, as can be seen in Table 16, were based on finding a good trade-off.

Table 16: Mooring line element length specification.

	Top-line[m]	**Middle line [m]**	**Bottom line[m]**
Element length	0.275	0.5	0.275

Finally, one model was created using state of the art SIMO-RIFLEX coupled analysis, as presented in Section 5.1.5. While another was created with identical dimensions in stand-alone SIMO. This was done in order to facilitate comparisons of coupled and uncoupled analysis. A 3D visualisation of both models in waves can be seen in Figure 37 and Figure 38.

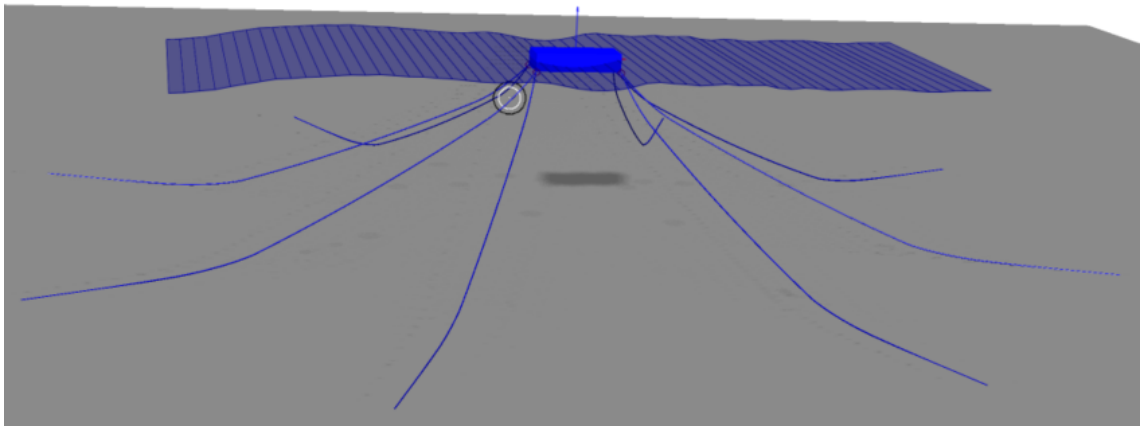

Figure 37: 3D visualisation in SIMA of uncoupled SIMO model.

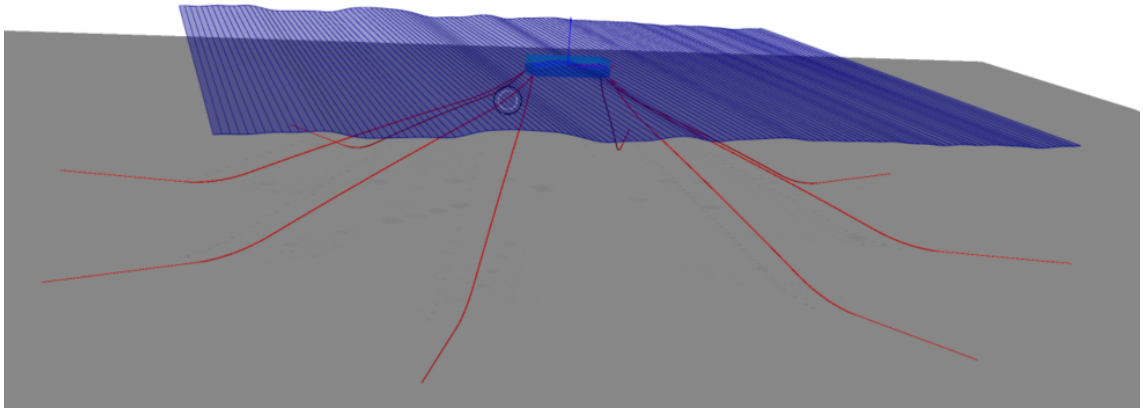

Figure 38: 3D visualisation in SIMA of coupled SIMO-RIFLEX model.

5.2.3 Environment

The choice of which environmental conditions to run were largely influenced by the cooperation with ScaleAQ. Since ScaleAQ had performed real-life model tests of a similar setup, identical environmental conditions for my analyses were thought to facilitate good grounds for comparisons. The model tests was performed with conditions equal to *Load combination 1 & 2* in Table 17. In addition, NS9415 allows for regular wave analysis instead of irregular waves, following Equation 55. *Load combination 3 & 4* corresponds to *load combination 1 & 2* under this requirement, respectively.

The time steps seen in Table 17 were decided from a parameter study. For the harshest irregular load, *load combination 1*, the time-steps were decreased steadily until good numerical stability was achieved. Resulting in a time-step of 0.02 for irregular waves, and 0.01 for regular waves. The reason behind the lower time-step for the regular wave analysis, was large initial motions before the vessel *settled* in the waves.

The simulation length was decided as a compromise between computational time, and good irregular response representation. According to the research performed in Section 3.7.3, simulation length should be longer than 5 minutes to account for wave-drift forces in deep water. However, since this thesis considers 65m water depth, this wave-drift period will be smaller. Simultaneously, simulation length should be between 20 minutes and 3 hours to statistically account for most wave combinations in the specific sea state, as presented in Section 3.3. A compromise of 20 minute simulation length were therefore found to give good response coverage and acceptable computational time.

The amount of runs with random seeds for the irregular analysis were decided from the amount of n runs required to achieve convergence of the mean value and standard deviation of the response. This is a commonly used method to determine statistical convergence. As can be seen in Figure 39, after 12 runs adequate convergence was achieved. Initially,it was intended to have more runs in order to use the extreme value distribution, presented in Section 3.4.3. This would have made it possible to compare 10 -and 50 year extreme responses. However, it would have required too many runs to get a good statistical foundation, and the time available did not allow for this.

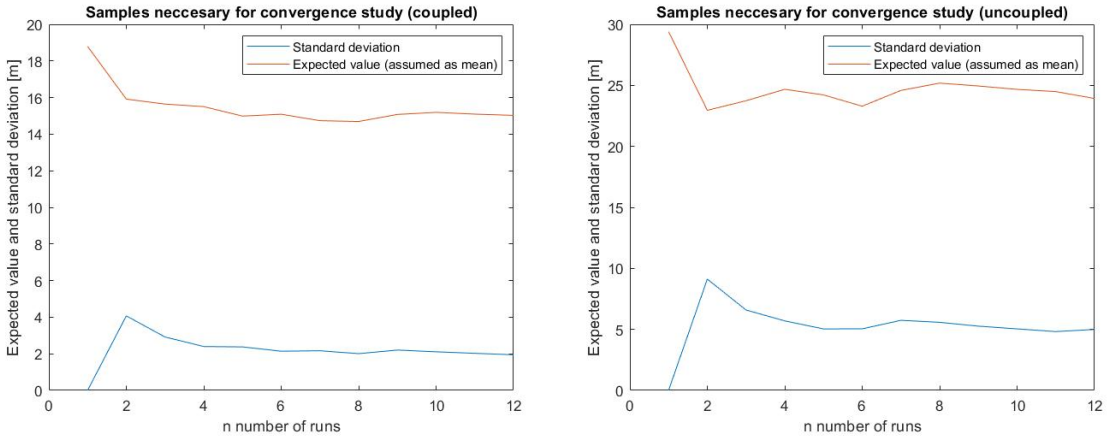

(a) Coupled

(b) Uncoupled.

Figure 39: Convergence plots for mean and standard deviation for vessel response for both coupled and uncoupled analysis.

The runs detailed in Table 17 were conducted for both the coupled and uncoupled model in SIMA with random seed numbers (except for load combination 5, where identical seed number was used for the coupled and uncoupled analysis). The JONSWAP 2-parameter wave spectrum was used to describe the wave-field (see Section 3.3.3) and a constant current along the water column was used. An overview of the mooring setup and wave -and current direction can be seen in Figure 40.

Table 17: Environment and simulation definition

Simulations				**Seeds [n]**	**Time-step [s]**	**Length [min]**
Irregular	**V_c [m/s]**	**H_s [m]**	**T_p [s]**			
Load combination 1	0.5	6	11	12	0.02	20
Load combination 2	0.5	4	8.5	12	0.02	20
Load combination 5	0.5	2	7	1	0.02	20
Regular	**V_c [m/s]**	**Wave height [m]**	**Period [s]**			
Load combination 3	0.5	11.4	11	1	0.01	20
Load combination 4	0.5	7.6	8.5	1	0.01	20

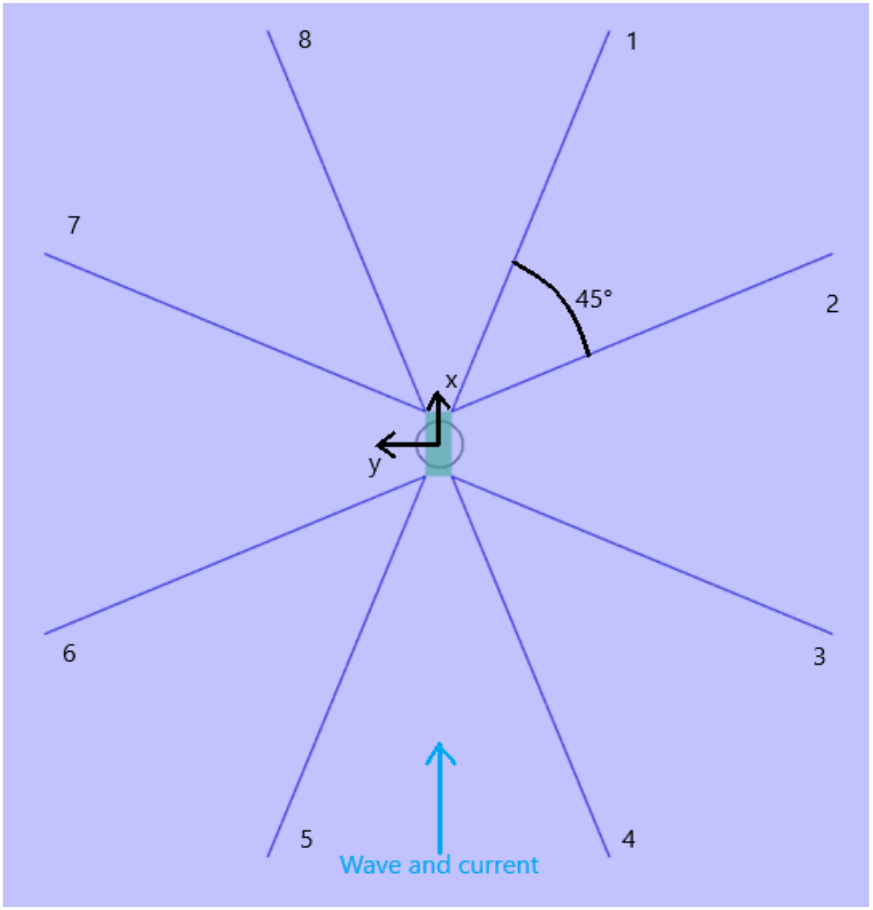

Figure 40: Model setup overview, picture from SIMA.

5.3 Comparison between coupled and uncoupled analysis

One of the main goals of this thesis was to investigate differences in state of the art time domain analysis methods, in irregular exposed wave conditions. Two frequently used methods were identified to be *coupled* and *uncoupled* analysis. This section will describe the methodology of how a comparison between these methods were performed.

5.3.1 Mooring line tension

The mooring line tension from the top element in line 5 and 8 (see Figure 40) was extracted for all runs at a sampling rate of 0.5 seconds. This was done in order to make comparison between a leeward and windward line possible. The tension force was filtered in a low and high frequency response spectrum and compared for the coupled and uncoupled model. The tension was filtered using MATLAB functions *lowpass* and *highpass*, with passband frequencies of $\frac{1}{60}Hz$ and $\frac{1}{20}Hz$ for low -and wave frequency, respectively (Mathworks, 2022a,b). The MATLAB code utilized for post-processing can be seen in Appendix G.

5.3.2 Vessel response

The barge response was extracted for x, y and z directions at a sampling rate of 0.5 seconds. The total response was then calculated using Equation 62. The code utilized for post-processing can be seen in Appendix F

$$X_{tot} = \sqrt{(X_x^2 + X_y^2 + X_z^2)} \tag{62}$$

This total response was then post-processed:

- The response was filtered into low and high frequency response and frequency response spectrums were created for both coupled and uncoupled model (see Section 3.4.1).
- Weibull distribution fitting was performed for the peaks of both coupled and uncoupled analysis (see Section 3.4.2). The *peak over threshold* method was used to identify peaks. This method is mentioned as a valid method in NS9415.

The results from different load combinations were compared to discover trends and discuss results. An additional small analysis, *load combination 5* in Table 17, was performed to support or contradict trends.

5.3.3 Regular and irregular response

The requirement from NS9415, as discussed in Section 3.8.5, was investigated by comparing the irregular load combination 1 and 2 to the corresponding regular load combination 3 and 4, respectively. The code utilized for regular analysis post processing can be seen in Appendix H.

5.3.4 Comparison to small scale model test

A results plot for a windward line in load combination 2, from ScaleAQ's small-scale model test was made available. This plot was compared to the corresponding

analysis plots from the coupled and uncoupled models. This was done in order to validate the models.

5.3.5 Discussion of results

Finally, the results are discussed up against the feed barge risk picture, with the risk assessment performed in Section 4 in mind, and the governing standard, NS9415 (Standard Norway, 2021).

6 Results and discussion

This section will present the results gained from the methods presented in Section 5, some intermediate observations and thoughts will be given. At the end of the section, these results will be discussed up against the goals of the thesis.

6.1 Vessel response

The vessel response results for analyses presented in Table 17 will be presented in this subsection.

Useful for interpreting analysis results is the eigenperiods for the system. SIMA calculates these for the entire coupled combined system, and the results are given in Table 18. The same feature is not available for the uncoupled model. Most likely because the mooring works as springs on the barge, and each spring stiffness is dependant on vessel position and mooring line tension, as shown in Section 3.1. However, one can assume that the uncoupled model will express similar eigenperiods since the models are identical, and the main difference are in form of damping (see Section 3.7). Damping, as shown in Section 3.6.1 and Equation 48, makes for a slight reduction in the natural frequency. Meaning that the uncoupled model should have a bit higher natural frequencies, or lower natural periods.

Table 18: Calculated eigenperiods for the coupled model in SIMA

Motion	**Eigenperiod [s]**
Surge	57.5
Sway	61.0
Yaw	34.1

6.1.1 Load combination 1

The response from the coupled and uncoupled analysis, with identified peaks, can be seen in Figure 41 and Figure 50. It was noted that the coupled response appeared rather consistent for various seed numbers when compared to the uncoupled response. This is most likely due to lack of damping effects from the mooring lines in the uncoupled analysis (see Section 3.6.2), making it easier for the uncoupled model to be excited by eigenmodes.

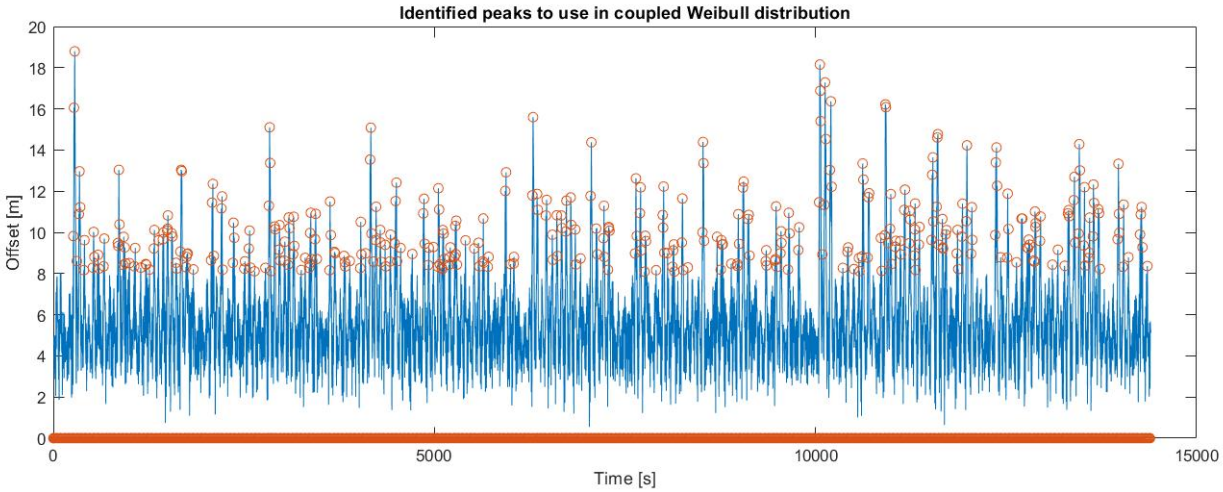

Figure 41: Plot of identified peaks in coupled response time series for use in Weibull fitting of load combination 1.

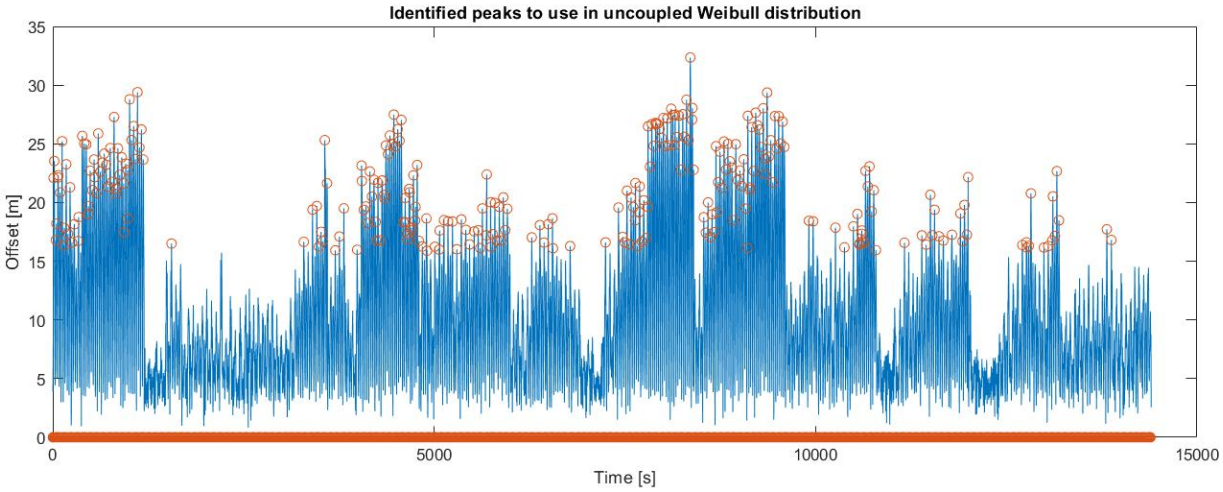

Figure 42: Plot of identified peaks in uncoupled response time series for use in Weibull fitting of load combination 1.

Fitting of a Weibull distribution for peaks larger than the mean value plus the standard deviation of each response time series was performed (peak over threshold method). The two fitted distributions can be seen in Figure 43. It is clearly visible from these distributions that the uncoupled analysis consists of much larger response.

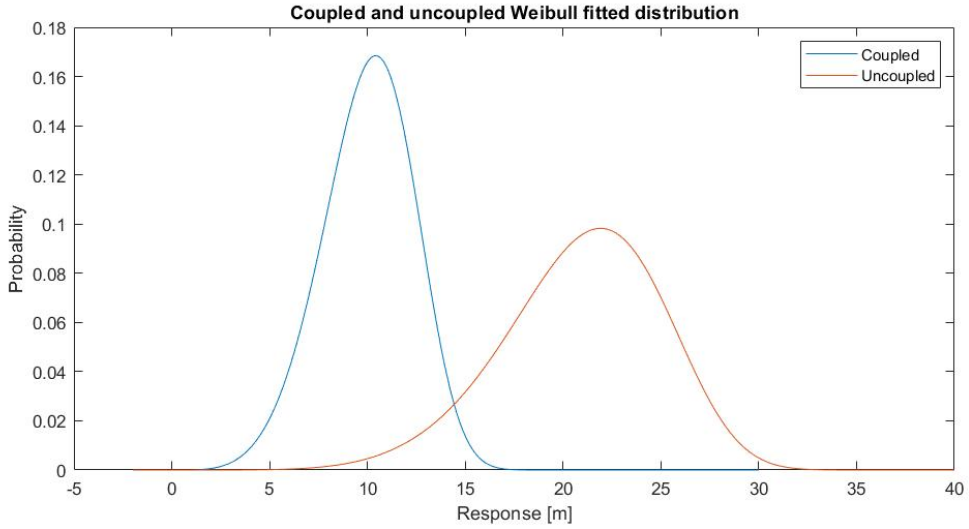

Figure 43: Coupled and uncoupled peaks fitted to Weibull distribution of load combination 1

A quantile-quantile plot of each distributions were made, to see if the Weibull distribution gave a good fit, and if it was suited for predicting extreme response values. These plots can be seen in Figure 44. It was discovered that the uncoupled QQ-plot made a good fit at the extreme, while the coupled QQ-plot did not fit at all. It was therefore concluded that the distribution fitting was unsuitable for predicting extreme response values. Comparison between the analyses should therefore not be performed by extreme value approximation with this distribution.

Theoretically, this can be explained partly by the assumptions that the Weibull distribution makes, as explained in Section 3.4.2. The response data is not narrow-banded.

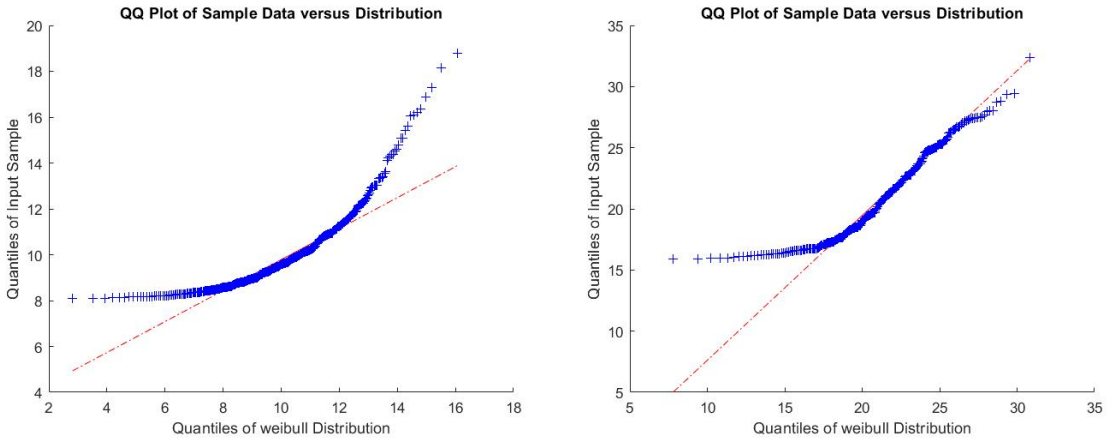

(a) Coupled (b) Uncoupled

Figure 44: Coupled and uncoupled QQ plot for Weibull distribution fitting for load combination 1.

The response was filtered into low-and wave frequency response (see post processing

code in Appendix F), and a frequency response spectrum was made for both models, as can be seen in Figure 45 and Figure 46. The Y-axis of these plots were made in decibel-scale, meaning that it is generally only the largest peak of each plot that is of most interest. For the coupled model, the most dominating low frequency response period was $\frac{1}{0.0149} = 67.11s$, while it was $\frac{1}{0.03883} = 25.7s$ for the uncoupled model.

For the wave-frequency response, the most dominating period for the coupled model was $\frac{1}{0.09838} = 10.16s$, while it was $\frac{1}{0.07888} = 12.67$ for the uncoupled model.

Even though the difference was quite large for the low-frequency range, it is clearly visible that roughly the same response frequencies are present at both the coupled and uncoupled model, at different strengths. A possible explanation for this, is that the yaw eigenperiod for the uncoupled model is being excited with no damping from the mooring lines, causing large motions. The yaw eigenperiod for the coupled model, as stated in Table 18, was found to be $34.1s$. The largest peak for the uncoupled response of 25.7s is close to the coupled yaw eigenperiod, which strengthens this hypothesis. It is additionally strengthened by the fact that a undamped natural period is shorter than damped, as shown in Section 3.6.1.

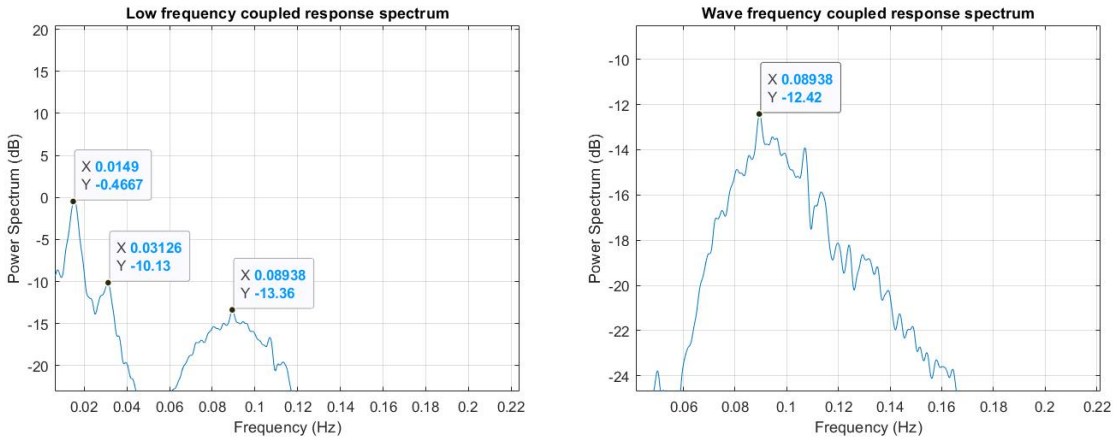

(a) Coupled low frequency response spectrum (b) Coupled wave frequency response spectrum

Figure 45: Coupled frequency spectrum power plots for load combination 1.

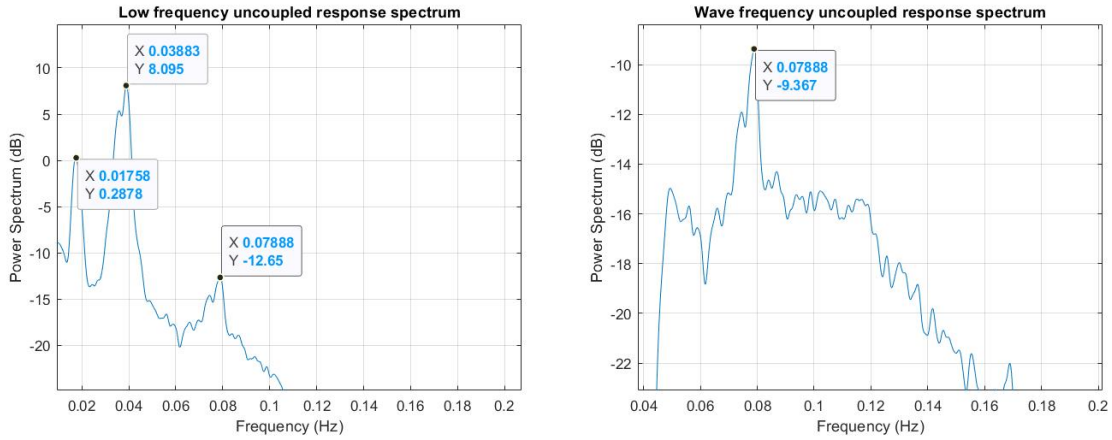

(a) Uncoupled low frequency response spectrum

(b) Uncoupled wave frequency response spectrum

Figure 46: Uncoupled frequency spectrum power plots for load combination 1.

From Figure 47 and Figure 48, the difference in scale for low -and wave frequency response becomes apparent. This was expected, as it is in compliance with the literature review, more specifically Section 3.5.2. It is worth to note that the uncoupled low frequency response is larger than coupled low frequency response, again supporting the hypothesis that low-frequency eigenmodes are being excited in this model.

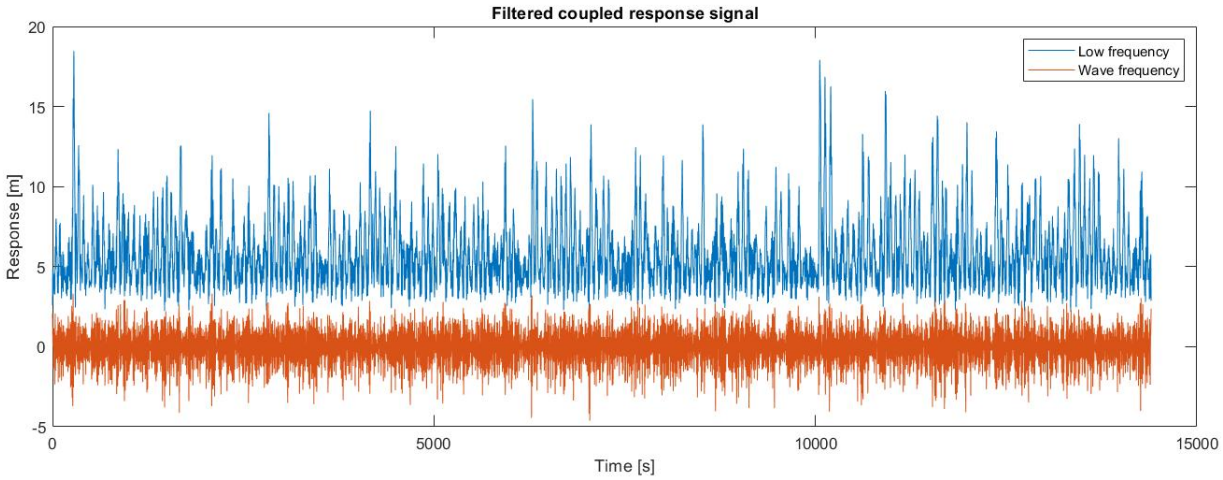

Figure 47: Plot of filtered response for total coupled response time series for load combination 1.

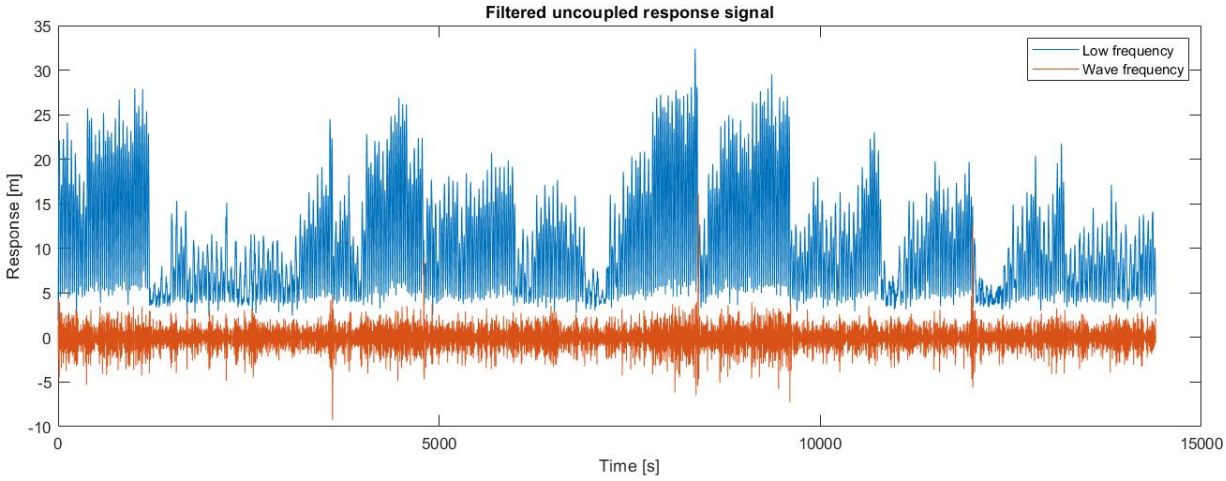

Figure 48: Plot of filtered response for total uncoupled response time series for load combination 1

Since the Weibull distribution was a poor fit for response data, it was deemed more appropriate to use mean, standard deviation and maximum values to compare the response. This data is collected and presented in Table 19. From a design standpoint, the uncoupled analysis gives max response $\frac{32.3551}{18.7936} = 1.72$ times higher when compared to the coupled analysis. Which naturally would lead to much larger mooring loads, demanding a system capable of higher loads. Additionally, the wave-frequency max load is $\frac{16.1285}{3.3133} = 4.86$ times higher for the uncoupled analysis. Larger wave-frequency loads are not crucial for mooring line design, but will definitely have impact on barge stability and fatigue life (see Section 3.5).

Table 19: Mean and standard deviation for the presented filtered and total response for load combination 1.

Response type	**Mean [m]**	**Standard deviation [m]**	**Max [m]**
Coupled			
Total response	5.8450	2.2342	18.7936
Low frequency response	5.8446	2.0423	17.7952
Wave frequency response	-3.3043e-05	1.0325	3.3133
Uncoupled			
Total response	10.1284	5.6870	32.3551
Low frequency response	10.1282	5.5293	32.4139
Wave frequency response	-0.0011	1.2558	16.1285

6.1.2 Load combination 2

The response from coupled and uncoupled response, with identified peaks, can be seen in Figure 49 and Figure 50. The same observation can be made for this load case, as for load combination 1: The coupled response seems more consistent when compared to the uncoupled model.

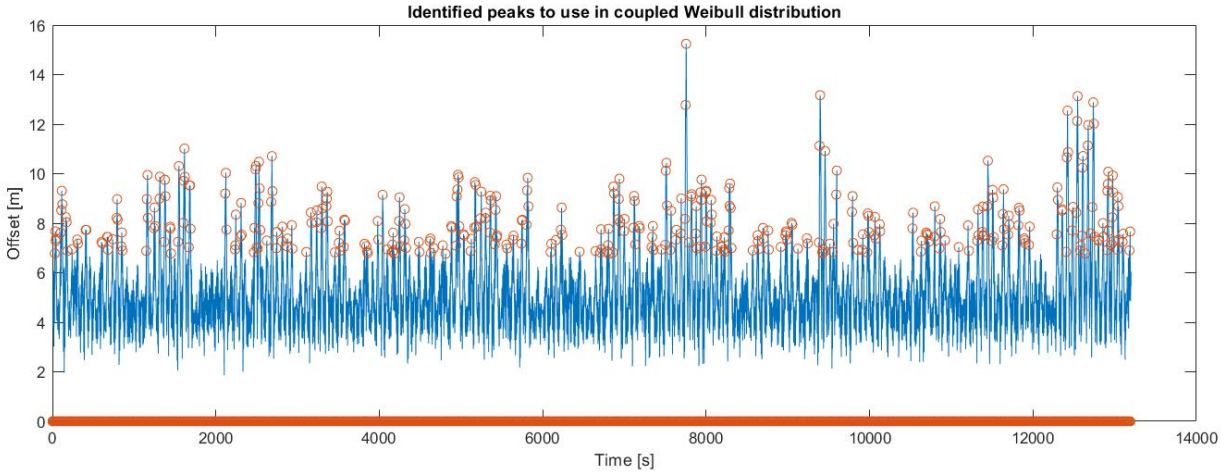

Figure 49: Plot of identified peaks in coupled response time series for use in Weibull fitting of load combination 2.

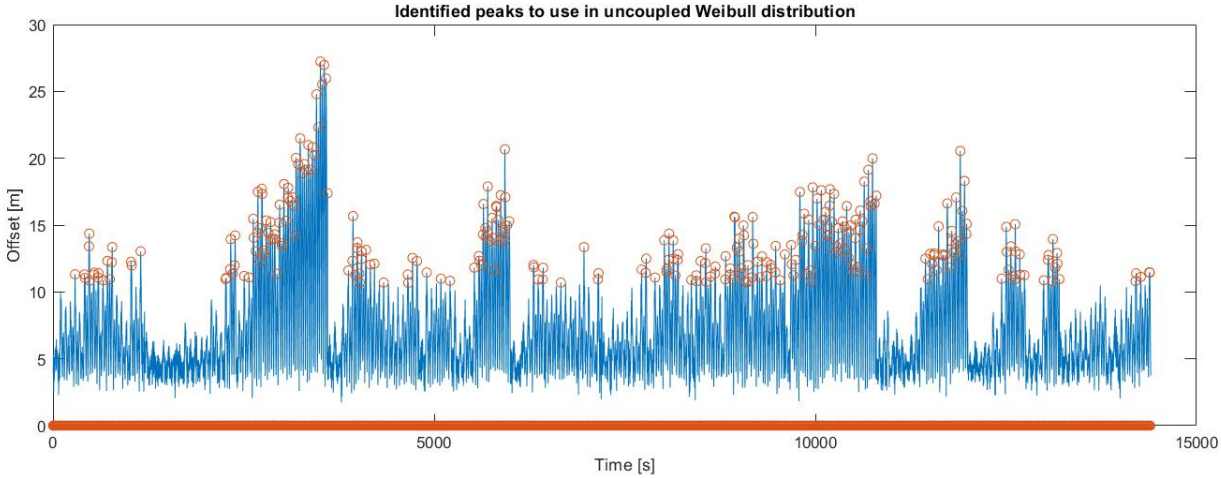

Figure 50: Plot of identified peaks in uncoupled response time series for use in Weibull fitting of load combination 2.

Fitting of a Weibull distribution for peaks larger than the mean value plus the standard deviation of each response time series was performed for this load combination also. The two fitted distributions can be seen in Figure 51. As with the distributions for load combination 1, it is clearly visible that the uncoupled model consists of much larger responses.

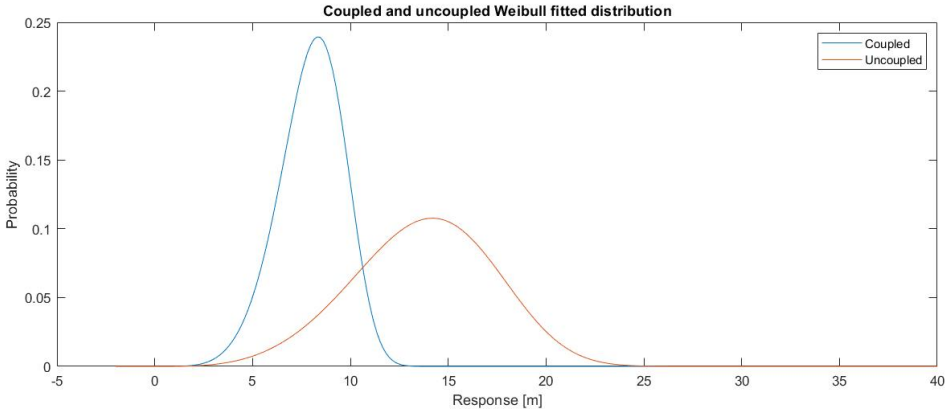

Figure 51: Coupled and uncoupled peaks fitted to Weibull distribution of load combination 2.

A quantile-quantile plot of each distributions were made, to see if the Weibull distribution gave a good fit, and if it was suited for predicting extreme response values. These plots can be seen in Figure 52. For this load combination, is can be seen that both the coupled and uncoupled response made a bad fit for the extreme values (right hand side tails). It was therefore concluded, similarly with load combination 1, that the distribution fitting was unsuitable for predicting extreme response values. Comparison between the analyses should therefore not be performed by extreme value approximation with Weibull distribution.

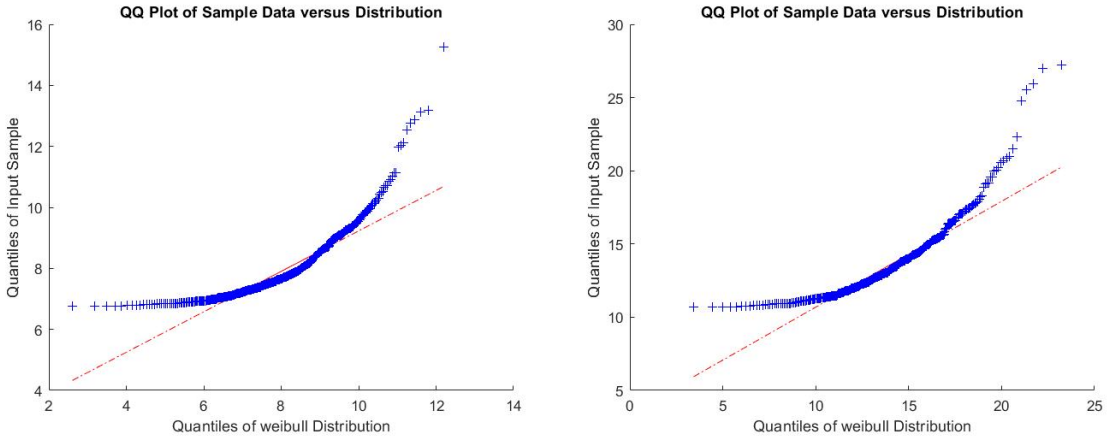

(a) Coupled (b) Uncoupled

Figure 52: Coupled and uncoupled QQ plot for Weibull distribution fitting for load combination 2.

The response was filtered into low -and wave frequency response for this load combination also (see post processing code in Appendix F), as can be seen in Figure 53 and Figure 54. For the coupled model, the most dominating low frequency response period was $\frac{1}{0.01612} = 62s$, while it was $\frac{1}{0.03883} = 25.7s$ for the uncoupled model.

The most dominating wave frequency was $\frac{1}{0.1187} = 8.4s$ and $\frac{1}{0.07131} = 14s$ for the coupled and uncoupled response, respectively. Although, the same frequencies are

visible in both spectrums.

The same low-frequency trends were visible in load combination 1, and the explanation is thought to be identical. The excitation of yaw-eigenmode in the uncoupled model due to lack of mooring damping is causing the large response at 25.7s. It should be noted that it is difficult to confirm this by hand calculations, as natural period estimates of moored systems is difficult because of stiffness change by vessel offset, as shown in Section 5.2.2.

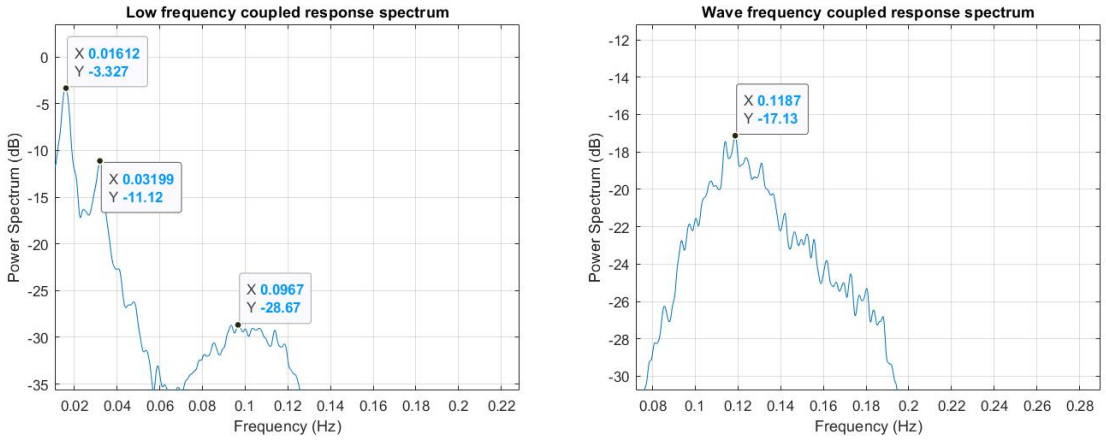

(a) Coupled (b) Coupled

Figure 53: Coupled frequency spectrum power plots for load combination 2

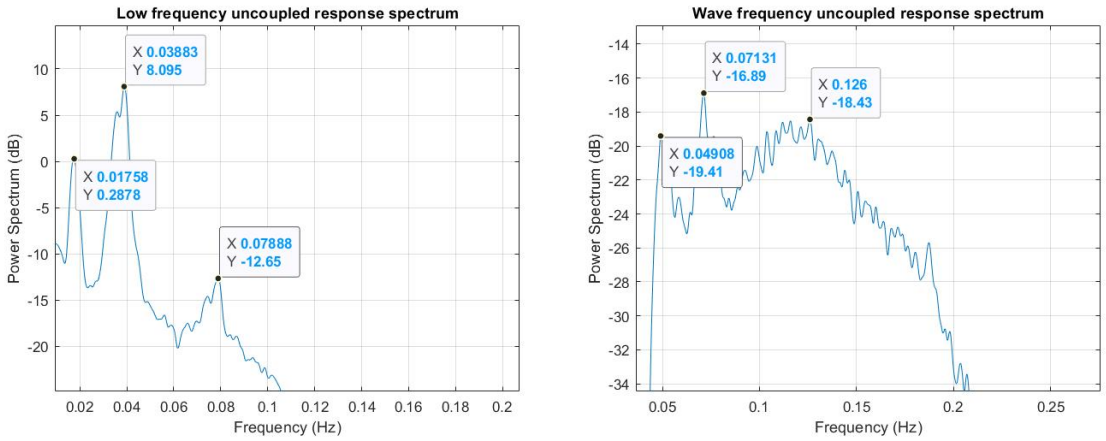

(a) Uncoupled low frequency response (b) Uncoupled wave frequency response

Figure 54: Uncoupled frequency spectrum power plots for load combination 2.

Figure 55 and Figure 56 shows the low -and wave frequency filtered response for load combination 2. Similarly as found for load combination 1, it is observed that the uncoupled low-frequency response is visibly larger than the coupled. Again supporting the hypothesis that low-frequency eigenmodes are being excited in the uncoupled model.

From Figure 56, a few very large wave-frequency responses can be seen. It is worth

to note that these individual responses could be induced by the filtering method used, and might not represent real wave frequency response.

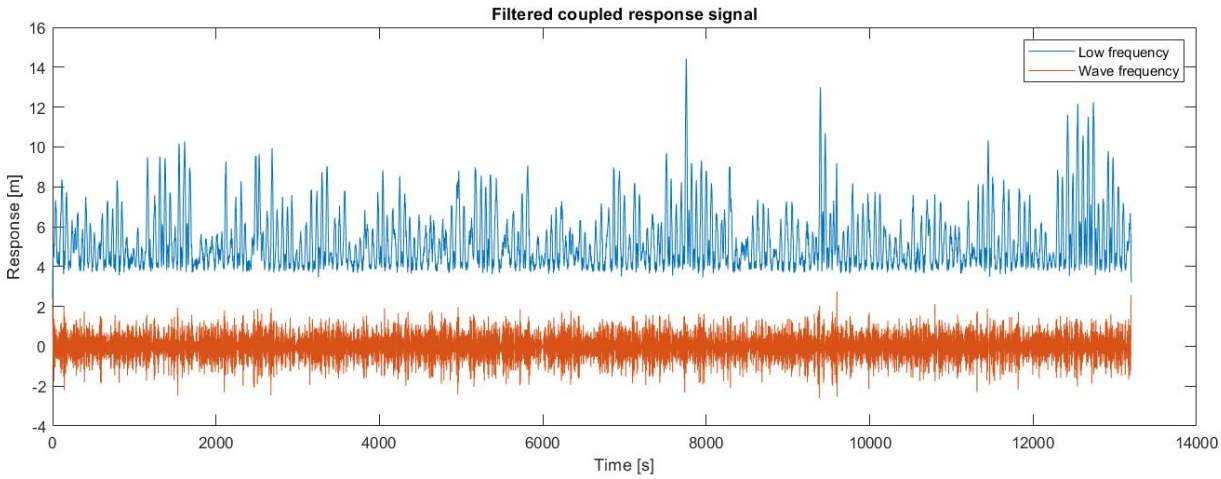

Figure 55: Plot of filtered response for total coupled response time series for load combination 2.

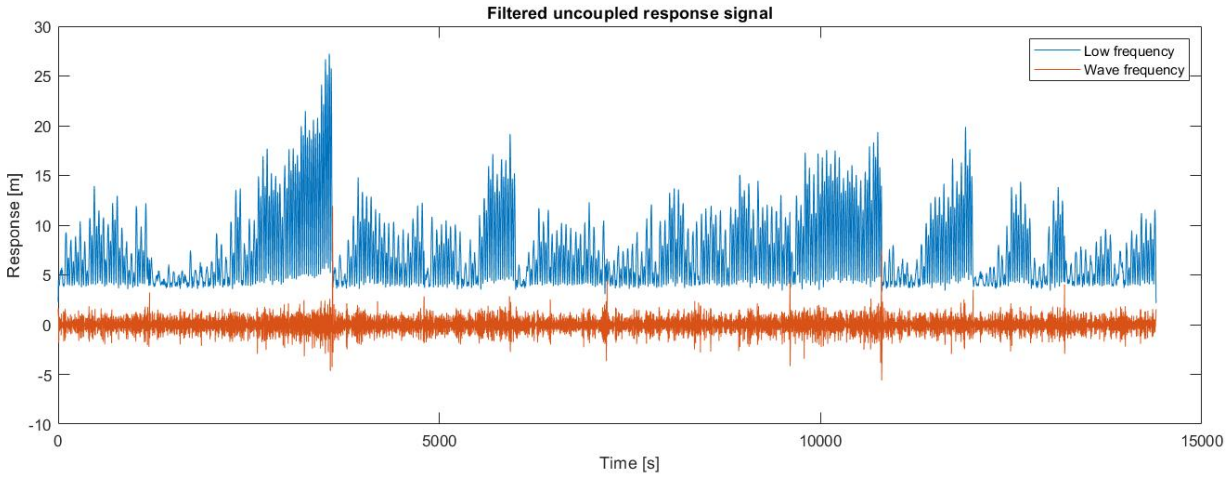

Figure 56: Plot of filtered response for total uncoupled response time series for load combination 2.

Since the Weibull fitting also gave poor approximation for extreme response in this load combination, mean, standard deviation and maximum values were thought more appropriate to compare. These results can be seen in Table 20. For load combination 2, the max response of the uncoupled analysis were $\frac{27.320}{15.2430} = 1.79$ times larger than the coupled max response. While the wave frequency uncoupled max response were $\frac{11.9294}{2.7488} = 4.33$ timer larger than the coupled. As states earlier, the max response is important for ULS design criteria, where a larger response will demand larger mooring system component dimensions. While, the wave frequency response is more important for barge stability and FLS.

Table 20: Mean, standard deviation and maximum values for the presented filtered and total response for load combination 2.

Response type	**Mean [m]**	**Standard deviation [m]**	**Max [m]**
Coupled			
Total response	5.2285	1.5299	15.2430
Low frequency response	5.2280	1.4055	14.4255
Wave frequency response	7.7092e-05	0.6277	2.7488
Uncoupled			
Total response	7.1824	3.4885	27.3230
Low frequency response	7.1821	3.4028	27.2370
Wave frequency response	4.6282e-04	0.7289	11.9294

6.2 Comparison of load combinations and discussion

This section will be dedicated to discuss the trends and differences discovered between the load combinations.

6.2.1 Load combination 1 and 2

This subsection will be dedicated to discuss the difference in results between load combination 1 and 2. Information was gathered from Table 19 and Table 20, to create Table 21, Table 22 and Table 23. In these tables, the uncoupled to coupled ratio of various interesting values are presented.

From these tables, some interesting potential trends are discovered. It seems that both the difference in *uncoupled/coupled* ratio is declining for both mean values and standard deviation for total response. Meaning that the differences increases with harsher environmental conditions. Also interesting, is the observation of max value change from load combination 1 to 2. This does not follow the same trend as mean values and standard deviation, on the contrary a small increase in ratio is observed from load combination 1 to 2.

Table 21: Uncoupled mean values divided by coupled mean values for load combination 1 and 2, and the change in these.

Mean values	**Load combination 1 [-]**	**Load combination 2 [-]**	**Change from 1 to 2 [%]**
Uncoupled/coupled			
Total response	1.74	1,37	-21
Low frequency response	1.73	1,37	-21
Wave frequency response	-	-	-

Table 22: Uncoupled standard deviation divided by coupled standard deviation for load combination 1 and 2, and the change in these.

Standard deviation	**Load combination 1 [-]**	**Load combination 2 [-]**	**Change from 1 to 2 [%]**
Uncoupled/coupled			
Total response	2.55	2.28	-11
Low frequency response	2.71	2.42	-11
Wave frequency response	1.22	1.61	32

Table 23: Uncoupled max values divided by coupled max values for load combination 1 and 2, and the change in these.

Max values	**Load combination 1 [-]**	**Load combination 2 [-]**	**Change from 1 to 2 [%]**
Uncoupled/coupled			
Total response	1.72	1.79	4
Low frequency response	1.82	1.89	4
Wave frequency response	4.86	4.34	-11

6.2.2 Additional analysis

In an attempt to confirm the trends discussed above, two more runs were performed with the models, with specifications given in Table 24. Milder environmental conditions were chosen to see if the trends discovered would continue, and the runs were performed on identical seed numbers to highlight only the coupled/uncoupled model differences. This method was performed due to lack of time. Preferably, this environmental condition should have been performed with an identical number of runs as load combination 1 and 2. This load combination was named *load combination 5.*

Table 24: Load combination 5.

Variable	**Coupled model**	**Uncoupled model**
Hs [m]	2	2
Tp [s]	7	7
Seed number [-]	2	2

The results from load combination 5 runs are given in Table 25.

Table 25: Mean, standard deviation and maximum values for the filtered and total response for load combination 5.

Response type	**Mean [m]**	**Standard deviation [m]**	**Max [m]**
Coupled			
Total response	4.2194	0.4207	6.0634
Low frequency response	4.2153	0.3240	5.5994
Wave frequency response	0.0070	0.3081	1.8761
Uncoupled			
Total response	5.2215	1.1622	8.6653
Low frequency response	5.2173	1.1322	8.3460
Wave frequency response	0.0070	0.2900	1.8247

To verify if the trends were continuous, Table 26, Table 27 and Table 28 were made. The downward trend in *uncoupled/coupled* response ratio seems to continue for this load combination, as can be seen from Table 26. This is also supported by the downward trend in the max responses, as can be seen in Table 28. The standard deviation is, however, larger for this load combination when compared to load combination 2.

Due to the fact that this load combination only contains one run of 1200s for each coupled and uncoupled model, the results should also be treated thereafter. However, the mean and max values does further indicate a lower difference between coupled and uncoupled response for milder weather conditions.

Table 26: Uncoupled mean values divided by coupled mean values for load combination 2 and 5, and the change in these.

Mean	**Load combination 2 [-]**	**Load combination 5 [-]**	**Change from 2 to 5 [%]**
Uncoupled/coupled			
Total Response	1.37	1.24	-9
Low frequency response	1.37	1.24	-9
Wave frequency response	-	-	

Table 27: Uncoupled standard deviation divided by coupled standard deviation for load combination 2 and 5, and the change in these.

Standard deviation	**Load combination 2 [-]**	**Load combination 5 [-]**	**Change from 2 to 5 [%]**
Uncoupled/coupled			
Total Response	2.28	2.76	21
Low frequency response	2.42	3.49	44
Wave frequency response	1.61	0.94	-42

Table 28: Uncoupled max values divided by coupled max values for load combination 2 and 5, and the change in these.

Max values	**Load combination 2 [-]**	**Load combination 5 [-]**	**Change from 2 to 5 [%]**
Uncoupled/coupled			
Total Response	1.79	1.43	-20
Low frequency response	1.89	1.49	-21
Wave frequency response	4.34	0.97	-78

6.3 Mooring line tension

This section will present line tension data from line 5, the windward line, and line 8, the leeward line (see Figure 40) and discuss the findings. The post-processing code utilized can be seen in Appendix G.

6.3.1 Load combination 1

In this subsection, data from load combination 1 will be presented and discussed.

Coupled

Figure 57 and Figure 58 shows coupled axial tension for the most and least loaded line, filtered into low -and wave frequency. As expected, the most loaded line has a higher total load when compared to the least loaded line. In addition, it is noted that the wave-frequency tension appears similar in magnitude for both lines.

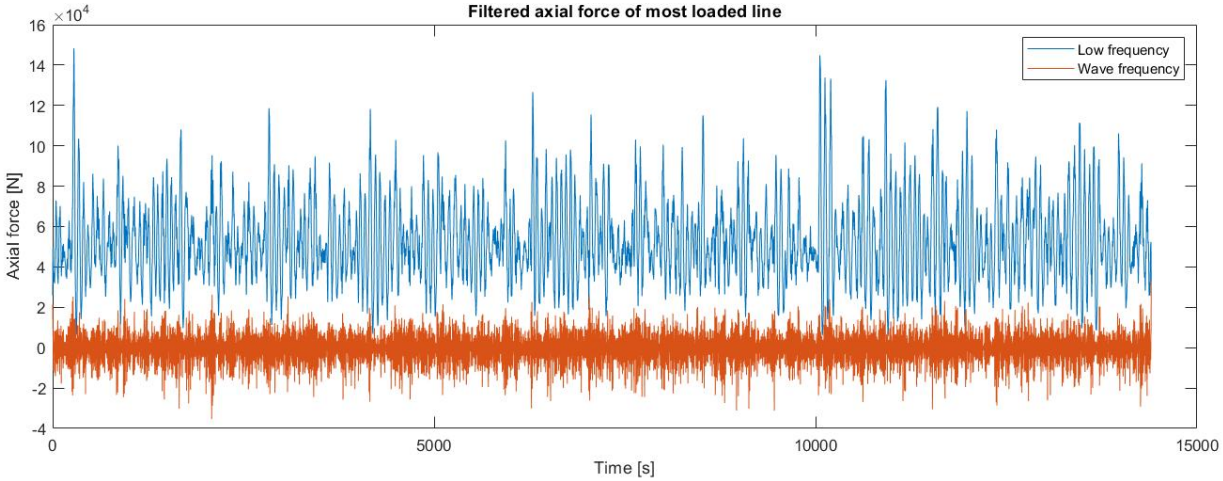

Figure 57: Plot of filtered axial force for most loaded line for load combination 1.

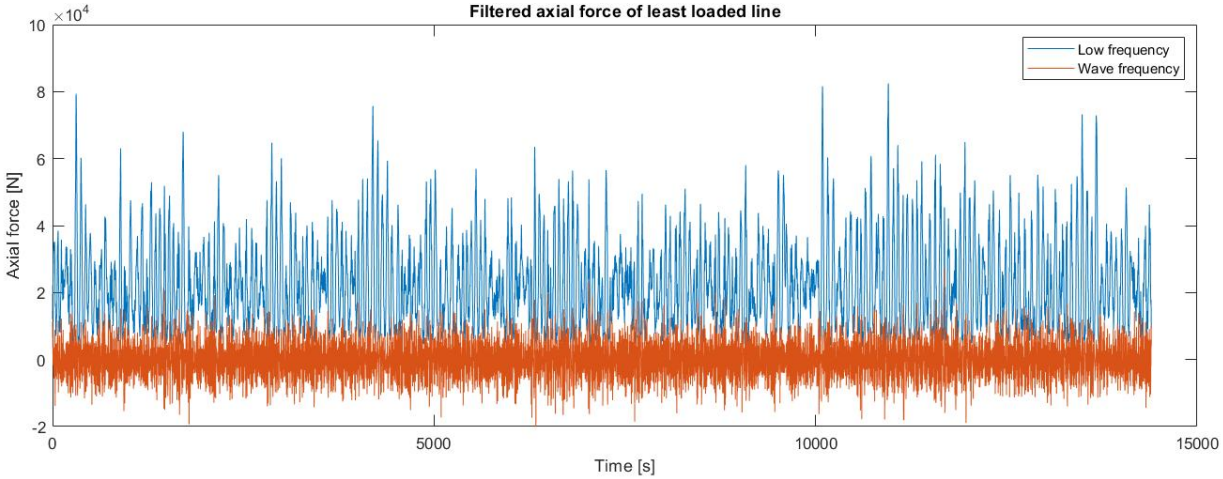

Figure 58: Plot of filtered axial force for least loaded line for load combination 1.

Frequency spectrums of the most loaded line in low -and wave frequency was created, as seen in Figure 59.

In the low frequency spectrum, $\frac{1}{0.01587} = 62.9s$ is the dominating response period. While it is $\frac{1}{0.08962} = 11.15s$ for the wave frequency response. The low frequency tension corresponds well with the slow-drift period found for the vessel response in Section 6.1.1. The wave-frequency tension corresponds well with the 11s peak period of this load combination.

It is also observed a minor peak in the wave-frequency spectrum at $\frac{1}{0.2132} = 4.7s$, which is most likely due to a local line eigenperiod being excited.

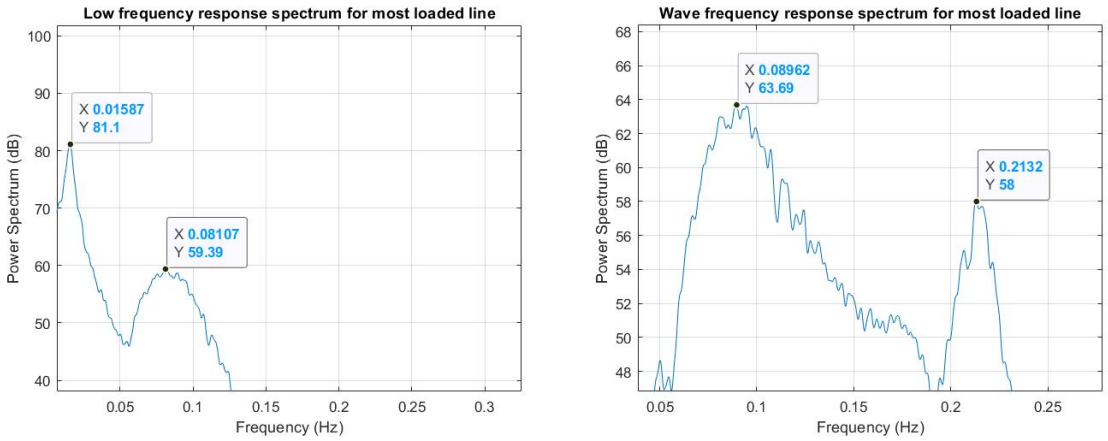

(a) Coupled low frequency

(b) Coupled wave frequency

Figure 59: Uncoupled frequency spectrum power plots for load combination 1.

Uncoupled

Figure 60 and Figure 61 shows uncoupled axial tension for most and least loaded line. It is immediately observed, as with the vessel response, that the line tension seem less consistent when compared to the coupled results. In addition, the wave frequency tension contributes less to the total load picture in the most loaded line when compare to the least loaded line.

The load pictures is expected given that the vessel response have a similar appearance. As discussed in Section 6.1, this erratic response picture is most likely caused by eigenmode excitation due to lack of mooring line damping.

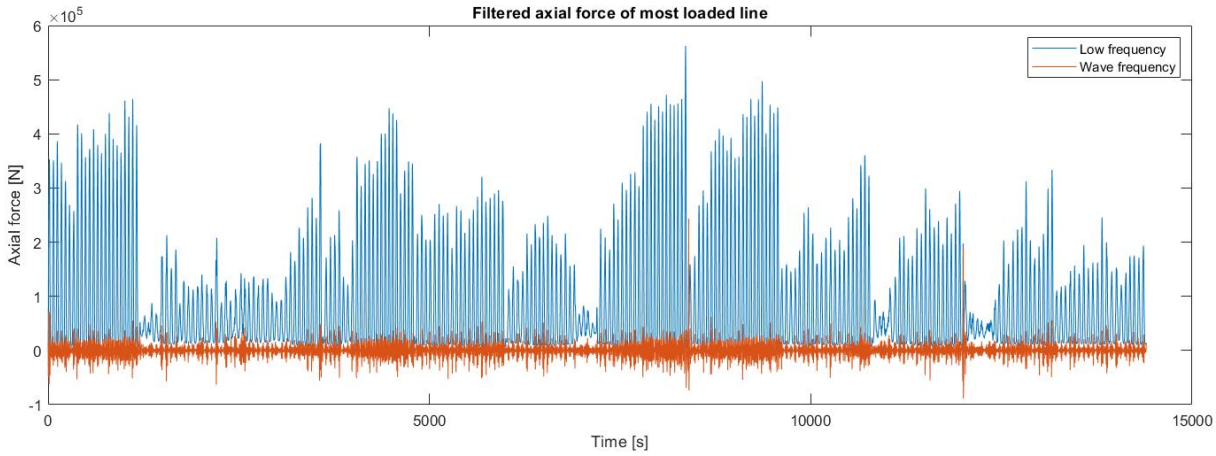

Figure 60: Plot of filtered axial force for most loaded line for load combination 1.

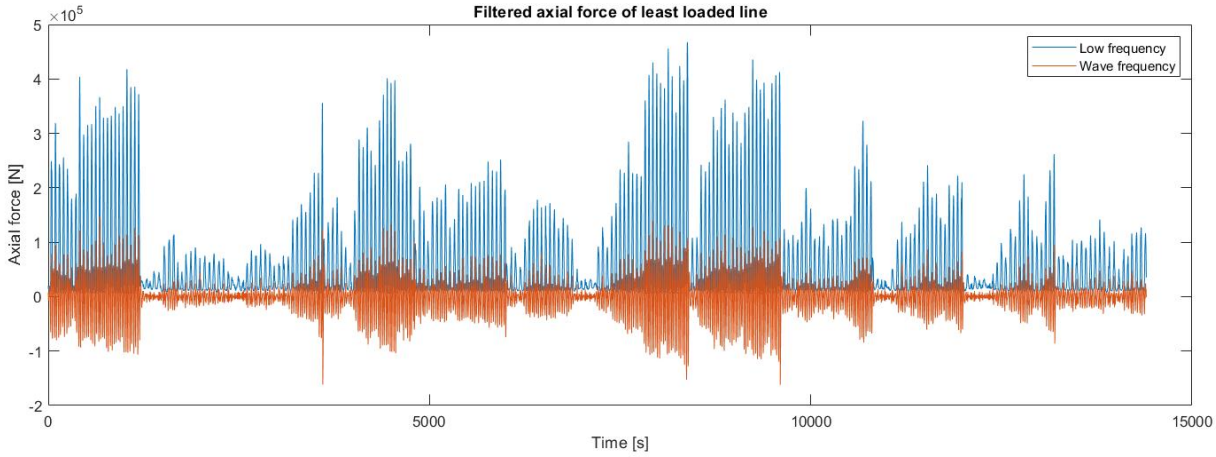

Figure 61: Plot of filtered axial force for least loaded line for load combination 1.

The uncoupled frequency response spectrums can be seen in Figure 62. The most prominent period was $\frac{1}{0.01905} = 52.5s$ for the low frequency tension, and $\frac{1}{0.05836} = 17.1s$ for the wave frequency response. When compared to the uncoupled vessel frequency response spectrum (Figure 46), this is quite interesting. The most dominant low frequency line tension period was around the sway and surge eigenperiods, while the vessel response was most dominating around the yaw eigenperiod. This seems to indicate that even though the vessel was most excited in yaw, it was still surge and/or sway motions that caused the largest line tensions. Intuitively this also makes sense since the weather came in towards the surge direction, then the slowly varying wave-drift forces will also act in this direction.

While the wave frequency spectrum does have peaks at the same frequencies to that of the coupled model, it has larger response at 17.1s for some reason. A possible explanation is that this is also caused by a local mooring line eigenmode.

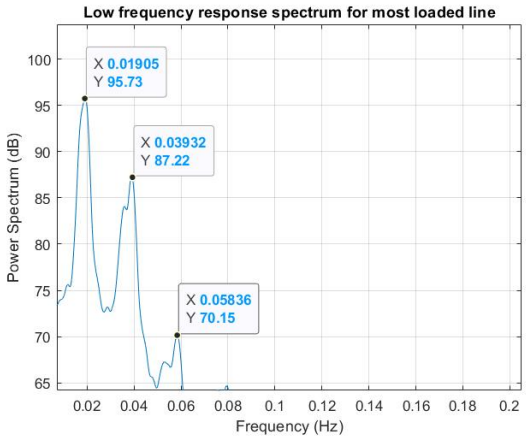

(a) Uncoupled low frequency

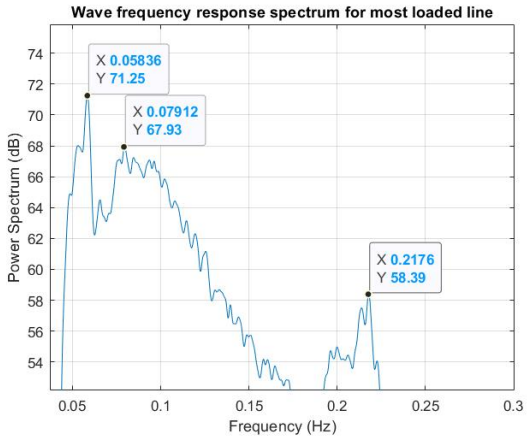

(b) Uncoupled wave frequency

Figure 62: Uncoupled frequency spectrum power plots for load combination 1.

Statistical values for load combination 1 is summarized in Table 29. Here it can be seen that the uncoupled line tension are larger than the coupled, with a drastically larger standard deviation. The max value of the uncoupled most loaded line is $\frac{561.3}{156.7} = 3.58$ times larger than the coupled most loaded line. The difference is even more extreme for the least loaded line, where the uncoupled line is $\frac{466.4}{85.6} = 5.44$ times larger than the coupled least loaded line.

Table 29: Line tension results for load combination 1.

Data Load comb. 1	**Mean [kN]**	**Std [kN]**	**Max [kN]**
Coupled			
Most loaded line	52.3	21.0	156.7
Low frequency	52.9	20.1	148.3
Wave frequency	0	7.1	33.0
Least loaded line	21.8	13.5	85.6
Low frequency	21.9	13.0	82.4
Wave frequency	0	5.1	27.4
Uncoupled			
Most loaded line	83.0	97.9	561.3
Low frequency	83.0	97.0	563.1
Wave frequency	0.1	13.2	243.6
Least loaded line	58.4	78.9	466.4
Low frequency	58.4	78.7	467.3
Wave frequency	0	32.9	146.4

6.3.2 Load combination 2

In this subsection, line tension data from load combination 2 will be presented and discussed.

Coupled

Figure 63 and Figure 64 presents coupled axial tension for the most and least loaded line, filtered into low -and wave frequency. As for the previous load combination, it is noted that the wave-frequency tension appears similar in magnitude for both lines, while the low-frequency tension is larger for the most loaded line.

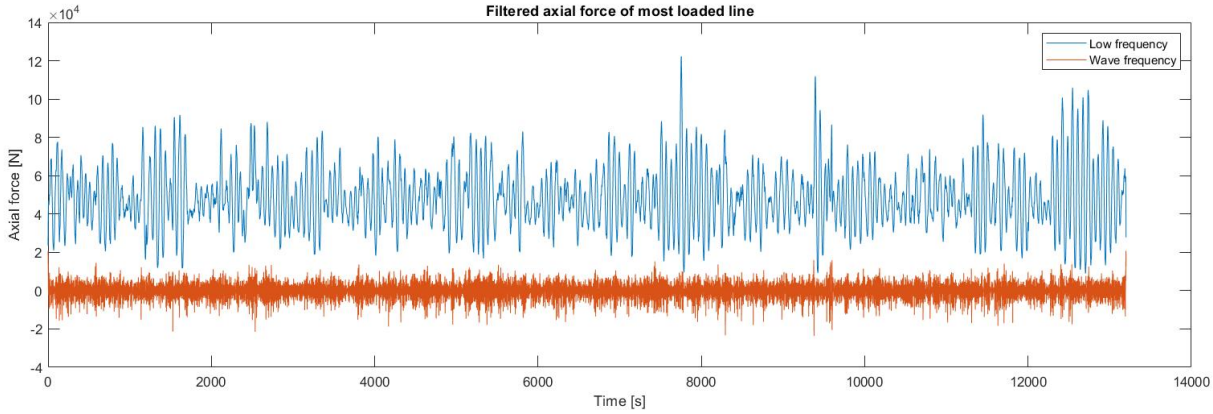

Figure 63: Plot of filtered axial force for most loaded line for load combination 2.

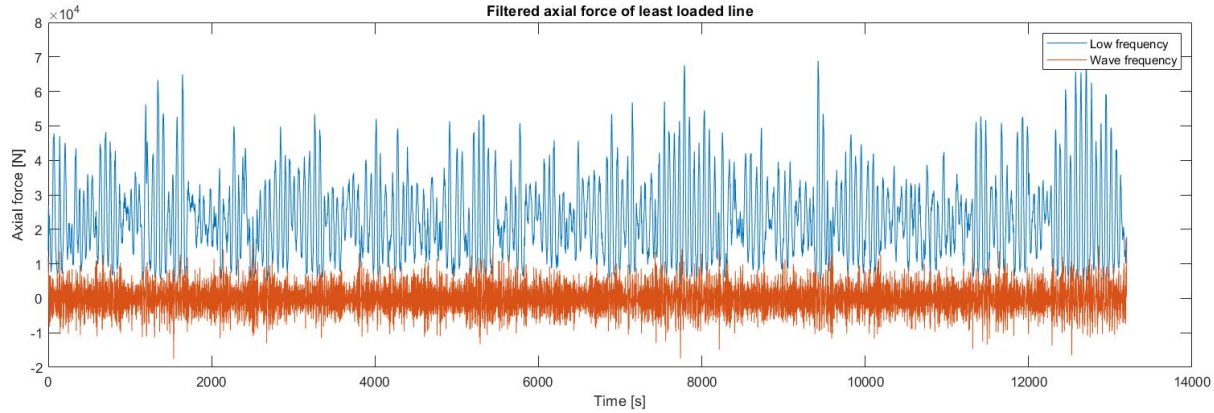

Figure 64: Plot of filtered axial force for least loaded line for load combination 2.

Figure 65 shows frequency spectrums for the coupled most loaded line, filtered into low -and wave frequency. The most dominating low-frequency period can be seen as $\frac{1}{0.01538} = 65s$, which corresponds well to the most dominating coupled vessel response period found in Section 6.1.2.

The wave-frequency spectrum has two peaks with roughly the same power. These corresponds to periods of $\frac{1}{0.1143} = 8.7s$ and $\frac{1}{0.2139} = 4.7s$. The first period is to be expected because the peak period in this load combination is 8.5s. The peak at 4.7s was also visible at the wave frequency spectrum for coupled load combination 1, and is similarly assumed to be caused by a local mooring line eigenmode. More excitation at this load combination make sense since the peak period is closer to the excited local period.

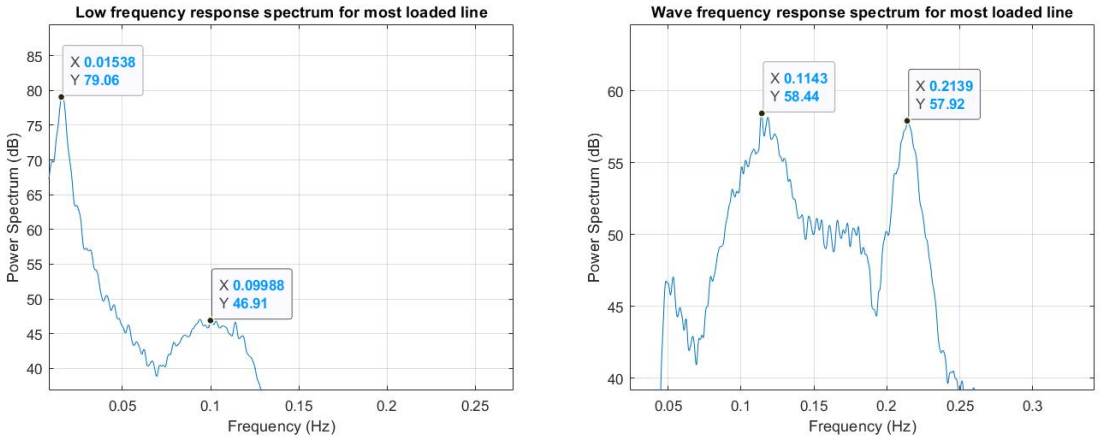

(a) Coupled low frequency (b) Coupled wave frequency

Figure 65: Uncoupled frequency spectrum power plots for load combination 2.

Uncoupled

Figure 66 and Figure 67 displays the uncoupled filtered tension of the most and least loaded line. Is is seen that the low frequency response dominates the load picture in both lines. It also matches the erratic nature of the uncoupled vessel response seen in Section 6.1.2.

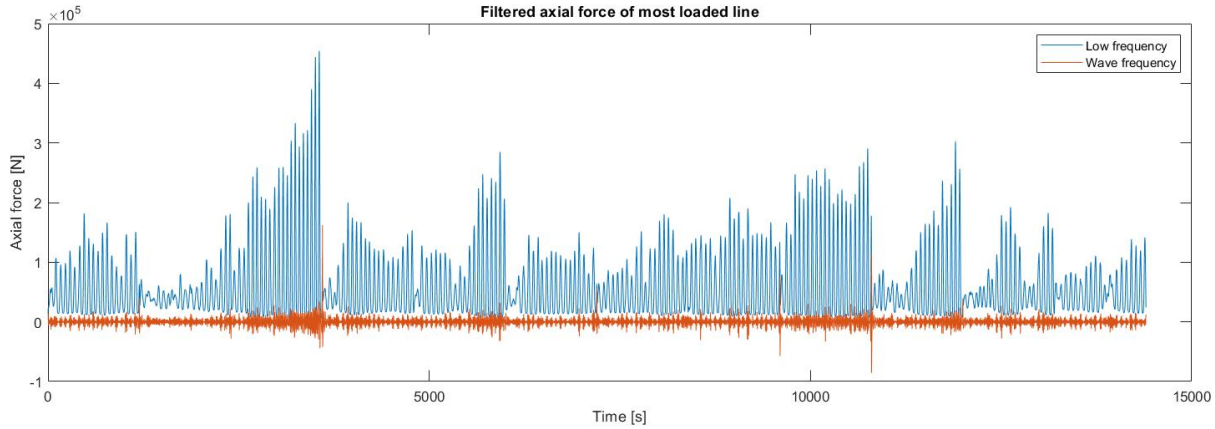

Figure 66: Plot of filtered axial force for most loaded line for load combination 2.

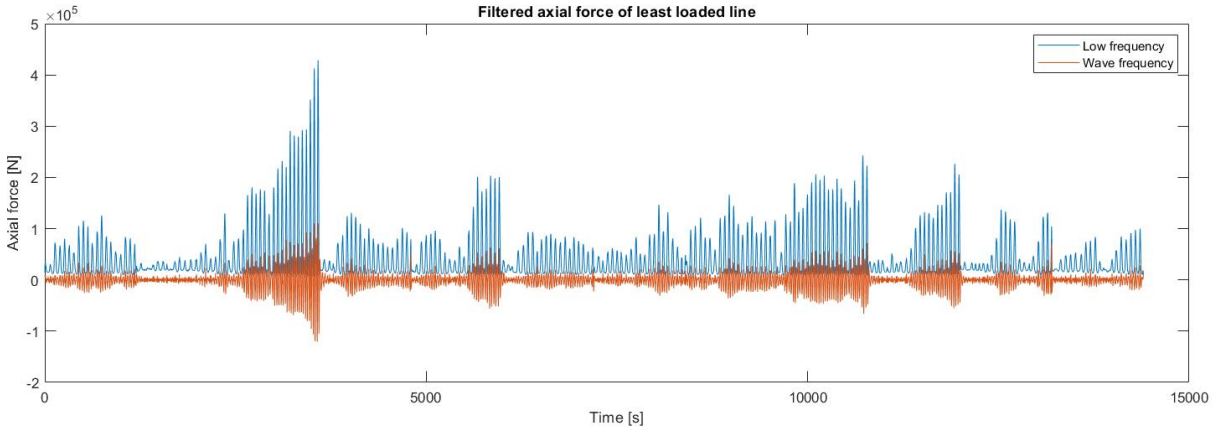

Figure 67: Plot of filtered axial force for least loaded line for load combination 2.

A frequency spectrum for the uncoupled most loaded line, filtered into low -and wave frequency can be seen in Figure 68. It can be seen that the dominating low-frequency response period is $\frac{1}{0.01709} = 58.5s$, while it is $\frac{1}{0.05324} = 18.78s$ for the wave-frequency spectrum.

It should be noted that also for this load combination, the dominating low frequency tension is similar to the surge/sway eigenperiod, while the dominating uncoupled vessel response period was 25.7s, corresponding to the yaw eigenperiod.

While the wave frequency spectrum does have peaks at the same frequencies as the coupled spectrum, the largest peak frequency differ. For some reason the uncoupled lines have larger response at 18.78s. As mentioned for load combination 1, where this also occurred, it might be caused by a local mooring line eigenmode.

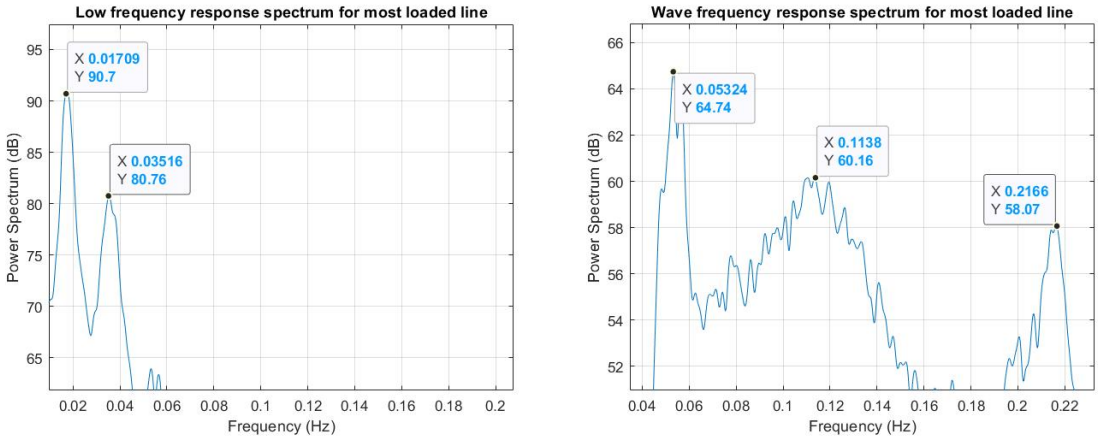

(a) Uncoupled low frequency

(b) Uncoupled wave frequency

Figure 68: Uncoupled frequency spectrum power plots for load combination 2.

Statistical values for load combination 2 is summarized in Table 30. As for load combination 1, it can be seen that the uncoupled tension is drastically larger than the coupled. Especially the standard deviation and max values differ drastically. The max value for the uncoupled most loaded line is $\frac{461.2}{125.5} = 3.67$ time larger than

the most loaded coupled line. The uncoupled least loaded line is $\frac{438.4}{73.6} = 6$ times larger than the coupled least loaded line.

Table 30: Line tension results for load combination 2.

Data Load comb. 2	**Mean [kN]**	**Std [kN]**	**Max [kN]**
Coupled			
Most loaded line	48.4	16.1	125.5
Low frequency	48.4	15.6	122.3
Wave frequency	0	4.2	20.7
Least loaded line	23.2	12.0	73.6
Low frequency	23.2	11.6	70.2
Wave frequency	0	3.7	17.9
Uncoupled			
Most loaded line	57.2	54.7	461.2
Low frequency	57.2	54.2	454.5
Wave frequency	0	6.6	162.0
Least loaded line	38.2	42.3	438.4
Low frequency	38.2	42.2	428.6
Wave frequency	0	15.8	110.3

6.4 Regular response criteria

This section is dedicated to explore a design criteria given in NS9415, stating that irregular wave analysis can be substituted with regular wave analysis as long as the regular wave height is equal to 1.9 times the significant wave height for the ULS sea-state.

While performing these analyses, it was noticed that the uncoupled analysis did not seem to converge after 20min. It was therefore decided to run 100 minutes to check if the response would converge better.

6.4.1 Load combination 3

The response from the regular wave coupled and uncoupled analysis can be seen in Figure 69 and Figure 70. The coupled analysis reached convergence after approximately 500s (indicated by black line), while the uncoupled model did not reach an equilibrium condition. Even though the uncoupled analysis length was increased from 20min to 100min. Around 3000s in the uncoupled analysis, a change in response pattern can be seen, this is caused by initiating yaw-motion.

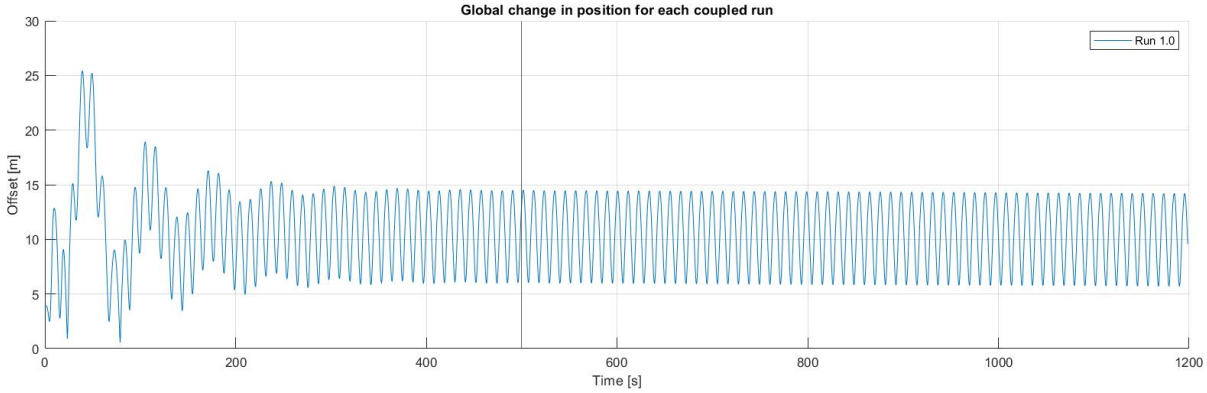

Figure 69: Total response for coupled model in load combination 3.

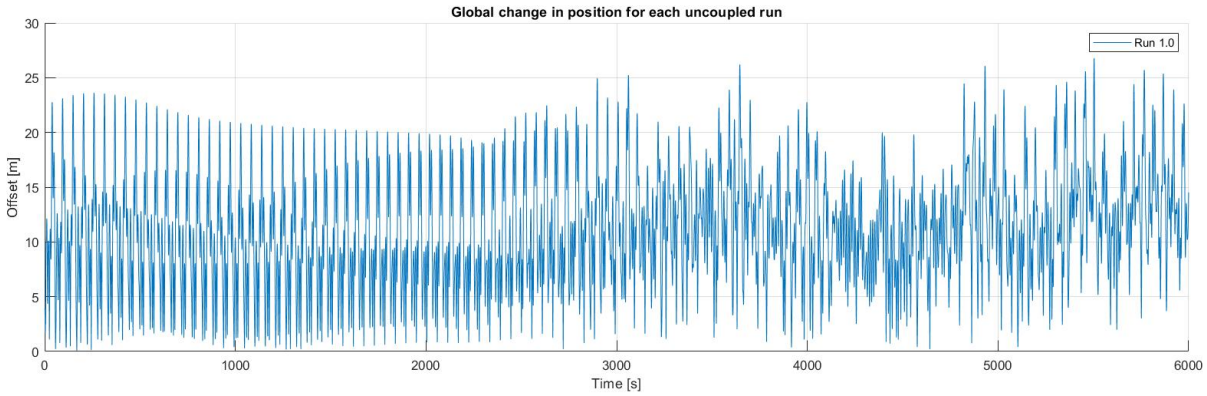

Figure 70: Total response for uncoupled model in load combination 3.

Response data was gathered from the analyses and presented in Table 31. For the coupled analysis, only data after the equilibrium point was used. For the uncoupled analysis, the entire time-series was used, since it did not achieve equilibrium.

When Table 31 is compared to the corresponding irregular analysis results in Table 19, it is seen that max values are actually smaller for the regular analysis, both for coupled and uncoupled. While the mean values are larger for the regular analysis.

The difference in max response values might seem counter-intuitive since the regular analysis method is supposed to give conservative results and should therefore be larger. However, it is important to remember that total response from the equilibrium position is not a crucial design factor. The important design factors are the induced loads.

Table 31: Mean, standard deviation and maximum values for filtered and total response for load combination 3.

Response type	**Mean [m]**	**Standard deviation [m]**	**Max [m]**
Coupled			
Total response	10.4746	2.9748	14.5098
Low frequency response	10.4523	1.5986	12.8587
Wave frequency response	-	2.9590	5.6505
Uncoupled			
Total response	11.0384	5.0725	26.7825
Low frequency response	11.0367	4.5446	24.9039
Wave frequency response	-	2.7384	8.0947

More interestingly for ULS mooring design, is the mooring line tensions. These are gathered in Table 32 (converged area for the coupled analysis is used). When compared to the line tensions in the corresponding irregular analysis in Table 29, some interesting finds are made. The coupled analysis gave lower maximum values when compared to the irregular analysis, even though the mean values are larger for the regular analysis. The uncoupled analysis also follows this pattern. The irregular analysis gave drastically larger tensions when compared to the regular analysis. $\frac{561.3}{368.1} = 1.52$ and $\frac{466.4}{169.0} = 2.76$ times larger in the irregular analysis for the most and least loaded line, respectively.

Table 32: Line tension results for load combination 3

Data Load comb. 3	**Mean [kN]**	**Std [kN]**	**Max [kN]**
Coupled			
Most loaded line	89.8	23.5	124.2
Low frequency	89.7	12,9	111.3
Wave frequency	0	23.8	50.3
Least loaded line	10.5	4.9	18.2
Low frequency	10.5	3.5	16.8
Wave frequency	0	5.0	11.9
Uncoupled			
Most loaded line	103.0	96.4	368.1
Low frequency	102.9	91.6	329.5
Wave frequency	0	35.6	100.9
Least loaded line	32.9	34.7	169.0
Low frequency	32.9	32.6	149.8
Wave frequency	0	22.1	94.4

6.4.2 Load combination 4

The total response from the regular wave coupled and uncoupled response of load combination 4 can be seen in Figure 71 and Figure 72. The uncoupled analysis experienced large movements in sway and yaw, starting at 1500s, causing the large

response seen in Figure 72.

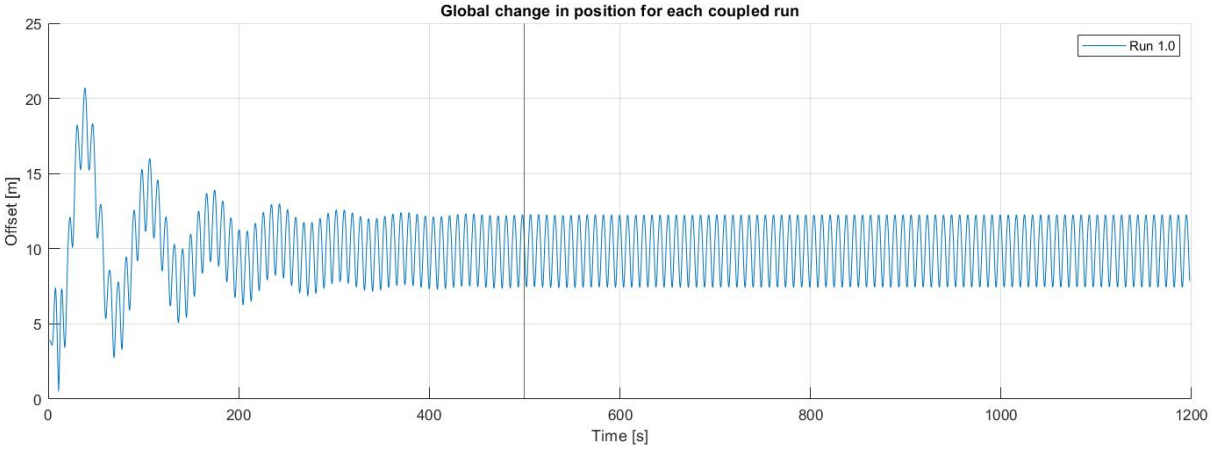

Figure 71: Total response for coupled model in load combination 4.

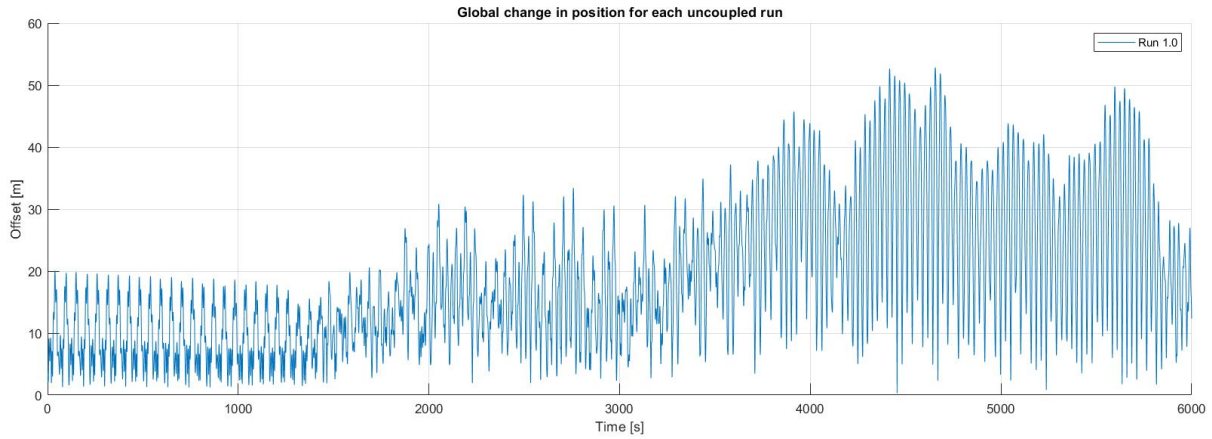

Figure 72: Total response for uncoupled model in load combination 4.

Statistical values for the regular analysis of load combination 4, is given in Table 33. The entire time-series was also used here, due to not reaching a state of convergence.

When these results are compared to the corresponding results of load combination 2, in Table 20, it is observed that the coupled max response is lower for the regular analysis. Following the trend seen between load combination 1 and 3. While the opposite is observed for the uncoupled model, here the response is almost doubled for the regular regular analysis. Both coupled and uncoupled follows the trend in regards to increase in mean response.

Table 33: Mean, standard deviation and maximum values for filtered and total response for load combination 4.

Response type	**Mean [m]**	**Standard deviation [m]**	**Max [m]**
Coupled			
Total response	10.0123	1.7134	12.2785
Low frequency response	9.9967	0.4720	10.9737
Wave frequency response	-	1.6977	2.9698
Uncoupled			
Total response	18.5634	11.2845	52.8207
Low frequency response	18.5618	11.0717	52.7388
Wave frequency response	-	1.9331	4.9161

Again, more interestingly than vessel response, is the line tensions. These are given in Table 34 for the regular analysis of load combination 4. Also for this analysis, it is observed that the regular max values are smaller when compared to the corresponding irregular load combination, seen in Table 30. While the mean tension values for both uncoupled and coupled are larger for the regular analysis. This is in accordance with the trend of load combination 1 and 3.

Table 34: Line tension results for load combination 4

Data Load comb. 4	**Mean [kN]**	**Std [kN]**	**Max [kN]**
Coupled			
Most loaded line	89.1	11.0	105.1
Low frequency	89.0	3.5	96.8
Wave frequency	0	10.7	18.3
Least loaded line	9.2	5.8	19.2
Low frequency	9.2	2.25	12.6
Wave frequency	0	5.8	10.2
Uncoupled			
Most loaded line	97.3	83.2	297.3
Low frequency	97.2	81.3	267.0
Wave frequency	0	17.7	78.5
Least loaded line	26.7	22.7	104.6
Low frequency	26.7	21.7	89.9
Wave frequency	0	11.1	41.2

6.5 Comparison to small scale model test

Figure 73 was made available from ScaleAQ's small-scale model test on an identical moored barge setup. This plot corresponds then to Figure 74 and Figure 75 for the coupled and uncoupled models, respectively. Since no more data was made available, it is difficult to draw many conclusions.

However, it can be seen that the max tension value is quite a bit larger for the model test. Approximately 240kN, while it was approximately 125kN for the coupled model

analysis. It would then seem like the coupled model underestimates the maximum mooring line tensions. Although, no information was given as to the scaling of these properties from small-scale, meaning that these results are hard to compare. The uncoupled model can be seen to predict larger responses than what were observed in the model test.

Most interesting is perhaps the shape of the graphs. The model-test tensions looks more similar to the coupled results than the uncoupled. As mentioned earlier when presenting the mooring line tension results, this is thought to be due to eigenmode excitation. However, in light of the model test tension plot and discussions with Professor Pål Lader, the possibility of numerical errors in the uncoupled model cannot be excluded.

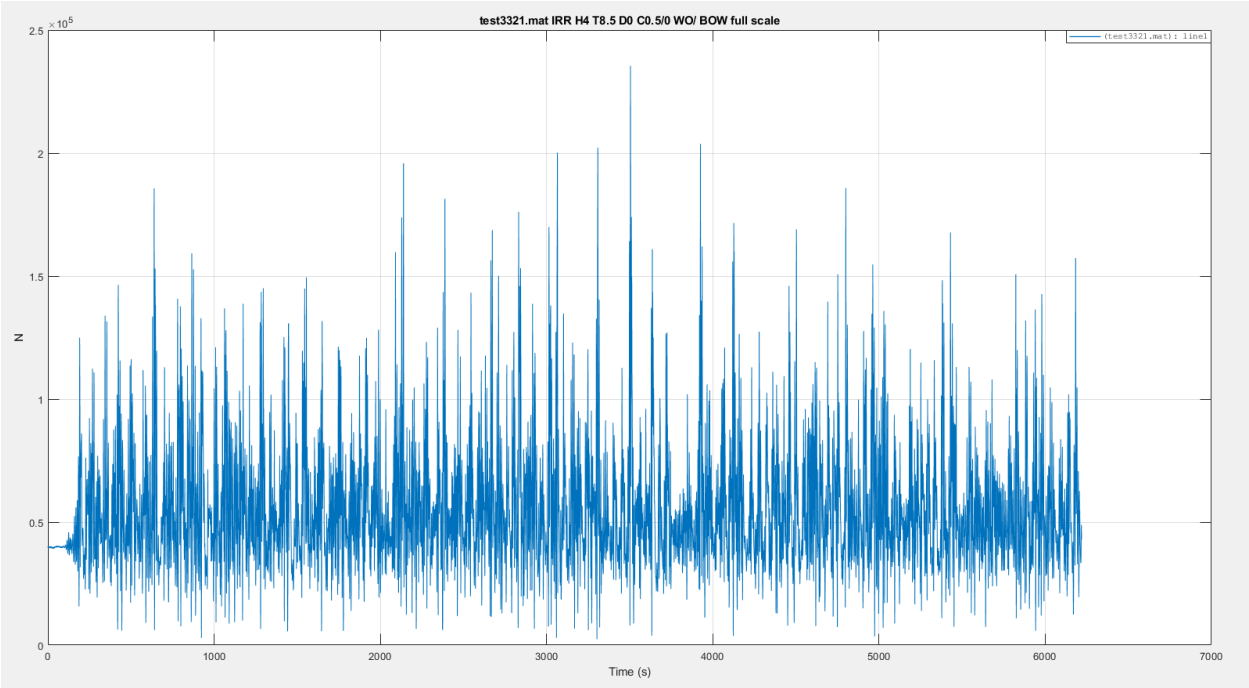

Figure 73: Line tension of windward line from small-scale model test performed by ScaleAQ, corresponding to load combination 2.

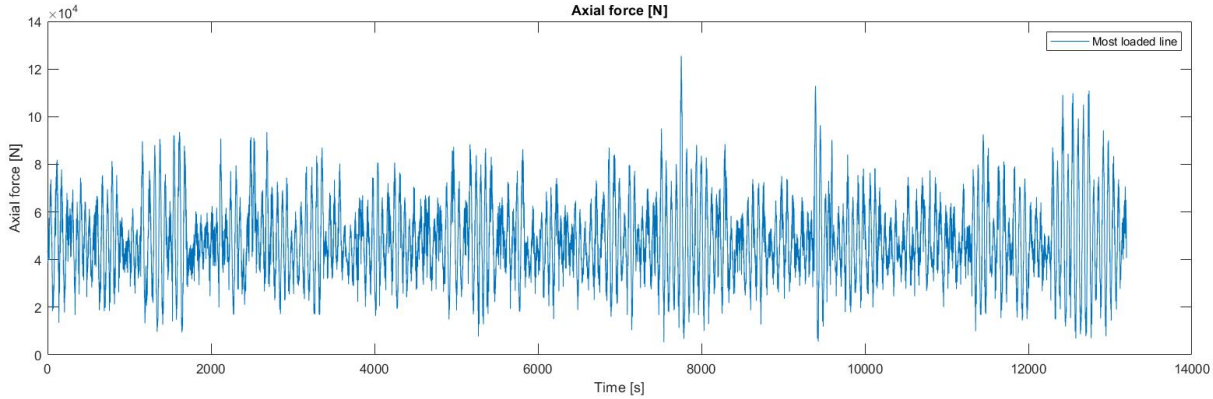

Figure 74: Line tension of windward line from coupled analysis for load combination 2

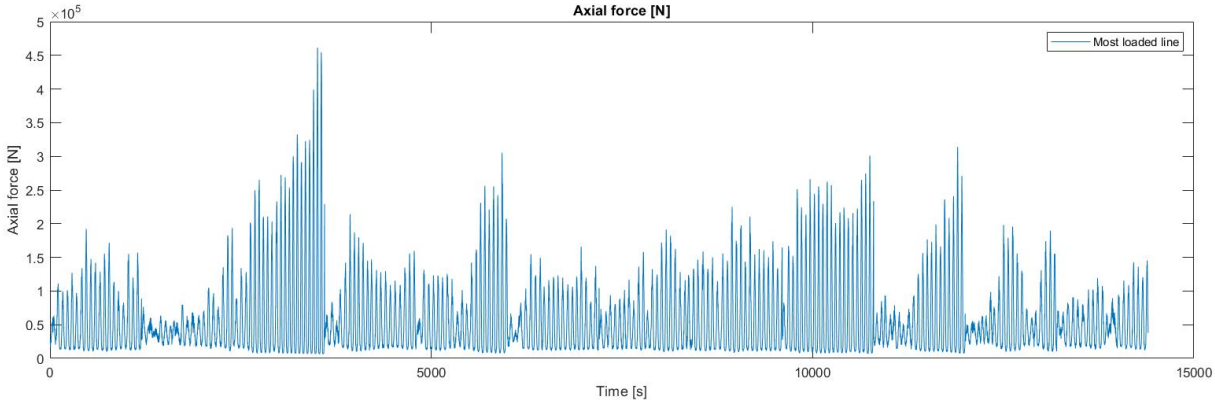

Figure 75: Line tension of windward line from uncoupled analysis for load combination 2.

6.6 Discussion of results

This thesis was written partly due to increasing concern regarding the risk of installing feed barges in more exposed locations. This section will be dedicated to discuss the impact that the results has on the total moored feed barge risk picture. It will also be discussed up against the new governing aquaculture standard NS9415 (Standard Norway, 2021).

6.6.1 Coupled and uncoupled analysis

According to NS9415 §13.4, *relevant calculation methods for the construction in question should be used, and assessments shall be documented* (Standard Norway, 2021). It also states that the method of analysis utilized for barge mooring systems should be able to give local loads on important components. Both coupled and uncoupled analysis fulfill these demands, as FEM formulation of the mooring lines are possible in both, allowing one to retrieve tension in any element. Beyond this, the standard does not specify weather a coupled or uncoupled analysis method should be utilized. This means that it is up to the company performing the mooring analysis to consider which method should be used.

The coupled analysis method is considered state of the art, since it takes dynamic effects on the mooring lines into account. This fact makes it natural to question the usefulness of uncoupled analysis. The main reason why uncoupled analysis can be considered to have a vast advantage over coupled analysis, is computational time. For the analyses performed in this thesis, it took approximately 20 times longer to run coupled analyses with equal time steps and length.

The results presented in Section 6.1 and Section 6.2 shows that most of the relative differences between coupled and uncoupled analysis increase with increasing significant wave heights (except for max value between load combination 1 and 2). Still, the uncoupled analysis consistently give much larger response and line tensions compared to coupled, as seen in Table 35. This difference is thought to be caused

by eigenmode excitation in the uncoupled model due to lower damping levels from the mooring lines. It it believed that this could be remedied by manually applying additional damping to the uncoupled model. This additional damping could be dependant on several parameters, but care should be taken to preserve the conservative quality of the uncoupled analysis.

In addition, the vessel response plots in Section 6.1 for the uncoupled model appears strange, a certain sea-state contains the same energy independent of which wave seed is used. Meaning that large variations in vessel response from one wave seed to another, as can be seen in Figure 42, should not occur. It is possible that these variations are caused by insufficient simulation length, but the possibility of numerical errors in the models should not be excluded.

Table 35: Max value of loaded lines for all load combinations.

Max of most loaded line	**Coupled [kN]**	**Uncoupled [kN]**	**Change factor [Uncoupled/Coupled]**
Load comb. 1	157.7	561.3	3.56
Load comb. 2	125.5	461.2	3.67
Load comb. 3	124.2	368.1	2.96
Load comb. 4	105.1	297.3	2.89

As a preliminary and quick analysis, uncoupled models could be used as a useful tool. Then, knowing that uncoupled analysis will drastically overestimate the line tensions and vessel response, only coupled analysis should be used for final design decisions. Regarding the risk picture, these findings does not give cause for concern. The coupled analysis give good realistic results, while the uncoupled analysis vastly overestimate forces and response. Meaning that the worst case scenario, if a company is not aware of this, is that they over-dimension the mooring system and therefore waste material and money.

6.6.2 Regular criteria

The analysis criteria presented in Section 3.8.5, was investigated in Section 6.4. Here, some interesting results were discovered. The regular wave analysis tended to underestimate max response and line-tension compared to irregular wave analysis, as shown in Table 36. For ULS design, this is a concerning result, since this design principle takes the worst case scenario into account (E.g 10 -and 50 year wave condition). Therefore, applying this criteria for ULS design could lead to an underestimation of extreme response.

Table 36: Most loaded line max value of irregular analysis divided on the corresponding regular analysis, for coupled and uncoupled models.

Max of most loaded line	**Coupled [kN]**	**Uncoupled [kN]**
Load comb. 1/Load comb. 3	1.27	1.89
Load comb. 2/Load comb. 4	1.19	1.55

The mean response and line tension, however, was much larger for the regular analysis. Meaning that FLS design, based on regular wave analysis, can drastically

overestimate fatigue damage to system components. This, in and of itself might not be a bad thing, since one of the most common mooring failures found in Section 4.2 was due to fatigue.

The advantage of using regular waves is that only one run until steady-state condition is achieved, is necessary. While for irregular waves, several runs with different seeds must be run to account for all the possible wave combinations. The results found indicates that irregular waves should be used to accurately represent real-life sea-states and get a realistic response picture for design purposes. The risk of underestimating ULS response that occurs when using regular wave analysis seems unnecessary. It should be noted that NS9415 does include a comment stating that irregular waves should be considered for systems where slowly varying forces are of importance, which applies to moored structures.

7 Conclusion

This chapter will conclude and summarize the analysis results, and present suggestions for further work.

7.1 Concluding remarks

The main goal of this thesis was to investigate load components acting on a feed barge mooring system for different analysis methods, up against the new standard NS9415. While focusing especially on exposed conditions and irregular waves. Two commonly used methods were identified to be *coupled* and *uncoupled* analysis. It was therefore decided that a study of these state of the art methods would fulfill the main goal. To facilitate this study, common mooring concepts and components were presented. A literature review of relevant theory were conducted. A risk assessment of feed barges was performed to form a risk picture. The relevant technical regulations for moored feed barges, being mainly NS9415 (Standard Norway, 2021) and NYTEK (NYTEK, 2011), was presented.

The analysis software SIMA and modelling tool GeniE was used to develop two models of a generic moored feed barge system, which had been tested in small scale by ScaleAQ. The only difference between these two models were that one was coupled and the other uncoupled. The hydrodynamic vessel data used in simulations was gathered from an Exposed project (Zang, 2017).

Results from simulation of these two models showed that uncoupled analysis drastically overestimates vessel response and mooring line tension, compared to the coupled model. However, this difference was reduced for milder sea-states. It was found that the uncoupled model was excited by the yaw eigenmode to a much larger degree than the coupled. It was concluded that these differences most likely were caused by the lack of mooring line damping in the uncoupled model, seeing as both models had the exact same vessel-specific damping properties. However, the possibility that these differences were caused by numerical errors in the uncoupled model, could not be excluded.

The results impact on total risk picture was found to be significant. The uncoupled analysis overestimate the response and loads, therefore not causing any other risk factor besides the risk of over-dimensioning. The coupled model was found to give accurate response and tensions, which combined with the partial coefficient method, should give acceptable risk levels. Although, this was not confidently confirmed by the model test results supplied by ScaleAQ. The criteria in NS9415, regarding the use of regular wave to substitute irregular waves, was found to be of concern. The comparable regular wave analysis gave lower extreme response, and larger mean response. Meaning that ULS response could be underestimated, and FLS design life overestimated. It was therefore concluded that said criteria, given in NS9415 §9.4.4.3, should be avoided for moored feed barges. It should be noted however, that the standard does mention to some degree that special irregular waves should be considered for structures where slowly varying drift forces dominate.

It was concluded that uncoupled analysis had the advantage of being roughly 20 times faster than coupled. Therefore, it could have potential as an early-stage method of analysis. For uncoupled analysis to be useful, however, improvements will have to be made. A factor of over 3.5 times larger line tension for the uncoupled model compared to coupled is too large.

7.2 Proposal to further work

The results presented in this master thesis came from time consuming numerical analyses. For further work, a larger data-foundation could be established, especially for load combination 5 where only one run was performed. A larger database would further ground the conclusions reached. Additionally, a larger number of analyses would enable the use of the extreme value distribution, presented in Section 3.4.3. This distribution could then be used to compare extreme response, e.g. 10 -and 50 year response values, which could be of interest.

The software HydroD could be utilized to gain vessel-specific hydrodynamic data, as it was not accomplished in this thesis. Even though the alternative method used was found to be adequate, more specific hydrodynamic data would improve result accuracy.

One of the goals of this thesis was to investigate the risk picture of exposed feed barge moored systems. This proved difficult, as accident data was unobtainable. If such data could be found, a risk picture specific to feed barges could be established and suggestions for improvements to barrier strategies could be made.

An attempt to create a model for adding additional damping to the uncoupled model, mimicking the damping of the mooring lines could be performed. This could potentially make the uncoupled analysis much better. However, care should be taken as to not loose the uncoupled analysis' conservative properties. Additionally, the possibility of numerical errors in the uncoupled analysis should be investigated.

Bibliography

Berstad, A.J., L.F. Heimstad and J. Walaunet (2014).
Model testing of fish farms for validation of analysis programs. ASME.

Bjørkøy, M. (2017). *Stochastic mooring analysis of aquaculture installations*. Unpublished.

Bruset, M. (2019). *Dynamic analysis of a floating fish cage with feeding systems*. University of Stavanger.

Chakrabarti, S.K. (2005). *Handbook of offshore engineering*. Elsevier.

DNV (2013). *DNVGL-OS-E301 - Position mooring*. DNV.

— (2020). *GeniE User Documentation*. DNV GL - Digital Solutions.

— (2021). *GeniE User Documentation*. DNV GL - Digital Solutions.

— (2022a).
Frequency domain hydrodynamic analysis of stationary vessels - Wadam.
URL: https://www.dnv.com/services/frequency-domain-hydrodynamic-analysis-of-stationary-vessels-wadam-2412?utm_campaign=structure_sesam&utm_source=google&utm_medium=cpc&gclid=CjwKCAiA4KaRBhBdEiwAZi1zztuO2J4cSZW19UezcjZUkYzF3l2j-r-cWI2AvJRGZjkIHDw8vfma3BoCYL8QAvD_BwE&gclsrc=aw.ds (visited on 10th Mar. 2022).

— (2022b). *Hydrodynamic analysis and stability analysis software - HydroD*.
URL: https://www.dnv.com/services/hydrodynamic-analysis-and-stability-analysis-software-hydrod-14492 (visited on 10th Mar. 2022).

— (2022c). *Strength assessment of offshore structures - Sesam software*.
URL: https://www.dnv.com/services/strength-assessment-of-offshore-structures-sesam-software-1068?&utm_campaign=structure_sesam&utm_source=google&utm_medium=cpc&gclid=Cj0KCQiAmpyRBhC-ARIsABs2EApLatkbJd_7oVsNgCrvrBXWhFq_UuZLf6rUUwvDO0f7E6dLgCWOZxAaAjo7EALw_wcB&gclsrc=aw.ds (visited on 8th Mar. 2022).

Eltervåg, A. et al. (2004).
Principles for barrier management in the petrolium industry.
Petrolium safety authority.

Energo Engineering (2018).
Integrity Management Process of Tension Leg Platforms. Unpublished.

eSubsea (2021). *Padeye og Løftepunkter*. URL: https://www.esubsea.no/padeye-og-loftepunkter/ (visited on 8th Dec. 2021).

Exposed (2022). *Senter for forskningsdrevet innovasjon innen eksponerte havbruksoperasjoner*. URL: https://exposedaquaculture.no/ (visited on 26th Mar. 2022).

Faltinsen, O.M. (1990). *Sea loads on ships and offshore structures*. Cambridge university press.

Fon, M. (2021). *Tool for analysis of feed barges*. URL: https://exposedaquaculture.no/en/tool-analysis-of-feed-barges/ (visited on 23rd Oct. 2021).

Grøftrem, S. (2021). *Preliminary investigation into theory, risk assessment and analysis of aquaculture feed barge mooring systems*. Unpublished.

Haver, S. (2019). *Metocean modelling and prediction of extremes*. Haver & havet, University in Stavanger, NTNU.

Holmen, I.M. and T. Thorvaldsen (2018). *Occupational health and safety in Norwegian aquaculture*. SINTEF Ocean AS.

Hydro (2021). *Deepwater Turret Mooring Monitoring Offshore Mozambique*. URL: https://www.hydro-international.com/content/news/sofec-selects-bmt-and-sonardyne-for-deepwater-turret-mooring-monitoring-offshore-mozambique (visited on 26th Oct. 2021).

Ikhennicheu, M. et al. (2020). *D2.1 Review of the state of the art of mooring and anchoring designs, technical challenges and identification of relevant DLCs*. Corewind.

ISO 31000 (2018). *NS-ISO 31000:2018 - Risk management and guidelines*. Standard Norway.

Kvitrud, A. (2014). *Lessons learned from the Norwegian mooring line failures 2010-2013*. Petroleum Safety Authority Norway (PSA).

Lader, P. (Feb. 2021). *Lecture notes in TMR4141 - Aquaculture structures*.

Larsen, C.M. et al. (2019). *Marine Dynamics*. Department of Marine Technology, Faculty of Engineering Science and Technology - NTNU.

Larsen, K. (Feb. 2018). *Static equilibrium of a mooring line - Lecture note*.

— (2022). *Time domain analysis overview - Lecture note*.

Marintek (2018). *SIMA user guide*. Marintek.

Mathworks (2022a). *Highpass filter signals*.
URL: https://www.mathworks.com/help/signal/ref/highpass.html (visited on 13th May 2022).

— (2022b). *Lowpass filter signals*.
URL: https://www.mathworks.com/help/signal/ref/lowpass.html (visited on 13th May 2022).

Matsumoto, K. (1991). *The influence of mooring line damping on the prediction of low frequency vessels at sea*. Proc. OTC, Houston, USA.

Moen, T. (2003).
TMR4190 - Finite element modelling and analysis of marine structures.
Department of Marine Technology.

Negi, A. and S.S. Dhavalikar (2009).
'Estimation of roll damping for transportation barges'.
In: *Researchgate - Conference paper*.

Newman, J.N. (1977). *Marine Hydrodynamics*. Cambridge, MA: MIT Press.

NYTEK (2011). *NYTEK*. Norwegian Ministry of Trade, Industry and Fisheries.

OrcaFlex (2021). *Vessel theory: Wave drift and sum frequency loads*.
URL: https://www.orcina.com/webhelp/OrcaFlex/Content/html/Vesseltheory, Wavedriftandsumfrequencyloads.htm (visited on 20th Oct. 2021).

Pettersen, B. (2007). *Marin teknikk 3: Hydrodynamikk*.
Department of Marine Technology, NTNU.

Pike, D. (2021). *Is it a Fair Lead?*
URL: https://boattest.com/article/is-it-a-fair-lead (visited on 8th Dec. 2021).

ScaleAQ (2021a). *Anchor chains*.
URL: https://scaleaq.com/product/anchor-chains/ (visited on 10th Nov. 2021).

— (2021b). *Anker*.
URL: https://scaleaq.no/produkt/anker/ (visited on 10th Nov. 2021).

— (2021c). *Forankringsbolt*.
URL: https://scaleaq.no/produkt/forankringsbolt/ (visited on 10th Nov. 2021).

— (2021d). *Fôrflåter*. URL: https://scaleaq.no/produktkategori/seabased/forflaater/ (visited on 14th Oct. 2021).

ScaleAQ (2021e). *Fortøyningsplate*.
URL: https://scaleaq.no/produkt/fortoyningsplate/ (visited on 10th Nov. 2021).

— (2021f). *Sjakler*.
URL: https://scaleaq.no/produkt/sjakler/ (visited on 10th Nov. 2021).

SINTEF (2021). *Sima*.
URL: https://www.sintef.no/programvare/sima/ (visited on 8th Dec. 2021).

Solheim, R. et al. (2004).
Gransking av ankerkjetting utrausing på Ocean Vanguard 14.12.2004.
Petroliumstilsynet.

SSB (2021). *Akvakultur (avsluttet i Statistisk sentralbyrå)*.
URL: https://www.ssb.no/fiskeoppdrett (visited on 11th Dec. 2021).

Standard Norway (2021).
NS9415 - Floating aquaculture farms. Site survey, design, execution and use.
Standard Norway.

The Aquaculture Act (2006). Norwegian Ministry of Fisheries and Coastal Affairs.

Vinnem, J. and W. Røed (2020). *Offshore Risk Assessment Vol. 2 - Principles, Modelling and Applications of QRA Studies*. Springer.

Weiby, A.J. (2018). *Frequency-domain Roll Motion Analysis of a Transportation Barge Using Stochastic Linearization of Viscous Roll Damping*.
NTNU, Department of Marine Technology.

Wikipedia (2021). *Klyss*.
URL: https://no.wikipedia.org/wiki/Klyss (visited on 8th Dec. 2021).

Zang, Y. (2017). *Program of barge analysis and damping estimation*.
SINTEF - SFI Exposed.

Appendix

A MTO analysis of Ocean Vanguard incident

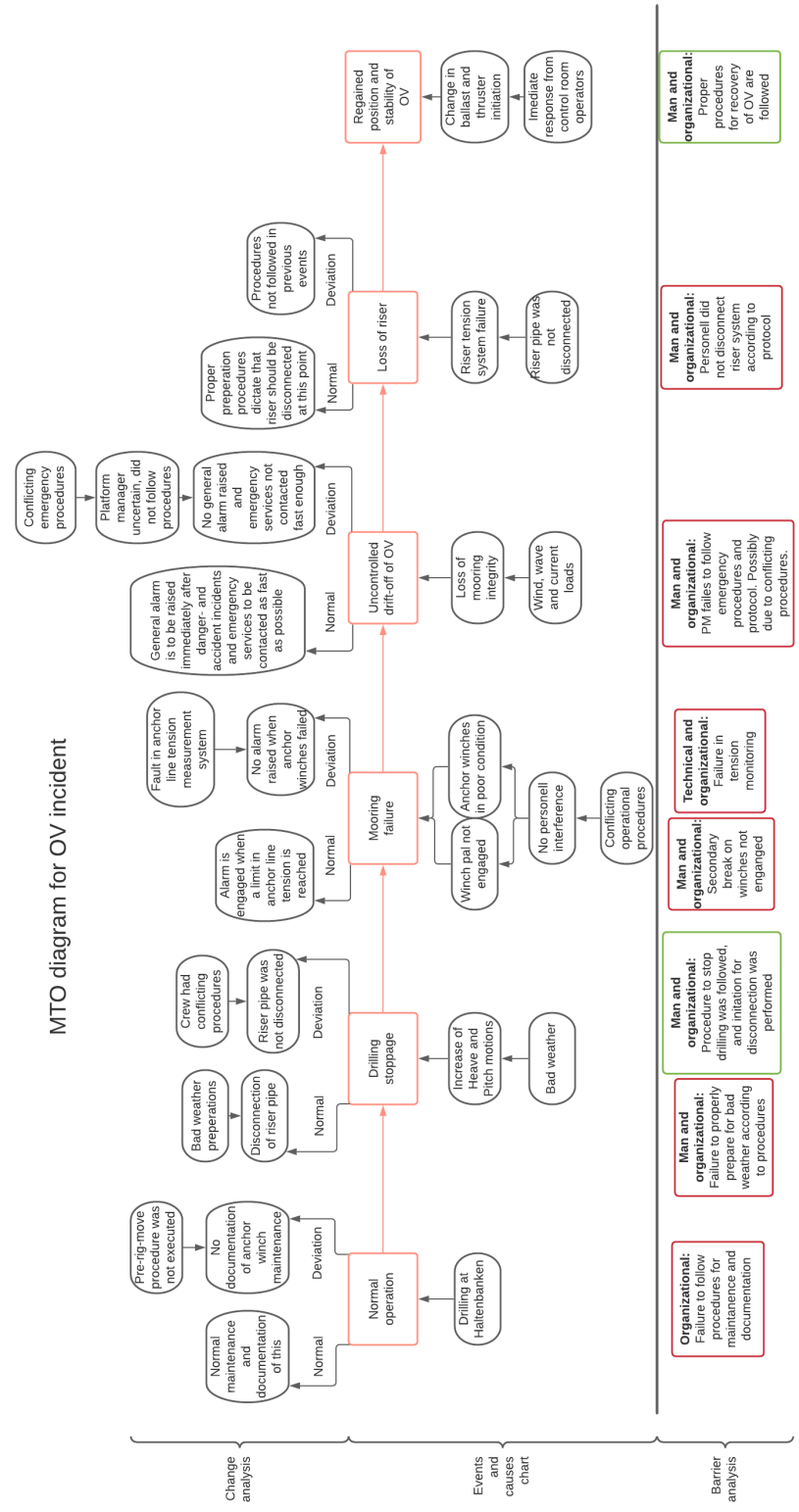

B Barrier strategy for moored vessel

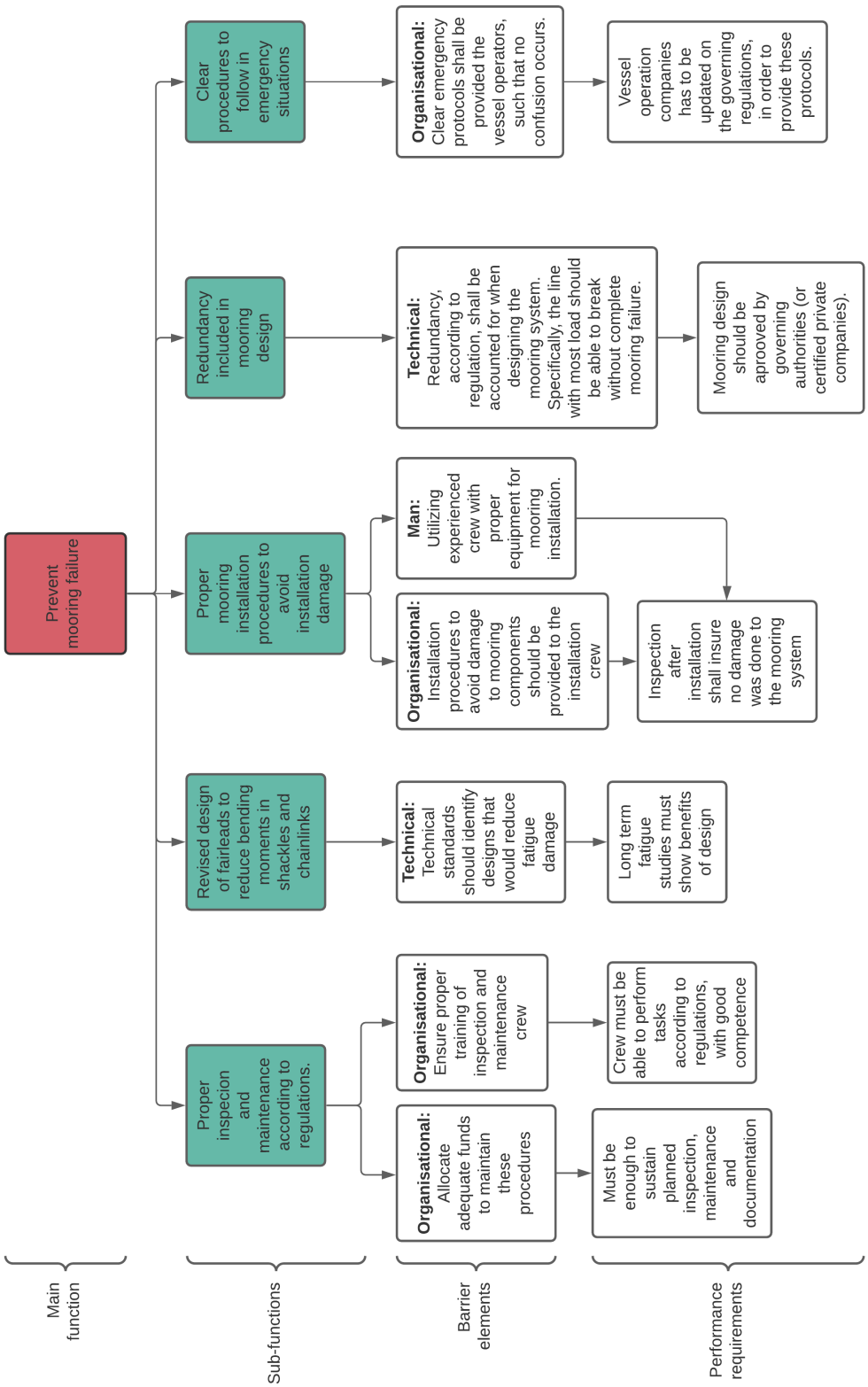

C HydroD transfer function example

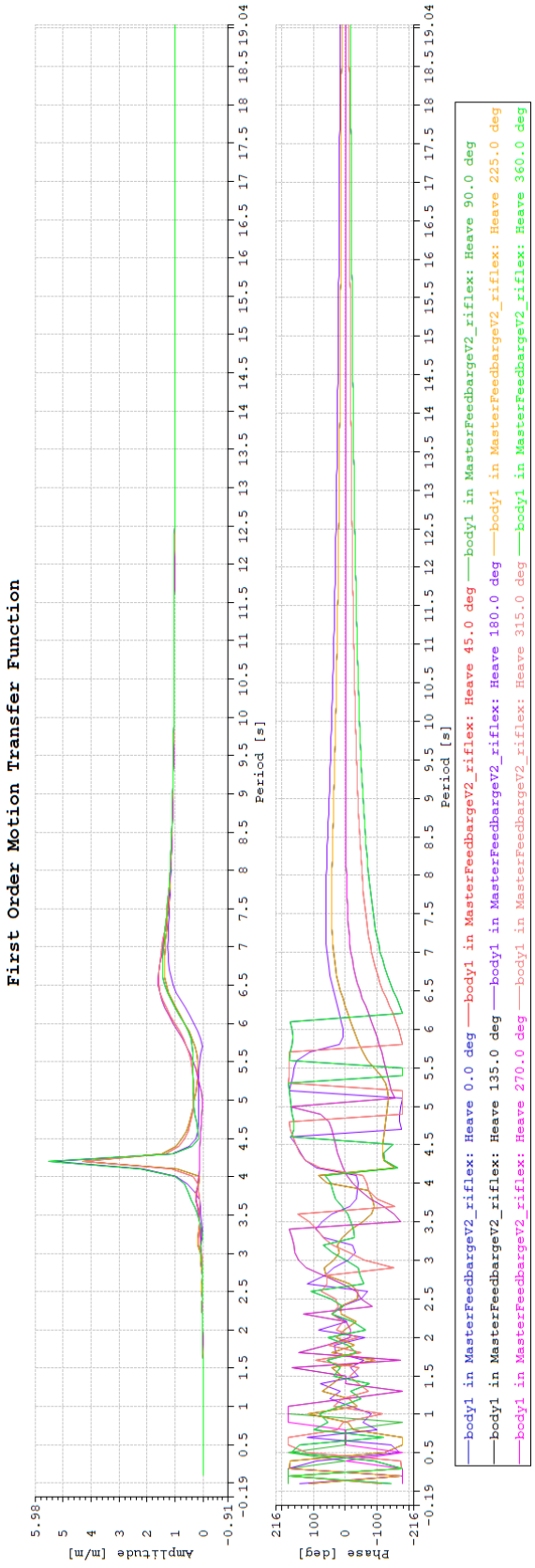

D MATLAB catenary comparison code

Contents

- Declaration of variables
- Calculation of line tension and offset for zero elastic chain
- Calculation of line tension and offset including elasticity
- Calculation of line tension and offset only accounting for elastic stiffness (almost no weight)
- Plotting all graphs of interest.

```
% Mooring analysis with different line characteristics - Sindre Grøftrem
```

Declaration of variables

```
w=1000; %weight [N/m]
l=2000; %length of line [m]
y=200; %vertical height of mooring [m]
EA=5*10^8; %Elastic stiffness [N]
```

Calculation of line tension and offset for zero elastic chain

```
Tx_0=(0:1000:600000); %Vector of horisontal tension [N]
s_0=zeros(length(Tx_0),1); %length of free hanging mooring line
Xl_0=zeros(length(Tx_0),1); %Horisontal length after offset
x_0=zeros(length(Tx_0),1);
for i=1:length(Tx_0)
x_0(i)=Tx_0(i)/w*log(1+y*w/Tx_0(i)+sqrt((1+y*w/Tx_0(i))^2-1));
s_0(i)=Tx_0(i)/w*sinh(w*x_0(i)/Tx_0(i));
Xl_0(i)=l+Tx_0(i)/w*acosh(1+(w*y/Tx_0(i)))-sqrt(y*(y+(2*Tx_0(i)/w)));
end
offset_0=Xl_0-(l-y);
```

Calculation of line tension and offset including elasticity

```
Ty_1=w*y; %The vertical force when zero tension is present [N]
Tx_1=zeros(2000,1); %Horisontal force
x_1=zeros(2000,1); %Horisontal length of elevated mooring line
Xl_1=zeros(2000,1);
s_1=zeros(2000,1); %Length of elevated mooring line [m]
for i=1:2000
   Tx_1(i)=(Ty_1^2-(w*y-(Ty_1^2/(2*EA)))^2)/(2*(w*y-(Ty_1^2/(2*EA))));
   x_1(i)=Tx_1(i)/w*asinh(Ty_1/Tx_1(i))+(Tx_1(i)*Ty_1)/(w*EA);
```

```
   Xl_1(i)=(l-(Ty_1/w))*(1+(Ty_1/EA))+x_1(i);
   Ty_1=160+Ty_1;
   s_1(i)=Tx_1(i)/w*sinh(w*x_1(i)/Tx_1(i));

end
offset_1=Xl_1-(l-y);
```

Calculatio of line tension and offsett only accounting for elastic stiffness (almost no weight)

```
%This might need some work. I think that the results are somewhat correct,
%althoug i do not now if the values i have used are representable for such
%a system
w_rope=34; %Weight of rope [N/m]
d_rope=0.134; %Diameter of rope [m]
EA_rope=5.4E6; %Elastic stiffness of rope (no weight only elastic stiffness)
T_0=4000; %Initial load [N]
%l_0=T_0/(EA_rope)*l+l; %Initial elongated length of rope with T_0 of load
l_0=1989;
phi_0=(asin(y/l_0)); %Initial angle of mooring
x_init=cos(phi_0)*l_0;
dx=0; %length increment
for i=1:2000
    phi(i)=atan(y/(x_init+dx));
    dl(i)=cos(phi(i))*dx;
    T(i)=T_0+EA_rope/l_0*dl(i);
    Tx_2(i)=T(i)*cos(phi(i));
    Xl_2(i)=real(x_init+dx);
    dx=dx+0.09; %Increment
end
offset_2=Xl_2-x_init;
```

Plotting all graphs of interest.

```
figure(1);
plot(Tx_0/1000,s_0,'blue','linewidth',2);
hold on
plot(Tx_0/1000,x_0,'red','linewidth',2);
plot(Tx_1/1000,x_1,'k','linewidth',2);
plot(Tx_1/1000,s_1,'c','linewidth',2);
legend('s_0 (no elasticity [m]','x_0 (no elasticity) [m]',...
    'x_1 (with elasticity)','s_1 (with elasticity)');
title('Length of lines');
xlabel('Tension [kN]');
ylabel('Length [m]');
```

```
figure(2);
plot(Tx_0/1000,offset_0,'green','linewidth',2);
hold on
plot(Tx_1/1000,offset_1,'magenta','linewidth',2);
plot(Tx_2/1000,offset_2,'r','linewidth',2);
grid on
title('Offsets against line tension');
xlabel('Tension [kN]');
ylabel('Offset [m]');
legend('Offset of no elastic chain',
'Offset with elastic chain','Offset with only elasticity');
```

E MATLAB 2D catenary approximation code

Contents

09.03.2021 Pål Lader
12.03.2021 V2.0 Pål Lader
03.04.2021 Modified by Sindre Grøftrem to fit Master thesis

```
clear
close all

% - Initiation ---
% Two chains: 1 (left) and 2 (right)

% Water depth
d1=65;d2=65; % [m]

% Weight of chain in water pr. m
n1=4;% Number of lines
n2=4;

w1=n1*26.28*9.81; w2=n2*26.28*9.81; % [N/m]
% Chain: MSc. Smith, p 74, table 7. 50mm chain: 49 kg/m i water

% Length of anchor line
s1=4*d1;s2=4*d2; % [m] length of anchor line
s1=210;s2=210;
```

Anchor line geometry (Plots)

Plots the achorline geometry for the two anchorlines, with the different Th_0 as given in the Th_0 vector

```
CMLC1=catenary_mooring_line_characteristics(d1,s1,w1);
CMLC2=catenary_mooring_line_characteristics(d2,s2,w2);
```

```
Th_max = min([CMLC1.Th_max CMLC2.Th_max]);

% Pretensioning (same for both lines)
%Th_0=[Th_max/100 Th_max/20 Th_max/2]; % [N] Horizontal trension
Th_0=0.3*Th_max; % [N] Horizontal trension

% --> CALCULATES

for c=1:length(Th_0)
    % CCMLCulates the geometry
    CMLG1(c)=catenary_mooring_line_geometry(d1,s1,w1,Th_0(c))
    CMLG2(c)=catenary_mooring_line_geometry(d2,s2,w2,Th_0(c))

    % Converts to "left" and "right" coordinate system
    X_equilibrium_1(c)=X_of_Th(d1,s1,w1,Th_0(c));
    X_equilibrium_2(c)=X_of_Th(d2,s2,w2,Th_0(c));

    % Line geometry
    CMLG1(c).x =   CMLG1(c).x - X_equilibrium_1(c) - CMLG2(c).x(1);
    CMLG2(c).x = -(CMLG2(c).x - X_equilibrium_2(c))- CMLG2(c).x(1);

    CMLG1(c).y=CMLG1(c).y-d1;
    CMLG2(c).y=CMLG2(c).y-d2;

    % X_max and X_min
    X_max1(c) = CMLC1.X_max - X_equilibrium_1(c);
    X_min1(c) = CMLC1.X_min - X_equilibrium_1(c);

    X_max2(c) = -(CMLC2.X_max - X_equilibrium_2(c));
    X_min2(c) = -(CMLC2.X_min - X_equilibrium_2(c));
end

% --> PLOTS
figure
for c=1:length(Th_0)
    subplot(length(Th_0),1,c)
    hold on
    grid on
    % Plots the line and characteristic points
    plot(CMLG1(c).x,CMLG1(c).y,'b',...
        CMLG2(c).x,CMLG2(c).y,'r') % Line
    plot(CMLG1(c).x(1),CMLG1(c).y(1),'kX',...
        CMLG2(c).x(1),CMLG2(c).y(1),'kX')% Anchor point
    plot(CMLG1(c).x(2),CMLG1(c).y(2),'ko',...
        CMLG2(c).x(2),CMLG2(c).y(2),'ko')% Bottom point
    plot(CMLG1(c).x(end),CMLG1(c).y(end),'ko',...
        CMLG2(c).x(end),CMLG2(c).y(end),'ko') % Vessel point
    %Plots limits
```

```
    plot(X_max1(c)*[1 1], [-min([d1 d2])*0.5 0 ],'b')
    plot(X_min1(c)*[1 1], [-min([d1 d2])*0.5 0 ],'b')
    plot(X_max2(c)*[1 1], [-min([d1 d2])*0.5 0 ],'r')
    plot(X_min2(c)*[1 1], [-min([d1 d2])*0.5 0 ],'r')

    ax(c)=gca
    ax(c).XLim=[CMLG1(end).x(1) CMLG2(end).x(1)];
    ax(c).YLim=[-max([d1 d2]) 0 ];
    axis equal
    ylabel('y [m]')
    grid on
end
xlabel('x [m]')
```

Range as a function of Th_0

```
CMLC1=catenary_mooring_line_characteristics(d1,s1,w1);
CMLC2=catenary_mooring_line_characteristics(d2,s2,w2);

Th_max = min([CMLC1.Th_max CMLC2.Th_max]);

n_points=1000
Th_0=[Th_max/100 : 99/100*Th_max/(n_points-1) : Th_max];

for c=1:length(Th_0)

    % Converts to "left" and "right" coordinate system
    X_equilibrium_1(c)=X_of_Th(d1,s1,w1,Th_0(c));
    X_equilibrium_2(c)=X_of_Th(d2,s2,w2,Th_0(c));

    % X_max and X_min
    X_max1(c) = CMLC1.X_max - X_equilibrium_1(c);
    X_min1(c) = CMLC1.X_min - X_equilibrium_1(c);

    X_max2(c) = -(CMLC2.X_max - X_equilibrium_2(c));
    X_min2(c) = -(CMLC2.X_min - X_equilibrium_2(c));

    Range(c) = min([X_min2(c) X_max1(c)]) - max([X_min1(c) X_max2(c)]);

end

figure
plot(Th_0/Th_max,Range)
xlabel('Th 0 / Th max [-]');
ylabel('Range [m]');
grid on
```

```
figure
plot(X_min1,Th_0/Th_max,'--b',X_min2,Th_0/Th_max,'--r',...
    X_max1,Th_0/Th_max,'b',X_max2,Th_0/Th_max,'r')
ylabel('Th 0 / Th max [-]');
xlabel('Xmin og Xmax [m]');
grid on
```

Range and k as a function of Th_0

```
CMLC1=catenary_mooring_line_characteristics(d1,s1,w1);
CMLC2=catenary_mooring_line_characteristics(d2,s2,w2);

Th_max = min([CMLC1.Th_max CMLC2.Th_max]);

n_points=1000
Th_0=[Th_max/100 : 99/100*Th_max/(n_points-1) : Th_max];

for c=1:length(Th_0)

    % Converts to "left" and "right" coordinate system
    X_equilibrium_1(c)=X_of_Th(d1,s1,w1,Th_0(c));
    X_equilibrium_2(c)=X_of_Th(d2,s2,w2,Th_0(c));

    % X_max and X_min
    X_max1(c) = CMLC1.X_max - X_equilibrium_1(c);
    X_min1(c) = CMLC1.X_min - X_equilibrium_1(c);

    X_max2(c) = -(CMLC2.X_max - X_equilibrium_2(c));
    X_min2(c) = -(CMLC2.X_min - X_equilibrium_2(c));

    Range(c) = min([X_min2(c) X_max1(c)]) - max([X_min1(c) X_max2(c)]);

    % Calculates X when Th=Th_0 (Equilibrium)
    X0_1=X_of_Th(d1,s1,w1,Th_0(c));
    X0_2=X_of_Th(d2,s2,w2,Th_0(c));

    % Th interval for each line
    n_points=10000;
    Th_1=[0.1 : (CMLC1.Th_max-0.1)/(n_points-1) : CMLC1.Th_max];
    Th_2=[0.1 : (CMLC2.Th_max-0.1)/(n_points-1) : CMLC2.Th_max];

    % Coordinate system shifted so that equilibrium is at x=0
    X1=CMLC1.X-X0_1;
    X2=-(CMLC2.X-X0_2);

    % Anchor line force on vessel is taken to be the horizontal tension in the
    % anchor line
```

```
    F1=Th_1;
    F2=Th_2;

    % Calculates the combined force
    % x is the displacement of the vessel. The possible x is limited by the
    % Xmax for each of the two lines
    n_points=1000;
    x=[-(CMLC2.X_max-X0_2) :...
        ((CMLC1.X_max-X0_1)+(CMLC2.X_max-X0_2))/(n_points-1) :...
        (CMLC1.X_max-X0_1)];

    % Since the X vectors is not evenly spaced it is necessary to look for x
    % values in the X1 and X2 vectors, and combine the corresponding force.
    for n=1:length(x)
        [dummy i1]=min(abs(X1-x(n)));
        F1_x(n)=F1(i1);

        [dummy i2]=min(abs(X2-x(n)));
        F2_x(n)=F2(i2);
    end

    F = F1_x - F2_x;


    % Calculates k at x=0

    [dummy i]=max(find(x>0));
    k(c)=(F(i+1)-F(i-1))/(x(i+1)-x(i-1));


end

figure
plot(Th_0/Th_max,Range)
xlabel('Th 0 / Th max [-]');
ylabel('Range [m]');
grid on

figure
plot(X_min1,Th_0/Th_max,'--b',X_min2,Th_0/Th_max,'--r',...
    X_max1,Th_0/Th_max,'b',X_max2,Th_0/Th_max,'r')
ylabel('Th 0 / Th max [-]');
xlabel('Xmin og Xmax [m]');
grid on

figure
plot(Th_0/Th_max,k)
xlabel('Th 0 / Th max [-]');
```

```
ylabel('k [N/m]');
grid on
```

Line characteristics of two separate anchor lines

```
[CMLC1]=catenary_mooring_line_characteristics(d1,s1,w1)
[CMLC2]=catenary_mooring_line_characteristics(d2,s2,w2)


% Plots Th
n_Th=figure;
hold on
plot(CMLC1.X,CMLC1.Th,'r',CMLC2.X,CMLC2.Th,'b')
xlabel('Horizontal distance between anchor point and vessel: X [m]');
ylabel('Horizontal anchor line force: Th [N]')
grid on

% Plots Th and Tv
n_ThTv=figure;
hold on
plot(CMLC1.X,CMLC1.Th,'r',CMLC1.X,CMLC1.Tv,'--r',...
    CMLC2.X,CMLC2.Th,'b',CMLC2.X,CMLC2.Tv,'--b')
xlabel('Horizontal distance between anchor point and vessel: X [m]');
ylabel('Horizontal and vertical anchor line force: Tv Th [N]')
grid on

% Plots Sa
n_sp=figure;
hold on
plot(CMLC1.X,CMLC1.s_p,'r',CMLC2.X,CMLC2.s_p,'b')
xlabel('Horizontal distance between anchor point and vessel: X [m]');
ylabel('Length of passive line, sp [m]')
grid on

% Plots Th Tv and Sa
n_all=figure;
subplot(2,1,1)
hold on
plot(CMLC1.X,CMLC1.Th,'r',CMLC1.X,CMLC1.Tv,'--r',...
    CMLC2.X,CMLC2.Th,'b',CMLC2.X,CMLC2.Tv,'--b')
xlabel('Horizontal distance between anchor point and vessel: X [m]');
ylabel('Horizontal and vertical anchor line force: Tv Th [N]')
grid on

subplot(2,1,2)
hold on
plot(CMLC1.X,CMLC1.s_p,'r',CMLC2.X,CMLC2.s_p,'b')
```

```
xlabel('Horizontal distance X [m]');
ylabel('Length of passive line, sp [m]')
grid on
```

Line characteristics of two combined anchor lines

```
n_points=1000;

[CMLC1]=catenary_mooring_line_characteristics(d1,s1,w1);
[CMLC2]=catenary_mooring_line_characteristics(d2,s2,w2);

Th_max = min([CMLC1.Th_max CMLC2.Th_max]);
% Pretensioning (needless to say same for both lines)
%Th_0=0.1*Th_max % [N] Horizontal trension
%Th_0=[Th_max/100 Th_max/10 Th_max/2];

Th_0=Th_max/10
% Calculates X when Th=Th_0 (Equilibrium)
X0_1=X_of_Th(d1,s1,w1,Th_0);
X0_2=X_of_Th(d2,s2,w2,Th_0);

% Th interval for each line
n_points=10000;
Th_1=[0.1 : (CMLC1.Th_max-0.1)/(n_points-1) : CMLC1.Th_max];
Th_2=[0.1 : (CMLC2.Th_max-0.1)/(n_points-1) : CMLC2.Th_max];

% Coordinate system shifted so that equilibrium is at x=0
X1=CMLC1.X-X0_1;
X2=-(CMLC2.X-X0_2);

% Anchor line force on vessel is taken to be the horizontal tension in the
% anchor line
F1=Th_1;
F2=Th_2;

% Calculates the combined force
% x is the displacement of the vessel. The possible x is limited by the
% Xmax for each of the two lines
n_points=1000;
x=[-(CMLC2.X_max-X0_2) :...
    ((CMLC1.X_max-X0_1)+(CMLC2.X_max-X0_2))/(n_points-1) :...
    (CMLC1.X_max-X0_1)];

% Since the X vectors is not evenly spaced it is necessary to look for x
% values in the X1 and X2 vectors, and combine the corresponding force.
for n=1:length(x)
    [dummy i1]=min(abs(X1-x(n)));
```

```
    F1_x(n)=F1(i1);

    [dummy i2]=min(abs(X2-x(n)));
    F2_x(n)=F2(i2);
end

F = F1_x - F2_x;

figure
plot(X1,F1,'b',X2,F2,'r',x,F,'k')
ax=gca;
ax.XLim=[max([x(1) X1(1)]) min([x(end) X2(1)])];
%ax.XLim=[X1(1) X2(1)];

xlabel('Displacement [m]')
ylabel('Force [N]')
grid on

% Calculates k at x=0

[dummy i]=max(find(x>0))
k=(F(i+1)-F(i-1))/(x(i+1)-x(i-1))
```

FUNCTIONS

```
function [CMLC]=catenary_mooring_line_characteristics(d,s,w)

% Estimates maximum Th (Th_max)
Th_max=(s^2-d^2)*w/(2*d); %Eq. 8.17
X_max=X_of_Th(d,s,w,Th_max);

X_min=s-d;

% Th interval
n_points=10000;
Th=[0.1:(Th_max-0.1)/(n_points-1):Th_max];
%cCMLCulates X from Th
X=X_of_Th(d,s,w,Th);


% Active length
s_a=d*sqrt(1+2./(w./Th*d));
% Passive length
s_p=(s-s_a);
% Vertical force
Tv=w*s_a;
```

```
% Put the values into the output struct
CMLC.Th=Th; CMLC.Tv=Tv; CMLC.X=X;
CMLC.s_a=s_a; CMLC.s_p=s_p;
CMLC.Th_max=Th_max; CMLC.X_max=X_max; CMLC.X_min=X_min;
end


function [CMLG]=catenary_mooring_line_geometry(d,s,w,Th)


%a=(w/Th);
%x_a=1/a*acosh(1+d*a); %

% Horizontal length active line Eq. 8.15 OMFaltinsen, Sealoads
x_a=1/(w/Th)*acosh(1+d*w/Th);

% CCMLCulates the catenary geometry
n_points=1000; % Number of points in the catenary cCMLCulation
x=[0:x_a/(n_points-2):x_a];
y=catenary(x,w,Th);

%cCMLCulates s_a (length of active line)
%s_a=sum(sqrt((x(1:end-1)-x(2:end)).^2+(y(1:end-1)-y(2:end)).^2));
s_a=d*sqrt(1+2./(w./Th*d));
%cCMLCulates s_p (length of passive line)
s_p=(s-s_a);

% Ads the anchor point to the coordinates
x=[-s_p x];
y=[0 y];

% Canges so that x=0 is at the anchor point
x=x-x(1);

% Put the values into the output struct
CMLG.x=x; CMLG.y=y;
end


function y=catenary(x,w,Th)
% Catenary equation
%
% w  [N/m] Weight of catenary pr m
% Th [N] Horisontal tension in the catenary
% x  [m] Hor. coordinate (Tv=0 at x=0 (bottom point))
% y  [m] Vert. coordinate (y=0 (bottom point)
a=w/Th;
y=(exp(a*x)+exp(-a*x))/(2*a)-1/a;
end
```

```
function X=X_of_Th(d,s,w,Th)
%cCMLCulates X from Th
a=w./Th;
x_a=1./a.*acosh(1+d*a);
s_a=d*sqrt(1+2./(a*d));
X=s-s_a+x_a;
end
```

F MATLAB irregular response post-processing code

Contents

- Uncoupled Data is loaded from .xlsx files
- Plotting total change in position for vessel for each run
- Plotting filtered response in LF and WF range
- Making response spectrum and plotting them
- Checking to see if n number of runs is sufficient
- Now doing the same operations with the coupled analysis data
- Coupled Data is loaded from .xlsx files
- Plotting total change in position for vessel for each run
- Plotting filtered response in LF and WF range
- Making response spectrum and plotting them
- Checking to see if n number of runs is sufficient

```
%MATLAB script for post-processing irregular data from SIMA runs, for
%Master thesis.
%23.04.22 Sindre Grøftrem


clc

clear all

close all
%Opening correct path, for this part of the script the Uncoupled analysis
%data will be gathered
```

Uncoupled Data is loaded from .xlsx files

```
path_directory_unc='C:\Users\si-gr\OneDrive\Dokumenter\Masteroppgave
\Simulering resultat\Uncoupled\H7.6T8.5Regular';
% Pls note the format of files,change it as required
original_files_unc=dir([path_directory_unc '/*.xlsx']);
for k=1:length(original_files_unc)
```

```
    filename_unc=[path_directory_unc '/' original_files_unc(k).name];
    data_unc{k}=xlsread(filename_unc);
    % Load files in cell array, each run is placed in a different cell
 end
```

Plotting total change in position for vessel for each run

```
 %Going through each run and plotting global change in position
 figure(); hold on
 title('Global change in position for each uncoupled run');
xlabel('Time [s]');
ylabel('Offset [m]');
grid on
legstring_unc=strings(1,k);
totposSeq_unc=zeros(length(data_unc{1,1}),length(data_unc));
 for k=1:length(original_files_unc)
    totpos_unc=sqrt((data_unc{1,k}(:,2)).^2+(data_unc{1,k}
    (:,3)).^2+(data_unc{1,k}(:,4)).^2); %calculating total response (y coord)
    time_unc=data_unc{1,1}(:,1); %Time steps (x coord)
plot(time_unc,totpos_unc,'linewidth',0.2); %Plotting each response
legstring_unc(k)=sprintf('Run %.1f',k); %Making legend for plots

totposSeq_unc(:,k)=totpos_unc; %Saving the total position for all runs in a matrix
 end
 legend(legstring_unc);
 hold off

  %Setting all the runs with different seeds in sequential order for
  %post-processing
 singleSeq_unc=reshape(totposSeq_unc,[length(data_unc{1,1})*length(data_unc),1]);
```

Plotting filtered response in LF and WF range

```
  %LF_unc=bandpass(singleSeq_unc,[1/300,1/30]);
  %WF_unc=bandpass(singleSeq_unc,[1/30,1/1.1]);
 %HF=bandpass(singleSeq,[1/10,1/1.1]);

  LF_unc=lowpass(singleSeq_unc,1/60,2);
  WF_unc=highpass(singleSeq_unc,1/20,2);
 figure();
 plot(linspace(0,length(singleSeq_unc)/2,length(singleSeq_unc)),LF_unc,
 'linewidth',0.2);
 hold on
 plot(linspace(0,length(singleSeq_unc)/2,length(singleSeq_unc)),WF_unc,
```

```
 'linewidth',0.2)
 legend('Low frequency','Wave frequency');
 xlabel('Time [s]');
 ylabel('Response [m]');
 title('Filtered uncoupled response signal');
 hold off

 %Making LF hand WF frequency response spectrums
figure();
pspectrum(LF_unc,2);
 title('Low frequency uncoupled response spectrum');

figure();
pspectrum(WF_unc,2);
title('Wave frequency uncoupled response spectrum');
```

Making response spectrum and plotting them

```
%Finner maksverdi for hver zero-upcrossing og lager weibullfordeling av
%disse verdiene.

[pks_unc,locs_unc] = findpeaks(singleSeq_unc);
peaks_unc=zeros(length(singleSeq_unc),1);

for i=1:length(pks_unc)
    if pks_unc(i)<= (mean(singleSeq_unc)+std(singleSeq_unc))
    %Chosing peaks larger than the average of total response plus
    standard deviation
        pks_unc(i)=0;
    end
    for k=1:length(singleSeq_unc)

        if pks_unc(i) == singleSeq_unc(k)
            peaks_unc(k)=singleSeq_unc(k);
        end
    end

end

figure();
plot(linspace(1,length(singleSeq_unc)/2,length(singleSeq_unc)),singleSeq_unc);
hold on
scatter(linspace(1,length(singleSeq_unc)/2,length(singleSeq_unc)),peaks_unc)
title('Identified peaks to use in uncoupled Weibull distribution');
xlabel('Time [s]');
ylabel('Offset [m]');
hold off
```

```
%Removing zero cells in pks_unc vector, for weibullfitting
pksW_unc = pks_unc(any(pks_unc,2),:);


%par_unc=evfit(pksW_unc);
par_unc=wblfit(pksW_unc);
x_unc=linspace(-2,40,200);
%pd_unc = makedist('GeneralizedExtremeValue','k',0,'mu',par_unc(1),'sigma'
,par_unc(2));
pd_unc= makedist('Weibull','A',par_unc(1),'B',par_unc(2));
Fiftyyear_unc=icdf(pd_unc,1-1/(50*365*3600/(20)))
Tenyear_unc=icdf(pd_unc,1-1/(10*365*3600/(20)))
y_unc=pdf(pd_unc,x_unc);
figure();
plot(x_unc,y_unc);
xlabel('Response [m]');
ylabel('Probability')
title('Uncoupled Weibull distribution')

figure();
qqplot(pksW_unc,pd_unc);
```

Checking if n number of runs is sufficient

```
% n contains the max response value for each run. The standard deviation
and expected
% value should converge when n is large enough.
for i=1:length(original_files_unc)
n_unc(i,1)=max(totposSeq_unc(:,i));
dev_unc(i,1)=std(n_unc);
exp_unc(i,1)=mean(n_unc);
end


figure();
plot(linspace(1,length(n_unc),length(n_unc)),dev_unc);
hold on
plot(linspace(1,length(n_unc),length(n_unc)),exp_unc);
xlabel('n number of runs');
ylabel('Expected value and standard deviation [m]');
title('Samples neccesary for convergence study (uncoupled)');
legend('Standard deviation','Expected value (assumed as mean)');
hold off
```

Now doing the same operations with the coupled analysis data

Coupled Data is loaded from .xlsx files

```
path_directory_cou='C:\Users\si-gr\OneDrive\Dokumenter\Masteroppgave\
Simulering resultat\Coupled\H7.6T8.5Regular';
% Pls note the format of files,change it as required
original_files_cou=dir([path_directory_cou '/*.xlsx']);
for k=1:length(original_files_cou)

   filename_cou=[path_directory_cou '/' original_files_cou(k).name];
   data_cou{k}=xlsread(filename_cou); % Load files in cell array,
   each run is placed in a different cell
end
```

Plotting total change in position for vessel for each run

```
%Going through each run and plotting global change in position
figure(); hold on
title('Global change in position for each coupled run');
xlabel('Time [s]');
ylabel('Offset [m]');
grid on
legstring_cou=strings(1,k);
totposSeq_cou=zeros(length(data_cou{1,1}),length(data_cou));
for k=1:length(original_files_cou)
   totpos_cou=sqrt((data_cou{1,k}(:,2)).^2+(data_cou{1,k}
   (:,3)).^2+(data_cou{1,k}(:,4)).^2); %calculating total response (y coord)
   time_cou=data_cou{1,1}(:,1); %Time steps 0,5s (x coord)
plot(time_cou,totpos_cou,'linewidth',0.2); %Plotting each response
legstring_cou(k)=sprintf('Run %.1f',k); %Making legend for plots

totposSeq_cou(:,k)=totpos_cou; %Saving the total position for all runs in a matrix
end
legend(legstring_cou);
hold off

 %Setting all the runs with different seeds in sequential order for
 %post-processing
singleSeq_cou=reshape(totposSeq_cou,[length(data_cou{1,1})*length(data_cou),1]);
```

Plotting filtered response in LF and WF range

```
 %LF_cou=bandpass(singleSeq_cou,[1/300,1/30]);
```

```
  %WF_cou=bandpass(singleSeq_cou,[1/30,1/2]);
 %HF=bandpass(singleSeq,[1/10,1/1.1]);

  LF_cou=lowpass(singleSeq_cou,1/60,2);
  WF_cou=highpass(singleSeq_cou,1/20,2);
 figure();
 plot(linspace(0,length(singleSeq_cou)/2,length(singleSeq_cou))
 ,LF_cou,'linewidth',0.2);
 hold on
 plot(linspace(0,length(singleSeq_cou)/2,length(singleSeq_cou))
 ,WF_cou,'linewidth',0.2)
 %plot(linspace(0,length(singleSeq),length(singleSeq)),HF,'linewidth',1.5)
 legend('Low frequency','Wave frequency');
 xlabel('Time [s]');
 ylabel('Response [m]');
 title('Filtered coupled response signal');
 hold off

 %Plotting frequency response spectrums
 figure();
pspectrum(LF_cou,2);
 title('Low frequency coupled response spectrum');

figure();
pspectrum(WF_cou,2);
title('Wave frequency coupled response spectrum');
```

Making response spectrum and plotting them

```
%Finner maksverdi for hver zero-upcrossing og lager weibullfordeling av
%disse verdiene.

[pks_cou,locs_cou] = findpeaks(singleSeq_cou);
peaks_cou=zeros(length(singleSeq_cou),1);

for i=1:length(pks_cou)
    if pks_cou(i)<= (mean(singleSeq_cou)+std(singleSeq_cou))
    %selecting peaks larger than the mean of total response plus the standard dev.
        pks_cou(i)=0;
    end
    for k=1:length(singleSeq_cou)

        if pks_cou(i) == singleSeq_cou(k)
            peaks_cou(k)=singleSeq_cou(k);
        end
    end
```

```
end

figure();
plot(linspace(1,length(singleSeq_cou)/2,length(singleSeq_cou)),singleSeq_cou);
hold on
scatter(linspace(1,length(singleSeq_cou)/2,length(singleSeq_cou)),peaks_cou)
title('Identified peaks to use in coupled Weibull distribution');
xlabel('Time [s]');
ylabel('Offset [m]');
hold off

%Removing zero cells in pks_cou vector, for weibullfitting
pksW_cou = pks_cou(any(pks_cou,2),:);


%par_cou=evfit(pksW_cou);
par_cou=wblfit(pksW_cou);
x_cou=linspace(-2,30,200);
%pd_cou = makedist('GeneralizedExtremeValue','k',0,'mu',
par_cou(1),'sigma',par_cou(2));
pd_cou= makedist('Weibull','A',par_cou(1),'B',par_cou(2));
Fiftyyear_cou=icdf(pd_cou,1-1/(50*365*3600/(20)))
Tenyear_cou=icdf(pd_cou,1-1/(10*365*3600/(20)))
y_cou=pdf(pd_cou,x_cou);
figure();
plot(x_cou,y_cou);
hold on
plot(x_unc,y_unc);
xlabel('Response [m]');
ylabel('Probability')
title('Coupled and uncoupled Weibull fitted distribution')
legend('Coupled','Uncoupled')
hold off

figure();
qqplot(pksW_cou,pd_cou);
```

Checking if n number of runs is sufficient

```
% n contains the max response value for each run. The standard deviation and
expected
% value should converge when n is large enough.
for i=1:length(original_files_cou)
n_cou(i,1)=max(totposSeq_cou(:,i));
dev_cou(i,1)=std(n_cou);
exp_cou(i,1)=mean(n_cou);
end
```

```
figure();
plot(linspace(1,length(n_cou),length(n_cou)),dev_cou);
hold on
plot(linspace(1,length(n_cou),length(n_cou)),exp_cou);
xlabel('n number of runs');
ylabel('Expected value and standard deviation [m]');
title('Samples neccesary for convergence study (coupled)');
legend('Standard deviation','Expected value (assumed as mean)');
hold off
```

G MATLAB line tension post-processing code

Contents

- Uncoupled Data is loaded from .xlsx files
- Sorting data
- Looking at low and wave frequency force

```
%MATLAB script for analysing line data from SIMA models, for master thesis
%28.04.22 Sindre Grøftrem


clc

clear all

close all

%Opening correct path, analysis
%data will be gathered
```

Data is loaded from .xlsx files

```
path_directory_cou='C:\Users\si-gr\OneDrive\Dokumenter\Masteroppgave\Simulering re
% Pls note the format of files,change it as required
original_files_cou=dir([path_directory_cou '/*.xlsx']);
for k=1:length(original_files_cou)

   filename_cou=[path_directory_cou '/' original_files_cou(k).name];
   linedata_cou{k}=xlsread(filename_cou); % Load files in cell array, each run is
end
```

Sorting data

```
%Sorting data into each line

for i=1:length(original_files_cou)
    mostLine_cou(:,i)=linedata_cou{1,i}(:,5);
    lessLine_cou(:,i)=linedata_cou{1,i}(:,2);
end



%Setting data in sequential order for each run
mostLineSeq_cou=reshape(mostLine_cou,[length(linedata_cou{1,1})*length(linedata_co
lessLineSeq_cou=reshape(lessLine_cou,[length(linedata_cou{1,1})*length(linedata_co

%For regular analysis, only evaluating the converged results (removed for
%the other analyses
%mostLineSeq_cou=mostLineSeq_cou(1000:length(mostLineSeq_cou));
%lessLineSeq_cou=lessLineSeq_cou(1000:length(lessLineSeq_cou));


%Plotting leeward line against most loaded line
time_cou=linspace(1,length(mostLineSeq_cou)/2,length(mostLineSeq_cou));

figure();
plot(time_cou,mostLineSeq_cou);
%hold on
%plot(time_cou,lessLineSeq_cou);
%hold off
legend('Most loaded line')
%'least loaded line');
title('Axial force [N]');
xlabel('Time [s]');
ylabel('Axial force [N]');
```

Looking at low and wave frequency force

```
 %LF_most_cou=bandpass(mostLineSeq_cou,[1/300,1/30]);
 %WF_most_cou=bandpass(mostLineSeq_cou,[1/30,1/1.1]);
%HF=bandpass(singleSeq,[1/10,1/1.1]);

 LF_most_cou=lowpass(mostLineSeq_cou,1/60,2);
 WF_most_cou=highpass(mostLineSeq_cou,1/20,2);
figure();
plot(linspace(0,length(mostLineSeq_cou)/2,length(mostLineSeq_cou)),LF_most_cou,'li
hold on
```

```
plot(linspace(0,length(mostLineSeq_cou)/2,length(mostLineSeq_cou)),WF_most_cou,'li
legend('Low frequency','Wave frequency');
xlabel('Time [s]');
ylabel('Axial force [N]');
title('Filtered axial force of most loaded line');
hold off

 LF_less_cou=lowpass(lessLineSeq_cou,1/30);
 WF_less_cou=highpass(lessLineSeq_cou,1/30);
figure();
plot(linspace(0,length(lessLineSeq_cou)/2,length(lessLineSeq_cou)),LF_less_cou,'li
hold on
plot(linspace(0,length(lessLineSeq_cou)/2,length(lessLineSeq_cou)),WF_less_cou,'li
legend('Low frequency','Wave frequency');
xlabel('Time [s]');
ylabel('Axial force [N]');
title('Filtered axial force of least loaded line');
hold off


%Making LF hand WF frequency response spectrums
figure();
pspectrum(LF_most_cou,2);
 title('Low frequency response spectrum for most loaded line');

figure();
pspectrum(WF_most_cou,2);
title('Wave frequency response spectrum for most loaded line');
```

H MATLAB regular analysis response post-processing code

Contents

- Uncoupled Data is loaded from .xlsx files
- Plotting total change in position for vessel for each run
- Plotting filtered response in LF and WF range
- Making response spectrum and plotting them
- Now doing the same operations with the coupled analysis data
- Coupled Data is loaded from .xlsx files
- Plotting total change in position for vessel for each run
- Plotting filtered response in LF and WF range
- Making response spectrum and plotting them

```
%MATLAB script for post processing regular data from SIMA runs, for
```

```
%Master thesis.
%23.04.22 Sindre Grøftrem


clc

clear all

close all
%Opening correct path, for this part of the script the Uncoupled analysis
%data will be gathered
```

Uncoupled Data is loaded from .xlsx files

```
 path_directory_unc='C:\Users\si-gr\OneDrive\Dokumenter\Masteroppgave\
 Simulering resultat\Uncoupled\H11.4T11RegularLong';
 % Pls note the format of files,change it as required
 original_files_unc=dir([path_directory_unc '/*.xlsx']);
 for k=1:length(original_files_unc)

    filename_unc=[path_directory_unc '/' original_files_unc(k).name];
    data_unc{k}=xlsread(filename_unc);
    % Load files in cell array, each run is placed in a different cell
 end
```

Plotting total change in position for vessel for each run

```
 %Going through each run and plotting global change in position
 figure(); hold on
 title('Global change in position for each uncoupled run');
xlabel('Time [s]');
ylabel('Offset [m]');
grid on
legstring_unc=strings(1,k);
totposSeq_unc=zeros(length(data_unc{1,1}),length(data_unc));
 for k=1:length(original_files_unc)
    totpos_unc=sqrt((data_unc{1,k}(:,2)).^2+(data_unc{1,k}
    (:,3)).^2+(data_unc{1,k}(:,4)).^2); %calculating total response (y coord)
    time_unc=data_unc{1,1}(:,1); %Time steps (x coord)
plot(time_unc,totpos_unc,'linewidth',0.2); %Plotting each response
legstring_unc(k)=sprintf('Run %.1f',k); %Making legend for plots

totposSeq_unc(:,k)=totpos_unc; %Saving the total position for all runs in a matrix
 end
 legend(legstring_unc);
```

```
 hold off

  %Cutting out the unsteady part of the results

singleSeq_unc = totposSeq_unc(1:length(totposSeq_unc));
```

Plotting filtered response in LF and WF range

```
  %LF_unc=bandpass(singleSeq_unc,[1/300,1/30]);
  %WF_unc=bandpass(singleSeq_unc,[1/30,1/1.1]);
 %HF=bandpass(singleSeq,[1/10,1/1.1]);

  LF_unc=lowpass(singleSeq_unc,1/60,2);
  WF_unc=highpass(singleSeq_unc,1/20,2);
 figure();
 plot(linspace(0,length(singleSeq_unc)/2,length(singleSeq_unc))
 ,LF_unc,'linewidth',0.2);
 hold on
 plot(linspace(0,length(singleSeq_unc)/2,length(singleSeq_unc))
 ,WF_unc,'linewidth',0.2)
 legend('Low frequency','Wave frequency');
 xlabel('Time [s]');
 ylabel('Response [m]');
 title('Filtered uncoupled response signal');
 hold off

 %Making LF hand WF frequency response spectrums
figure();
pspectrum(LF_unc,2);
 title('Low frequency uncoupled response spectrum');

figure();
pspectrum(WF_unc,2);
title('Wave frequency uncoupled response spectrum');
```

Making response spectrum and plotting them

```
%Finner maksverdi for hver zero-upcrossing og lager weibullfordeling av
%disse verdiene.

[pks_unc,locs_unc] = findpeaks(singleSeq_unc);
peaks_unc=zeros(length(singleSeq_unc),1);

for i=1:length(pks_unc)
    if pks_unc(i)<= (mean(singleSeq_unc)+std(singleSeq_unc)) %Chosing peaks larger
```

```
    than the average of total response plus standard deviation
        pks_unc(i)=0;
    end
    for k=1:length(singleSeq_unc)

        if pks_unc(i) == singleSeq_unc(k)
            peaks_unc(k)=singleSeq_unc(k);
        end
    end

end
```

Now doing the same operations with the coupled analysis data

Coupled Data is loaded from .xlsx files

```
 path_directory_cou='C:\Users\si-gr\OneDrive\Dokumenter\Masteroppgave\
 Simulering resultat\Coupled\H11.4T11Regular';
 % Pls note the format of files,change it as required
 original_files_cou=dir([path_directory_cou '/*.xlsx']);
 for k=1:length(original_files_cou)

    filename_cou=[path_directory_cou '/' original_files_cou(k).name];
    data_cou{k}=xlsread(filename_cou);
    % Load files in cell array, each run is placed in a different cell
 end
```

Plotting total change in position for vessel for each run

```
 %Going through each run and plotting global change in position
 figure(); hold on
 title('Global change in position for each coupled run');
xlabel('Time [s]');
ylabel('Offset [m]');
grid on
legstring_cou=strings(1,k);
totposSeq_cou=zeros(length(data_cou{1,1}),length(data_cou));
 for k=1:length(original_files_cou)
    totpos_cou=sqrt((data_cou{1,k}(:,2)).^2+(data_cou{1,k}
    (:,3)).^2+(data_cou{1,k}(:,4)).^2); %calculating total response (y coord)
    time_cou=data_cou{1,1}(:,1); %Time steps 0,5s (x coord)
plot(time_cou,totpos_cou,'linewidth',0.2); %Plotting each response
legstring_cou(k)=sprintf('Run %.1f',k); %Making legend for plots
```

```
totposSeq_cou(:,k)=totpos_cou; %Saving the total position for all runs in a matrix
 end
 xline(500);
 legend(legstring_cou);
 hold off

  %Cutting out the unsteady part of the results

singleSeq_cou = totposSeq_cou(1000:length(totposSeq_cou));
```

Plotting filtered response in LF and WF range

```
  %LF_cou=bandpass(singleSeq_cou,[1/300,1/30]);
  %WF_cou=bandpass(singleSeq_cou,[1/30,1/2]);
 %HF=bandpass(singleSeq,[1/10,1/1.1]);

  LF_cou=lowpass(singleSeq_cou,1/60,2);
  WF_cou=highpass(singleSeq_cou,1/20,2);
 figure();
 plot(linspace(0,length(singleSeq_cou)/2,length(singleSeq_cou
 )
 ,LF_cou,'linewidth',0.2);
 hold on
 plot(linspace(0,length(singleSeq_cou)/2,length(singleSeq_cou))
 ,WF_cou,'linewidth',0.2)
 %plot(linspace(0,length(singleSeq),length(singleSeq)),HF,'linewidth',1.5)
 legend('Low frequency','Wave frequency');
 xlabel('Time [s]');
 ylabel('Response [m]');
 title('Filtered coupled response signal');
 hold off

 %Plotting frequency response spectrums
 figure();
pspectrum(LF_cou,2);
 title('Low frequency coupled response spectrum');

figure();
pspectrum(WF_cou,2);
title('Wave frequency coupled response spectrum');
```

Making response spectrum and plotting them

```
%Finner maksverdi for hver zero-upcrossing og lager weibullfordeling av
%disse verdiene.
```

```
[pks_cou,locs_cou] = findpeaks(singleSeq_cou);
peaks_cou=zeros(length(singleSeq_cou),1);

for i=1:length(pks_cou)
    if pks_cou(i)<= (mean(singleSeq_cou)+std(singleSeq_cou))
    %selecting peaks larger than the mean of total response plus the standard dev.
        pks_cou(i)=0;
    end
    for k=1:length(singleSeq_cou)

        if pks_cou(i) == singleSeq_cou(k)
            peaks_cou(k)=singleSeq_cou(k);
        end
    end

end
```

Sindre Grøftrem

Master thesis 2022

NTNU
Norwegian University of
Science and Technology